Cosmochrony: A Pre-geometric Framework for Emergent Spacetime, Dynamics, and Matter

Jérôme Beau[1*]

[1*]Independent Researcher, France.

Corresponding author(s). E-mail(s): jerome.beau@cosmochrony.org;

Abstract

We present Cosmochrony, a foundational pre-geometric framework in which spacetime, inertia, mass, and interactions emerge from the irreversible relaxation of a single relational substrate $\boldsymbol{\chi}$. By postulating a principle of ontological poverty at the origin, we derive the expansion of the admissible configuration space as the primary driver of cosmic evolution.

A central result of the theory is the emergence of a Born–Infeld-like dynamics from the saturation of relational relaxation fluxes, providing a unified and non-singular resolution of both the initial cosmological singularity and the self-energy of charged particles. Within this framework, the speed of light and Planck's constant arise as complementary limits of projectability: $\boldsymbol{c}$ bounds the maximal admissible propagation of relational flux, while $\boldsymbol{h}$ sets the minimal resolvable granularity of the same underlying dynamics. In such regimes, effective thermodynamic and geometric quantities act as compensatory parameters encoding structural information lost under non-injective projection.

We further show that matter and electric charge emerge naturally as stable saturation and chiral-torsional invariants of the $\boldsymbol{\chi}$-flux, without invoking fundamental gauge fields. Numerical simulations indicate that Cosmochrony reproduces flat galactic rotation curves and provides a structural explanation of the Hubble tension as emergent effects of substrate relaxation, without dark matter particles or a fundamental dark energy component.

Finally, quantum indeterminacy and entanglement are derived as consequences of the non-injective projection of underlying $\boldsymbol{\chi}$-configurations onto effective observables. This mechanism naturally accounts for Bell inequality violations, the emergence of classical behavior in massive systems, and leads to concrete, falsifiable predictions, including precision spectral shifts in the Lamb regime, non-linear saturation in Schwinger pair-production, and signatures in ultra-high energy cosmic rays.

Keywords: Pre-geometric substrate, emergent spacetime, relational dynamics, Born–Infeld dynamics, spectral geometry, quantum non-injectivity

Contents

Part I
Foundations

1 Introduction and Motivation

Modern fundamental physics is built upon two highly successful yet conceptually distinct frameworks: quantum mechanics and general relativity [1, 2]. Quantum theory accurately describes microscopic phenomena, while general relativity provides a geometric account of gravitation and spacetime dynamics at macroscopic and cosmological scales. Despite their empirical success, these theories rely on incompatible foundational assumptions and resist unification within a single coherent conceptual framework [3–5].

In this work, we introduce *Cosmochrony*[1], a deliberately minimalist framework whose guiding hypothesis is that spacetime geometry, gravitation, and quantum phenomena emerge from the dynamics of a single continuous underlying entity, denoted χ, whose effective descriptions arise through a constrained projection process. This projection is generically non-injective, allowing distinct underlying χ-configurations to correspond to identical effective observables and, conversely, allowing a single underlying configuration to admit multiple correlated effective realizations. A detailed and formal treatment of this projection asymmetry is given in Section 2.10.

The substrate χ is not defined on a pre-existing spacetime manifold, nor is it interpreted as a conventional physical field propagating within spacetime. Instead, spacetime notions themselves arise as effective and relational descriptions, applicable only once suitable stability and projection conditions are satisfied. The precise ontological status of χ and the minimal assumptions governing its dynamics are introduced systematically in Section 2.

The fundamental dynamical postulate of Cosmochrony is that χ undergoes an irreversible relaxation process, locally bounded by an invariant structural propagation speed. The effective projection of this bound defines the observed causal limit c and induces an intrinsic ordering of physical processes, identified with physical time. Spatial relations emerge relationally from differences, gradients, and correlations of χ once a stable geometric regime is reached. Within this perspective, spacetime expansion, gravitation, particle-like excitations, radiation processes, and quantum correlations are emergent phenomena associated with specific configurations or interactions of the underlying substrate. In particular, discreteness, inertial mass, and quantum indeterminacy arise from structural constraints on projection and relaxation.

Convention on spacetime language

Throughout this article, spacetime coordinates, metric quantities, variational principles, and differential geometry are employed strictly as effective descriptive tools, valid only in regimes where χ-configurations admit a stable geometric interpretation. They are not treated as fundamental postulates of the theory. Technical reconstructions and mathematical details are confined to the appropriate effective regimes and collected in the appendices. This point will not be reiterated in subsequent sections.

[1] From $\kappa\acute{o}\sigma\mu o\varsigma$ and $\chi\rho\acute{o}\nu o\varsigma$, denoting a framework in which cosmic structure and temporal ordering emerge from a common pre-geometric substrate.

Cosmochrony does not aim to replace the Standard Model or general relativity in their empirically validated domains, nor does it claim to provide a final unification of quantum theory and gravitation. It offers an exploratory and internally coherent framework designed to clarify the physical origin of time, geometry, gravitation, and quantum correlations within a single relational dynamics. The unifying thread is the idea that apparent multiplicity, indeterminacy, and nonlocality reflect structural features of projection.

1.1 The Unification Problem

Quantum mechanics and general relativity differ not only in their mathematical formalisms but also in their foundational concepts. Quantum theory is intrinsically probabilistic, relies on a fixed causal structure, and treats time as an external parameter [1, 6]. General relativity describes gravitation as the dynamics of spacetime geometry itself, with time acquiring a coordinate-dependent and observer-relative status [2, 3].

This conceptual mismatch becomes acute in regimes where both quantum effects and strong gravitational fields are relevant, such as near spacetime singularities or in the early universe [7, 8]. Direct attempts to quantize gravity encounter persistent difficulties, including the problem of time, non-renormalizability, and the absence of a preferred background structure. These difficulties suggest that the tension may reflect a deeper incompatibility in the assumed ontological status of time and geometry.

Several major research programs have sought to address these challenges. Quantum field theory in curved spacetime accounts for particle creation and vacuum effects but retains a classical spacetime background [4]. Canonical and covariant approaches to quantum gravity attempt to quantize spacetime geometry itself, often at the cost of substantial mathematical complexity and interpretational ambiguity. String theory introduces extended fundamental objects and higher-dimensional structures, offering deep mathematical unification but leading to a large space of possible low-energy realizations [5]. While internally rich, these approaches face ongoing challenges concerning empirical testability and the physical interpretation of their fundamental degrees of freedom.

These limitations motivate the exploration of alternative perspectives in which spacetime geometry, matter, and quantum behavior emerge from a common underlying mechanism operating at a pre-geometric level.

1.2 Minimalism as a Guiding Principle

The framework developed in this work adopts minimalism as a guiding principle. Rather than introducing multiple fundamental fields, additional dimensions, or independent quantization rules, we explore whether a single continuous fundamental entity can account for temporal ordering, spatial relations, and quantum features within a unified relational dynamics.

The quantity χ is not interpreted as a conventional matter field, nor as a component of spacetime geometry. It represents a pre-geometric substrate whose irreversible relaxation underlies the emergence of both duration and separation. In this view, time and space are not independent primitives but complementary aspects of a single

dynamical process. Effective geometric and quantum descriptions arise only through coarse-grained, generally non-injective projections of the underlying χ-configurations.

1.3 Time, Irreversibility, and Cosmological Expansion

A central motivation for the Cosmochrony framework is the close connection between time, irreversibility, and cosmological expansion. In standard cosmology, expansion is described kinematically through the scale factor, while the arrow of time is typically attributed to boundary conditions or entropy growth [7–9].

In Cosmochrony, the monotonic relaxation of χ provides a unified origin for both phenomena. Irreversibility follows directly from the intrinsic directionality of the relaxation process, while cosmological expansion is interpreted as its large-scale geometric manifestation in the effective, projected description. Expansion does not require an externally imposed energy component but arises as an emergent consequence of the underlying pre-geometric dynamics. In the effective description, this manifestation is encoded geometrically as a large-scale compensatory response to sustained relational relaxation.

1.4 Conceptual Context and Related Approaches

The idea that spacetime geometry and gravitation may be emergent has been explored in a variety of contemporary theoretical frameworks. Several approaches interpret the spacetime metric as an effective description arising from deeper geometric, informational, or dynamical structures, and recast gravitation as a collective phenomenon [10, 11]. Cosmochrony belongs to this broad conceptual lineage while adopting a deliberately minimalist ontological stance: a single pre-geometric relational substrate χ whose irreversible relaxation governs the emergence of physical observables.

Like Loop Quantum Gravity (LQG), Cosmochrony holds that spacetime geometry is not fundamental [5]. However, the two frameworks operate at distinct conceptual levels. LQG provides a quantized description of geometry once a spacetime structure is already assumed, encoding areas and volumes through spin networks and holonomies. Related ideas have also appeared in modern holographic approaches formulated in asymptotically flat spacetimes, such as celestial holography, where scattering amplitudes are reorganized as conformal correlators on the celestial sphere [12].

Cosmochrony addresses an earlier and more primitive level. It does not quantize geometry but seeks to explain how geometric notions themselves arise as effective, coarse-grained descriptions of underlying χ-configurations. The emergence of spacetime is mediated by a non-injective projection from the pre-geometric substrate to effective observables, allowing geometric, dynamical, and quantum features to appear only once specific relational and spectral conditions are met. From this perspective, Cosmochrony does not compete with LQG but conceptually precedes it: it aims to account for the physical origin of the geometric degrees of freedom that may subsequently be quantized within such approaches, while remaining agnostic about the detailed form of their quantization at the effective level.

1.5 Scope and Limitations

The aim of this work is exploratory rather than definitive. Cosmochrony does not seek to replace established theories within their empirically validated domains, but to offer a coherent reinterpretation that may clarify persistent conceptual difficulties concerning time, geometry, and quantization. Emphasis is placed on internal consistency, conceptual clarity, and qualitative contact with observable phenomena, while openly acknowledging open questions and limitations.

1.6 Structure of the Paper

The paper is organized in five parts. Part I introduces the χ substrate, its minimal structural properties, and its ontological status (Section 2). Part II develops the effective dynamics of χ (Section **??**), the emergence of particle-like excitations (Section 4), and the projection fiber with gauge emergence (Section **??**). Part III addresses gravity as a collective effect (Section 6) and cosmological implications (Section **??**). Part IV presents the unified treatment of quantum phenomena, entanglement, and the relation to quantum formalism (Section 8). Part V collects radiation and quantization (Section 9), the spectral mass spectrum (Section **??**), testable predictions (Section 11), and the discussion with conclusion (Section 12). Appendices **??**–**??** provide mathematical foundations, conceptual extensions, cosmological and numerical supplements, and a glossary of notation.

For convenience, a glossary summarizing the main quantities and operators used throughout the article is provided in Appendix E.

2 The χ Substrate: Definition, Properties, and Ontology

This section introduces the single fundamental entity at the core of Cosmochrony: the pre-geometric relational substrate χ. We identify the minimal structural properties required for effective descriptions of spacetime, dynamics, and physical observables to arise in appropriate regimes, and we clarify the ontological status of χ and its relation to emergent physical quantities.

No spacetime manifold, metric structure, or background geometry is assumed. Geometric and dynamical notions are recovered only through non-injective, coarse-grained projections of χ configurations once suitable stability conditions are met. This minimality principle, referred to as a regime of *ontological poverty*, is adopted as a foundational constraint.

2.1 Definition of the χ Field

We define the existence of a single pre-geometric relational substrate, denoted χ, which constitutes the primitive ontological basis of physical reality. The quantity χ is not defined on a pre-existing spacetime manifold and does not presuppose any metric, causal, or geometric structure. Spacetime notions arise only as effective descriptions of the relational, spectral, and dynamical properties of χ configurations.

Ontologically, χ is not a scalar order parameter and does not possess local values. Scalar order parameters arise only at the effective level, as coarse-grained descriptors of projected χ configurations once a geometric regime is established. Dimensional quantities associated with length, duration, or mass arise only when χ configurations admit a stable geometric interpretation. The monotonic ordering intrinsic to χ configurations gives rise, upon projection, to what is operationally perceived as temporal flow.

Ontological Status of χ

The χ substrate is **not**:

- A scalar field defined on spacetime (no background manifold).
- A discrete lattice or graph.

It is a **pre-geometric relational structure** from which spacetime, matter, and physical observables emerge through projection.

Temporal ordering and spatial separation are not fundamental primitives but arise respectively from the intrinsic ordering of χ configurations and from their relational structure once a quasi-stable geometric regime is reached. Effective time corresponds to ordering, while space corresponds to relational structure.

The analogy with thermodynamic order parameters applies only at the effective level: χ itself is not an order parameter but gives rise to effective order parameters once projected. The substrate χ therefore provides the minimal ontological basis from which time, space, inertial mass, gravitation, and quantum phenomena jointly emerge as harmonics of a single irreversible relaxation process.

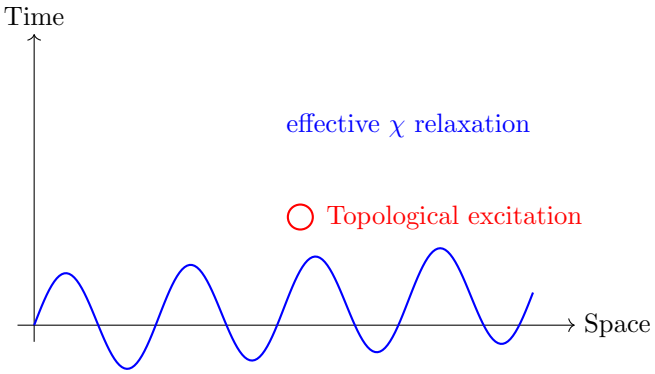

Fig. 1 Conceptual representation of Cosmochrony. An effective spacetime depiction of the projected scalar description of χ, used for visualization purposes only. The monotonic relaxation of χ gives rise to an effective temporal ordering, while localized topological excitations correspond to particle-like configurations in the emergent geometric regime.

Further interpretative clarifications and the fully relational formulation of χ are provided in Appendix B.1 and Appendix **??**.

2.2 The Geometric Effective Description of χ Dynamics

Effective Observables from χ Correlations

Quantities conventionally described in geometric terms—such as time intervals, spatial separation, and causal ordering—arise as effective summaries of relational patterns within the χ substrate, accessed only through projected, coarse-grained representations. The configurations σ represent internal relational states of χ and are defined without reference to external spacetime coordinates. The measure $d\mu(\sigma)$ denotes an invariant integration over configuration space, defined intrinsically from the correlation structure associated with χ.

Effective scalar descriptor.

In regimes where projected χ configurations admit a stable geometric interpretation, we introduce an *effective scalar descriptor* χ_{eff}. This quantity is a coarse-grained, projected representation of relational and spectral features of χ, defined only within the emergent spacetime description. It does not correspond to the fundamental substrate itself.

Operational time intervals are defined from the accumulated ordering of projected configurations along paths in configuration space:

$$\tau_{AB} \propto \int_{\gamma_{AB}} \mathcal{D}_\lambda \chi_{\text{eff}}\, d\lambda, \tag{1}$$

where $\mathcal{D}_\lambda \chi_{\text{eff}}$ is an effective relaxation functional and λ an ordering parameter.

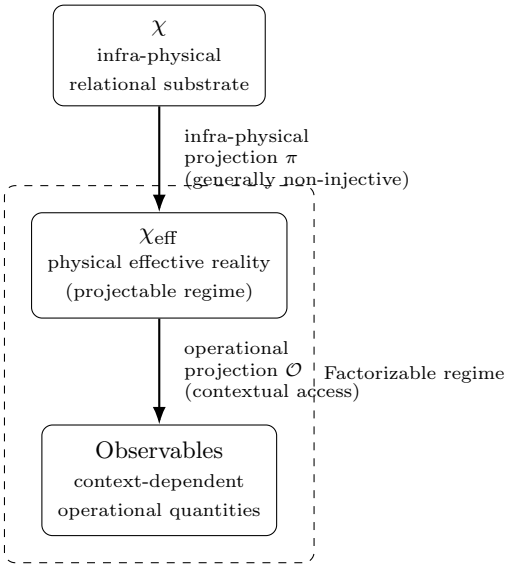

Fig. 2 Ontological pipeline in Cosmochrony. The infra-physical projection π maps the fundamental χ substrate to an effective physical reality χ_{eff} in projectable regimes, generally in a non-injective manner. Physical observables arise from an operational projection $\mathcal{O}$ that specifies how χ_{eff} is accessed under measurement contexts.

Operational spatial separation is quantified by the decay of correlations between effective descriptors:

$$d(x,y) \;\propto\; -\log\left(\frac{\langle \chi_{\text{eff}}(x)\,\chi_{\text{eff}}(y)\rangle}{\langle \chi_{\text{eff}}^2\rangle}\right), \tag{2}$$

where $\langle \chi_{\text{eff}}(x)\,\chi_{\text{eff}}(y)\rangle$ denotes an effective correlation functional encoding relational proximity between projected configurations x and y.

Effective Metric as a Descriptive Tool

In regimes where projected configurations exhibit smooth and stable correlation patterns, the relational observables may be summarized by an operational tensor $g_{\mu\nu}[\chi_{\text{eff}}]$. This effective metric is a derived descriptor summarizing relational correlations, not a fundamental geometric structure. No background $\eta_{\mu\nu}$ is assumed; Minkowski space appears only as an effective approximation in weak-gradient regimes.

In projectable regimes admitting a low-dimensional embedding, one may write locally

$$d(i,j)^2 \;\approx\; g_{\mu\nu}(x)\,\Delta x^\mu \Delta x^\nu.$$

The continuum line element ds^2 is therefore a derived descriptive construct.

Consistency with General Relativity

The effective metric reproduces the phenomenology of general relativity in appropriate regimes: the weak-field limit yields Einstein-like dynamics; near localized χ excitations,

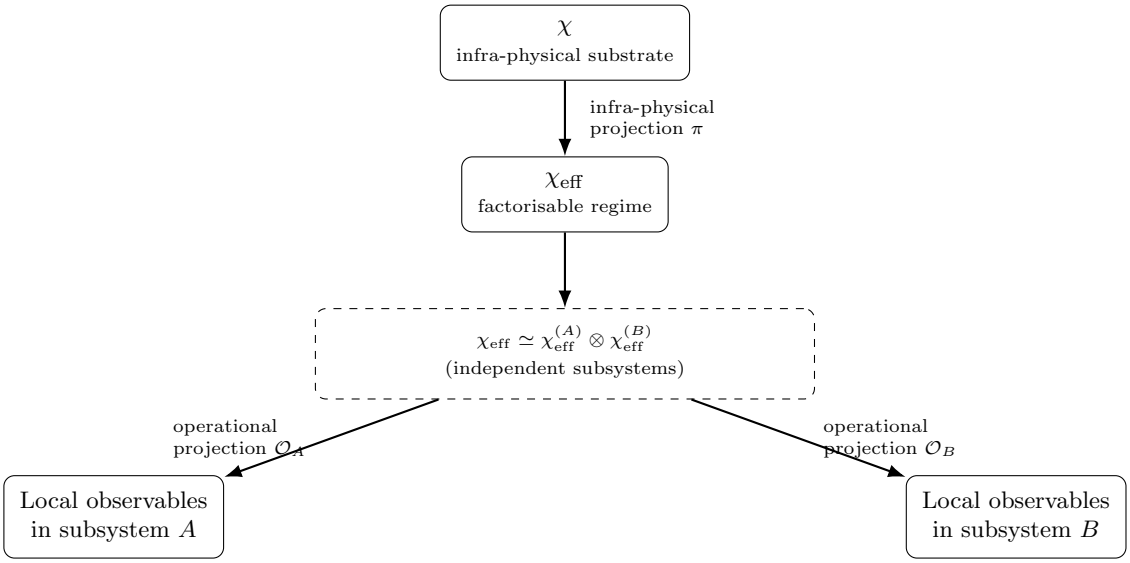

Fig. 3 Classical (factorisable) regime. After the infra-physical projection π, the effective description admits an approximate decomposition into independent subsystems. Operational projections then yield compatible local observables, recovering standard classical descriptions. This contrasts with the non-factorisable regimes discussed in Section 8.

the metric encodes time dilation and spatial curvature as emergent consequences of inhibited relaxation; homogeneous relaxation yields an effective Hubble-like expansion law. All predictive content resides in the underlying χ dynamics.

Operational origin of the effective metric.

The explicit construction of $g_{\mu\nu}$ from operational distances is given in Appendix E, where geometric quantities are shown to arise only in projectable regimes admitting a smooth continuum approximation.

2.3 Physical Interpretation

In regimes where the infra-physical projection from χ to an effective description χ_{eff} yields a factorisable structure, an approximate decomposition into subsystems and the definition of operational observables become possible. This factorisation underlies the emergence of classical locality, compatibility of measurements, and standard relativistic descriptions, as illustrated in Fig. 3.

Because the projection from χ to χ_{eff} is generically non-injective, distinct χ configurations may correspond to identical effective descriptions, while a single underlying configuration may admit multiple correlated operational realizations. This structural asymmetry is central to the emergence of both classical and quantum phenomenology. The physical content of the theory resides entirely in the dynamics of the fundamental substrate, while spacetime notions function as emergent, context-dependent descriptive tools.

2.4 Relational Projection and Spectral Admissibility

Admissible physical descriptions are defined by the spectral properties of the relational substrate χ.

Relational operator.

Let $\mathcal{H}_\chi$ denote the configuration space of admissible χ states. We introduce a relational operator

$$L_\chi : \mathcal{H}_\chi \to \mathcal{H}_\chi, \tag{3}$$

defined purely in terms of χ correlations. In discrete implementations (Appendix D), L_χ reduces to a graph Laplacian; in the continuum limit, it defines an effective self-adjoint operator encoding relational connectivity.

Spectral decomposition.

The operator L_χ admits a spectral decomposition

$$L_\chi \psi_n = \lambda_n \psi_n, \tag{4}$$

where $\{\lambda_n\}$ are non-negative eigenvalues and $\{\psi_n\}$ the associated eigenmodes.

Admissibility as spectral filtering.

Projectable configurations are selected by a spectral filter acting on L_χ. The infra-physical admissibility projection is

$$\Pi_{\lambda_*} \;\equiv\; f\left(\frac{L_\chi}{\lambda_*}\right), \tag{5}$$

where $f(x)$ is a fixed, smooth cutoff function satisfying $f(x) \to 0$ for $x \ll 1$ and $f(x) \to 1$ for $x \gg 1$. The scale λ_* sets the spectral threshold separating admissible from non-admissible relational modes.

Non-injectivity of the admissibility projection.

The projection Π_{λ_*} is intrinsically non-injective. Distinct configurations sharing identical spectral content below the cutoff λ_* are mapped to the same effective description. This structural non-injectivity—formalized here at the spectral level—constrains the class of admissible projected regimes and underpins the emergence of quantum correlations, internal degrees of freedom, and measurement processes developed in subsequent sections.

2.5 Structural Principles and Projective Regimes

All effective physical observables arise through a relational projection Π from the underlying configuration space Ω of the χ substrate. Effective descriptions are constrained by three structural principles that govern the admissibility of projected regimes.

Principle I: Substratic Locality and Bounded Relaxation.

The fundamental relaxation dynamics of χ is strictly local and subject to universal bounds. The transport of relational relaxation admits a maximal admissible flux, constraining the rate at which structural information can be redistributed. This bound arises from the intrinsic stability conditions of χ itself.

Principle II: Non-Injective Projective Realization.

The projection $\Pi : \Omega \to O$ from substratic configurations to effective observables is generically non-injective. Distinct configurations of χ may be structurally identified at the level of observable descriptions. This implies that effective descriptions need not admit a factorisable or locally complete representation, even when the underlying dynamics remains strictly local.

Principle III: Projective Compensation.

Whenever Π fails to resolve the full relational complexity of χ, effective descriptions compensate through the inflation of effective parameters—temperature, curvature, horizon structure—encoding unresolved relational structure within a reduced descriptive framework. These quantities function as Lagrange multipliers, not as additional fundamental degrees of freedom.

Together, these principles delineate distinct projective regimes. When the projection is approximately injective and relaxation is far from saturation, standard local and geometric descriptions apply. Near structural saturation or strong non-injectivity, effective parameters grow large, signaling the breakdown of spacetime-based descriptions.

2.6 Monotonicity and Arrow of Time

A central structural postulate is that the relational substrate χ admits an intrinsic, globally ordered relaxation structure. In effective descriptions, this ordering manifests as the monotonic behavior of the projected scalar descriptor along admissible ordering paths:

$$\mathcal{D}_\lambda \chi_{\text{eff}} \geq 0. \tag{6}$$

Here λ denotes an ordering parameter associated with relaxation, not a fundamental time coordinate. The inequality is a structural constraint on admissible projected representations.

Energy is interpreted as the remaining capacity of projected configurations to undergo further relaxation. Admissible ordering paths exclude any effective decrease of χ_{eff}, which would correspond to a restoration of relaxation capacity incompatible with the underlying ordering structure. The arrow of time is identified with this directional ordering: the progression from configurations with greater relaxation capacity toward configurations in which that capacity has been exhausted. This temporal orientation arises prior to any statistical or thermodynamic description [8, 13]. The relation to thermodynamic irreversibility is discussed further in Section 7.8.

Projectability and Kinematic Saturation.

A change of velocity corresponds to a modification of the relational coherence constraints maintained by the projection. As velocity increases, the informational demand on the projection grows, progressively saturating its capacity. The bound c_χ is a structural limit beyond which no stable and globally consistent projection can be maintained. Approaching saturation, part of the relational content of χ becomes inaccessible to the effective description, manifesting as time dilation, length contraction, and horizon formation. Relativistic kinematics thus emerges as a consequence of finite projection capacity[2].

Planck Scale and Relativistic Bounds as Projection Limits.

The constants c and h are interpreted as complementary manifestations of a finite resolution of the projection from χ to effective observables. The bound c limits the maximal admissible rate at which relational ordering can be projected, while h sets a lower bound on the granularity with which the relational flux can be resolved. Relativistic and quantum constraints thus emerge as complementary facets of a single structural limitation: the finite capacity and resolution of the projection.

2.7 Local Relaxation Speed

The effective local ordering rate associated with projected χ configurations is bounded. In effective geometric descriptions, this constraint takes the form

$$|\mathcal{D}_{\mathrm{loc}}\chi_{\mathrm{eff}}| \leq c, \tag{7}$$

where $\mathcal{D}_{\mathrm{loc}}\chi_{\mathrm{eff}}$ denotes an effective local relaxation functional. This inequality limits the maximal rate at which effective causal connectivity can be established within admissible descriptions. The quantity c characterizes the causal structure of the projected regime.

Local particle propagation, signal transmission, and field interactions are all constrained by this bound in effective spacetime descriptions. Apparent superluminal recession velocities at cosmological scales arise from cumulative global effects of projected ordering and do not violate this local causal constraint.

2.8 Relation to Conventional Fields

Effective descriptions derived from projected χ configurations may formally resemble scalar or tensor fields used in cosmology and particle physics. This resemblance reflects the emergence of a spacetime-based descriptive language, not the presence of an additional fundamental field.

Energy and quantization are not fundamental attributes of χ but arise at the effective level as consequences of the non-injective projection. Matter, radiation, and interactions correspond to effective degrees of freedom arising from structural constraints, spectral organization, and long-lived relational patterns of projected configurations. Standard

[2]This kinematic saturation concerns the ordering and coherence capacity of the projection itself and should not be conflated with thermodynamic entropy production.

Model fields are recovered as accurate effective descriptions within the appropriate coarse-grained regimes.

Cosmochrony does not extend the Standard Model by introducing new fundamental fields. It provides an ontological explanation for the emergence, applicability, and structural properties of effective field descriptions themselves.

2.9 Initial Conditions and Global Structure

The framework does not postulate initial conditions in the conventional temporal sense. It assumes that χ admits a minimal admissible ordering state, denoted χ_0, defining a structural boundary of admissible projected descriptions. This state does not correspond to a distinguished moment in time but to the earliest configurations for which an effective ordering interpretation becomes meaningful.

In effective geometric regimes, the characteristic scale near χ_0 coincides numerically with the Planck scale. This correspondence reflects the breakdown of projectability below this regime, not the presence of a fundamental cutoff or underlying discreteness.

Cosmic history is interpreted as the progressive and irreversible ordering of projected configurations away from this minimal admissible boundary. No spacetime singularity is required at the fundamental level. Apparent singular behavior arises only when classical notions are extrapolated beyond the regime in which projected configurations admit a stable geometric interpretation.

Ontological poverty and the growth of admissible structure.

The minimal state χ_0 corresponds to a regime of *ontological poverty*: only a severely restricted class of simple and highly coherent configurations can be projected. As relaxation proceeds, the space of admissible configurations expands, enabling the emergence of increasingly rich, localized, and hierarchical effective structures. The global structure of admissible descriptions is constrained by the ordering properties of the underlying substrate.

2.10 Ontological Interpretation

The χ Substrate as a Pre-Temporal Structural Plan

The substrate χ admits an ontological interpretation as a pre-temporal relational structure from which spacetime, matter, and effective physical laws emerge. It may be heuristically described as a *structural plan*: not a dynamical history, but a complete relational organization encoding the set of physically admissible configurations and the constraints that relate them. Temporal succession is emergent, corresponding to an oriented resolution of structural relations through irreversible relaxation. The notion of a structural plan does not introduce teleology, determinism, or a block-universe ontology: multiple effective histories may correspond to the same underlying relational structure through non-injective projection.

Relational Ontology and Conceptual Lineage

The relational character of χ bears a conceptual affinity with relational approaches in physics, notably those of Rovelli [5, 14], which trace part of their lineage to Aristotelian relational ontology [15, 16]. Cosmochrony shares the rejection of intrinsic, observer-independent properties but extends relationalism to a deeper ontological level: χ configurations are not relations *between* fundamental objects but relational structures that give rise to objects only upon projection. Relativistic causality emerges without postulating spacetime as fundamental [17]. Relationality is an intrinsic property of the pre-geometric substrate from which spacetime and physical entities jointly emerge.

Projection, Reality, and Ontological Asymmetry

The emergence of spacetime is a *projection* from χ, not a dual or bidirectional description. The projected universe is fully real at the level of physical experience but ontologically derivative: spacetime entities and dynamical laws do not possess ontological primacy [18]. While all physical descriptions depend on the projection of χ, the relational structure of χ does not admit a reformulation entirely in geometric or field-theoretic terms.

Apparent fine-tuning is reinterpreted as a selection effect imposed by projectability: only those configurations compatible with a stable emergent geometry appear as physically realized universes. Cosmochrony does not postulate a multiverse—the universe is unique at the level of physical reality, even though its underlying description in terms of χ may be non-unique.

The formal developments related to projection, including its fiber-bundle formulation and the emergence of gauge interactions, are developed in Section 5.

Configurational State Structure

The substrate χ defines a *configurational structure* specifying the set of admissible macroscopic states and the allowed transitions between them. Physical reality corresponds to a projected realization stabilized under finite resolution; no causal influence from projected configurations to χ is postulated. What appears as temporal evolution corresponds, at the level of χ, to an ordering of admissible configurations under projection. Universal bounds such as c_χ and $\hbar_\chi$ reflect intrinsic limits on admissible transitions within this configurational structure.

Intrinsic Structural Indeterminacy

A perfectly deterministic, fully symmetric relational substrate would remain physically inert. Cosmochrony therefore postulates an *intrinsic structural indeterminacy* at the level of χ: configurations are not exhaustively specified by a finite, closed set of relational conditions. This indeterminacy is ontological, not dynamical—it reflects the absence of perfect structural closure rather than random motion or noise.

Observable variability and probabilistic behavior arise only at the level of projected descriptions. Because the projection is non-injective, a single underlying configuration may correspond to multiple admissible effective realizations. Randomness is therefore

projective: it reflects the multiplicity of effective descriptions compatible with a given pre-geometric structure.

Relation to Holographic Descriptions

Cosmochrony is not a holographic theory in the technical sense. It does not posit a lower-dimensional boundary description or a dual equivalence between bulk and boundary physics. The limitation of physically accessible information within a given spacetime region reflects the degeneracy of underlying χ configurations corresponding to the same effective projection—a direct consequence of non-injectivity, not of boundary-localized degrees of freedom. Scaling behaviors reminiscent of holography are interpreted as emergent signatures of projection.

Similarly, Cosmochrony differs from thermodynamic approaches to gravity (Jacobson, Verlinde) in that it does not posit entropy or information as primitive quantities. Thermodynamic descriptions arise only at the effective level, as secondary languages applicable when projected configurations admit coarse-grained statistical interpretations.

2.11 Energy, Mass, and Fundamental Constants

Energy as Capacity for Relaxation

Energy is the effective capacity of projected χ configurations to relax unresolved structural constraints. It is not a fundamental conserved substance but an emergent quantity characterizing the degree to which a given projected configuration retains the ability to undergo further relaxation. Conservation laws arise only at the effective level, as structural regularities of projected dynamics. Without intrinsic structural indeterminacy (Section 2.10), the notion of energy would be ill-defined: a fully determined substrate would admit no unresolved tension and therefore no capacity for relaxation. The quantitative formulation is developed in Section 4.3.

Mass as Frozen Information

Localized and long-lived configurations of χ correspond to regions in which further relaxation is strongly inhibited. Such configurations trap a fixed amount of unresolved structural information, preventing it from participating in the global relaxation process. Mass represents *frozen energy*: structural information whose capacity for further relaxation has been locally suppressed[3]. Particle annihilation, decay, or radiation emission correspond to the partial or complete release of frozen structural information. The operational definition $m = E/c^2$ and its derivation from resistance to relaxation ordering are developed in Section 4.3.

Quarks as Non-Projectable Internal Modes

Quarks are not independent localized excitations but internal structural modes of composite solitonic configurations. They are required to characterize the internal

[3]This notion of frozen structural information should be distinguished from projection-induced entropy, which quantifies loss of distinguishability under non-injective projection.

organization of hadronic excitations but do not admit an autonomous projection into spacetime. Confinement reflects a structural constraint: isolated quark-like modes do not correspond to admissible standalone projections of χ_{eff}. Only collective configurations in which such internal modes are topologically and relationally closed admit a stable spacetime manifestation. Quark confinement thus appears as a direct consequence of the non-injective character of the projection.

The Role of the Universal Bound c_χ

The universal invariant bound c_χ characterizes an absolute structural limit on the degree to which relational information can be locally confined within admissible configurations of χ. It is non-metric and non-temporal: it is not associated with distances, durations, or lightcones, since none of these are defined prior to projection. The constant c_χ expresses a maximal admissible rate of structural ordering.

The effective causal constraint c observed in spacetime is the projected manifestation of c_χ:

$$c \equiv \Pi(c_\chi),$$

acquiring operational meaning only once notions of locality and causal ordering become meaningful. In strong-gravity or near-deprojection regimes, c may lose its geometric interpretation while c_χ remains invariant.

The Role of $\hbar_\chi$ and Reprojection

The parameter $\hbar_\chi$ characterizes a fundamental structural scale of χ, determined by its intrinsic relational density and constraint structure. It specifies a minimal quantum of *reprojection*: intrinsic structural information encoded in χ can enter an effective spacetime description only in discrete units set by this scale. As spacetime structure stabilizes, reprojection events become increasingly localized, manifesting phenomenologically as vacuum fluctuations.

The Origin of Planck's Constant

Within Cosmochrony, $\hbar$ is a **spectral invariant** of the relaxation and projection process. At the substrate level, the quantum of reprojection is fixed by

$$\hbar_\chi = \frac{c^3}{K_0\,\chi_c}, \tag{8}$$

where K_0 denotes the coupling density of relational constraints and χ_c the characteristic correlation scale. This relation expresses the *spectral rigidity* of the substrate.

In effective spacetime descriptions, the same scale appears as $\hbar_{\text{eff}}$, functioning as the quantum of action in Hilbert-space formulations. The apparent universality of $\hbar$ reflects the fact that K_0 and χ_c are global invariants of the current relaxation epoch. The transition from $\hbar_\chi$ to $\hbar_{\text{eff}}$ involves a change in representation, not in value.

Spectral Invariance of Planck's Constant and the Fine-Structure Constant

The fine-structure constant α emerges as a dimensionless spectral ratio, determined by the geometry of the projection fiber Π and the spectral rigidity encoded by K_0:

$$\alpha \;=\; \mathcal{F}\!\left(\frac{\text{geometry and topology of } \Pi}{K_0}\right), \tag{9}$$

where $\mathcal{F}$ is a functional fixed by the structure of admissible projections. If the structural parameters K_0 or χ_c were to vary—for example in primordial high-constraint regimes—both $\hbar$ and α would scale accordingly, preserving the internal structural coherence of the framework.

Part II
Dynamics and Particles

3 Effective Dynamics of the χ Substrate

3.1 Parameter-Independent Relaxation

Physical evolution appears only at the effective level, as an ordered sequence of projected χ configurations $(\chi_{\text{eff},\lambda})$, where λ is a strictly monotonic ordering parameter labeling admissible stages of relaxation. The ordering parameter λ does not represent time; it serves as an index ordering projected configurations once a macroscopic spacetime description becomes applicable.

Admissible projected descriptions are constrained by an effective relaxation condition:

$$\mathcal{D}_\lambda \chi_{\text{eff}} = \mathcal{R}[\chi_{\text{eff}}], \tag{10}$$

where $\mathcal{R}[\chi_{\text{eff}}]$ denotes an effective relaxation functional characterizing the ordering of projected configurations. This relation is a consistency condition on admissible projections, not a fundamental dynamical law. The functional $\mathcal{R}$ is defined only in regimes admitting a stable geometric interpretation.

Quantities commonly interpreted as temporal derivatives arise exclusively within effective descriptions. Within this framework, relaxation does not occur *in* time; the ordering of projected configurations defines what is operationally identified as physical duration.

3.2 Hamiltonian Derivation of the Evolution Equation

Once projected χ configurations admit a smooth, stable coarse-grained description, admissible local relaxation patterns may be summarized by a constraint formally analogous to a Hamiltonian condition. The effective local relaxation ordering is bounded by the invariant causal constant c:

$$\left(\mathcal{D}_{\text{loc}} \chi_{\text{eff}}\right)^2 + \mathcal{V}_{\chi_{\text{eff}}}^2 = c^2, \tag{11}$$

where $\mathcal{V}_{\chi_{\text{eff}}}$ denotes an effective internal variation functional encoding the resistance of projected configurations to further relaxation (e.g., solitonic or bound configurations).

Restricting to the monotonic ordering branch yields

$$\mathcal{D}_{\text{loc}} \chi_{\text{eff}} = c\sqrt{1 - \frac{\mathcal{V}_{\chi_{\text{eff}}}^2}{c^2}}, \tag{12}$$

expressing the universal slowdown of effective relaxation induced by localized structural constraints.

Emergent Gravitational Description

Projected configurations exhibiting strong resistance to relaxation locally reduce the admissible effective relaxation rate. In a spacetime interpretation, this reduction is conventionally described as gravitational time dilation. No independent gravitational field is postulated.

In weak-structure regimes, the spatial distribution of relaxation slowdown admits the simplified relation

$$\nabla \cdot \left(\frac{\nabla \chi_{\text{eff}}}{\sqrt{1 - |\nabla \chi_{\text{eff}}|^2 / c^2}} \right) \simeq \frac{4\pi G_{\text{eff}}}{c^2} \rho, \tag{13}$$

where ρ denotes the effective density of localized relaxation-resistant configurations and G_{eff} is an emergent coupling parameter. In the Newtonian limit, this yields an effective Poisson equation for a potential defined operationally by

$$\Phi \equiv c^2 \ln\left(\frac{\mathcal{D}_{\text{loc}} \chi_{\text{eff}}}{c} \right). \tag{14}$$

This potential is a compact summary of how localized variations in effective relaxation modulate physical clocks and rulers.

3.3 Microscopic Origin of the Coupling Tensor and the Poisson Equation

The effective coupling governing projected χ configurations depends on the internal structural state of the projected description. A convenient phenomenological parametrization is

$$K_{\text{eff}} = K_0 \exp\left(-\frac{(\Delta \chi_{\text{eff}})^2}{\chi_c^2} \right), \tag{15}$$

where $\Delta \chi_{\text{eff}}$ measures effective internal variation, K_0 is the maximal relaxation conductivity in a homogeneous background, and χ_c sets the scale beyond which inhomogeneities suppress relaxation efficiency.

Projected configurations exhibiting strong internal variation reduce the effective coupling and locally slow the admissible relaxation ordering, providing the microscopic origin of emergent gravitational phenomenology.

An effective gravitational potential Φ may then be introduced through

$$\frac{\mathcal{D}_{\text{loc}} \chi_{\text{eff}}}{\mathcal{D}_0} \simeq 1 + \frac{\Phi}{c^2}, \tag{16}$$

summarizing the relative slowdown of effective relaxation ordering. In the weak-structure regime, the spatial distribution of Φ admits a Poisson-type relation:

$$\nabla^2 \Phi \simeq 4\pi G_{\text{eff}} \rho, \tag{17}$$

where ρ is the effective density of relaxation-resistant configurations and G_{eff} an emergent coupling parameter. Gravitation appears as a descriptive manifestation of reduced relaxation conductivity induced by structured projected configurations.

A fully relational formulation is provided in Appendix **??**.

3.4 Variational Formulation and Born–Infeld Action

In regimes admitting a stable geometric interpretation, the effective relaxation constraints may be summarized in a compact variational form. Motivated by Born–Infeld-type non-linear actions [19, 20], we consider the effective Lagrangian density

$$\mathcal{L}_{\text{eff}} = -c^2\sqrt{1 - \frac{|\nabla\chi_{\text{eff}}|^2}{c^2}} + \mathcal{D}_{\text{loc}}\chi_{\text{eff}} - \frac{4\pi G_{\text{eff}}}{c^2}\,\rho\,\chi_{\text{eff}}, \tag{18}$$

where $\mathcal{D}_{\text{loc}}\chi_{\text{eff}}$ is the effective local relaxation ordering (Section 3.1) and ρ the effective density of localized relaxation-resistant configurations.

The linear dependence on $\mathcal{D}_{\text{loc}}\chi_{\text{eff}}$ enforces monotonicity without additional propagating degrees of freedom. The square-root structure acts as a non-linear regulator ensuring that effective spatial variations remain bounded by c. The Euler–Lagrange equation reproduces the non-linear elliptic relation

$$\nabla\cdot\left(\frac{\nabla\chi_{\text{eff}}}{\sqrt{1 - |\nabla\chi_{\text{eff}}|^2/c^2}}\right) = \frac{4\pi G_{\text{eff}}}{c^2}\,\rho, \tag{19}$$

coinciding with the effective relation obtained in Section 3.3.

This Born–Infeld-like action is an *auxiliary variational representation*. It does not define a fundamental action principle, nor equations of motion for the χ substrate. Its purpose is to regularize the effective description, enforce universal structural bounds, and facilitate comparison with standard gravitational phenomenology.

The physical interpretation is discussed in Appendix A.1, and the mathematical consistency with the relational dynamics is established in Appendix A.12.

Connection to Emergent Geometry.

In regimes where a geometric description is applicable, the Hessian of $\mathcal{L}_{\text{eff}}$ defines an emergent metric tensor $g_{\mu\nu}$, summarizing the effective geometric regularities of projected configurations.

Why This Is Not a Scalar–Tensor Theory.

The effective scalar descriptor χ_{eff} is not a fundamental dynamical field: it does not possess intrinsic values or conjugate momenta, and does not propagate independently. No modification of the gravitational sector is postulated, no scalar–tensor coupling of the form $f(\chi_{\text{eff}})R$ is introduced, and no additional propagating modes arise. Gravitation emerges from the local inhibition of relaxation ordering, not from the exchange of a scalar mediator.

3.5 Schwinger Effect as a Saturation Threshold of Relaxation Flux

In standard quantum field theory, the Schwinger effect is interpreted as a vacuum instability under an electric field exceeding a critical threshold. In Cosmochrony, the Born–Infeld-type effective dynamics provides a structurally different interpretation.

The Schwinger effect corresponds to a *threshold of flux saturation*. When the imposed electric field drives the effective relaxation flux beyond what can be transported smoothly through the projection fiber, the homogeneous relaxation regime becomes unstable. The system resolves this instability by activating additional admissible modes of the projection, corresponding to the nucleation of conjugate torsional excitations—naturally identified with electron–positron pairs. As discussed in Section 4.7, such pairs preserve global torsional neutrality, ensuring charge conjugation symmetry.

Pair production thus originates from a topological reconfiguration of the projection fiber under maximal relaxation stress, not from vacuum fluctuations. Matter creation acts as a dissipation channel that restores admissibility by redistributing excess relaxation flux into stable, projectable vortical modes. This enlarges the space of admissible configurations, in accordance with the principle of monotonic growth of admissible states.

Cosmochrony therefore predicts the existence of a Schwinger-like threshold *ab initio*, without invoking the Dirac sea or field quantization. The effect emerges as a universal transition between smooth relaxation and topologically mediated dissipation.

Dissipation by structure creation.

This mechanism illustrates a more general principle: when directional relaxation fluxes approach their maximal transport capacity, admissibility is restored by creating new stable structures that enlarge the space of admissible configurations. This suggests a unified interpretation of pair-loaded astrophysical jets, primordial matter production, and ultra-high-energy excitations in extreme curvature regimes (Section 11).

3.6 Causality and Locality

Within effective descriptions, the relaxation ordering encoded by χ_{eff} exhibits locality and causality. Effective locality follows from the fact that variations of χ_{eff} at a given effective event depend only on correlated neighboring projected configurations. Causality is enforced through the universal bound

$$|\mathcal{D}_{\text{loc}}\chi_{\text{eff}}| \leq c,$$

constraining the maximal rate at which correlations between effective configurations may be established. No superluminal propagation of signals or causal influence occurs within effective descriptions. Apparent superluminal recession velocities in cosmological contexts arise from cumulative integration of locally constrained relaxation ordering over extended regions and remain consistent with effective locality.

The effective causal bound c corresponds to the projected manifestation of the invariant structural bound c_χ defined at the level of the pre-temporal substrate (Section 2.11). Effective causality arises as a derived property of bounded projective realizations.

3.7 Homogeneous Cosmological Limit

In a homogeneous and isotropic regime, projected configurations exhibit no effective spatial variations and the admissible relaxation rate attains its maximal value:

$$\mathcal{D}_{\mathrm{loc}}\chi_{\mathrm{eff}} = c. \tag{20}$$

Expressed in terms of an effective cosmological time parameter t, this yields

$$\chi_{\mathrm{eff}}(t) = \chi_{\mathrm{eff},0} + c\,t, \tag{21}$$

where $\chi_{\mathrm{eff},0}$ is a reference value. This linear regime underlies the emergent Hubble law derived in Section 7.5.

As shown in Appendix A.6, the monotonicity requirement in an expanding regime implies a minimal residual structural inhomogeneity in projected configurations, manifesting as a non-vanishing lower bound on gravitational acceleration. This bound provides a natural route to MOND-like phenomenology without postulating dark matter particles [21, 22].

3.8 Influence of Local Structure

In regions where projected configurations exhibit non-vanishing effective structural variations, the admissible local relaxation ordering is reduced. Localized relaxation-resistant configurations—describable as particle-like solitonic structures—act as constraints on the admissible ordering of projected configurations. By increasing the effective structural complexity, they locally inhibit relaxation without introducing any additional interaction or mediator.

When a geometric description is applicable, this inhibition manifests as gravitational time dilation and spatial curvature. Gravitation arises as a collective consequence of locally constrained effective relaxation ordering.

3.9 Unified Origin of Geometric and Field Effects

The relation between the χ substrate and the effective spacetime metric $g_{\mu\nu}$ is strictly hierarchical and may be summarized in three levels. First, at the fundamental level, physical reality is described solely in terms of χ and its intrinsic relational structure. Second, in regimes where projected configurations admit a stable and slowly varying description, the spacetime metric arises as an effective descriptor summarizing correlations and relaxation ordering. Third, localized relaxation-resistant projected configurations—describable as solitonic structures—are identified with matter degrees of freedom, and gravitational phenomena correspond to local modulations of effective relaxation ordering induced by such structures.

No independent gravitational interaction or fundamental field is postulated. Matter, geometry, and gravitation emerge as complementary aspects of the same constrained ordering of projected configurations.

3.10 Limitations and Scope

Equation (12) is intentionally minimal. It constrains admissible projected descriptions in regimes where a stable geometric interpretation is applicable, but does not provide a first-principles account of quantum fluctuations or correlations at the level of χ itself. Such phenomena arise from non-injective projection and coarse-graining. Higher-order structural effects and strongly non-projectable regimes lie outside the present scope.

Within these limitations, the constrained ordering relation provides a unified kinematic backbone from which gravitational, quantum, and cosmological phenomena can be consistently recovered at the effective level. More refined treatments of effective fluctuations and extended relational structures are left for future work.

4 Particles as Localized Excitations of the χ Field

4.1 Particles as Stable Wave Configurations

Particles are not fundamental point-like entities. They arise at the level of effective descriptions as stable, localized configurations within projected χ descriptions [23]. Such configurations correspond to persistent patterns that locally constrain the admissible relaxation ordering. In effective geometric regimes, they may be described using soliton-like language. Their stability reflects localized regions in which further relaxation is strongly inhibited. Apparent particle propagation corresponds to a continuous reorganization of admissible projected descriptions, not to the motion of an object through a fundamental spacetime.

4.2 Topological Stability

The stability of particle-like excitations does not rely on fundamental conserved charges postulated *a priori*. Certain projected configurations exhibit non-trivial internal organization that prevents them from being continuously deformed into homogeneous effective descriptions without violating admissibility conditions.

This stability is topological in character: it reflects the existence of inequivalent classes of admissible projected configurations that cannot be smoothly connected through continuous reconfiguration while preserving monotonic relaxation ordering. The long-lived character of solitonic structures follows from this topological incompatibility, not from a dynamical balance of forces.

Detailed geometric constructions of topological solitons, including vortex, skyrmion, and knotted configurations, are provided in Appendix B.2. The fully relational formulation is developed in Appendix **??**.

4.3 Mass as Resistance to χ Relaxation

Building on the ontological interpretation of mass as frozen structural information (Section 2.11), we develop the quantitative formulation. Mass emerges at the effective level as a measure of how strongly a localized projected configuration resists admissible relaxation ordering.

The effective structural energy associated with a projected solitonic configuration $\chi_{\text{eff},s}$ is

$$E[\chi_{\text{eff},s}] \equiv \int_{\Sigma} \left(\frac{1}{\sqrt{1 - |\nabla \chi_{\text{eff},s}|^2/c^2}} - 1 \right) d\Sigma, \tag{22}$$

where Σ denotes a hypersurface of constant effective ordering parameter and $|\nabla \chi_{\text{eff},s}|$ quantifies effective structural deformation. The inertial mass is then defined operationally as

$$m \equiv \frac{E[\chi_{\text{eff},s}]}{c^2}. \tag{23}$$

For example, the electron mass m_e reflects its topological stability as a 4π-periodic soliton (Section B.4), while the proton mass arises from a composite 3-soliton configuration.

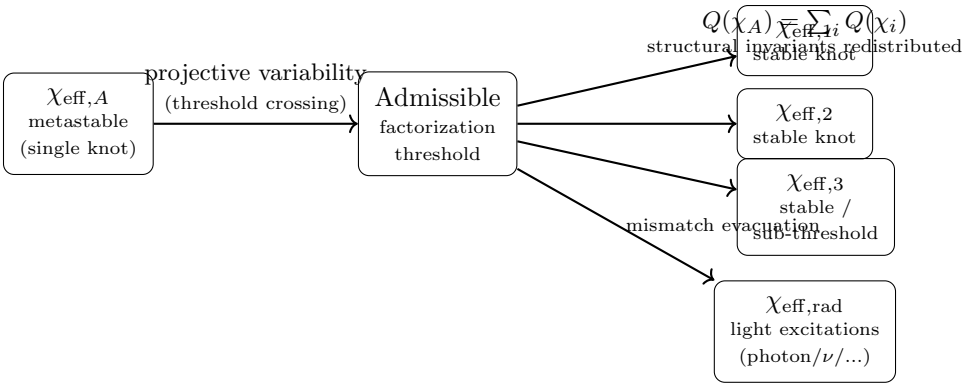

Fig. 4 Structural interpretation of particle decay. A metastable localized projected configuration transitions, via an admissible factorization threshold, into several more stable configurations plus weak excitations that evacuate the residual structural mismatch.

The relation $E = mc^2$ is interpreted as a kinematic identity: mass quantifies relaxation resistance, while energy expresses the same quantity in relaxation units. The question of how distinct particle masses arise from different classes of projected configurations is addressed in Appendix B.2.

4.4 Metastability, Projection, and Particle Decay

A stable particle corresponds to a deep basin of admissible projected configurations; an unstable particle occupies a shallow or fragile basin. Particle decay is interpreted as the structural reorganization of a metastable configuration: when the concentration of constraints exceeds what can be sustained by a single projected entity, admissibility is recovered through factorization into less constrained localized configurations, possibly accompanied by weakly structured excitations.

Entanglement and decay represent two regimes of the same projection structure. Entanglement corresponds to non-factorizability without fragmentation, while decay corresponds to non-factorizability that forces fragmentation. The distinction lies in the stability properties of the projected description under admissible fluctuations.

The finite lifetime of unstable particles reflects the probability of crossing a structural reorganization threshold under admissible variations, yielding the observed exponential decay law as a statistical signature of metastability.

A more technical characterization of metastability, admissible factorization channels, and decay widths is provided in Appendix B.14.

4.5 Energy–Frequency Relation

The energy associated with a particle-like excitation is linked to a characteristic internal spectral scale of the corresponding projected configuration. Configurations associated with higher characteristic frequencies correspond to more tightly constrained structures and encode greater effective resistance to relaxation. This yields

$$E \propto \nu, \tag{24}$$

where ν characterizes the spectral scale of internal organization. Planck's constant appears as an effective proportionality factor whose universality reflects the robustness of spectral scales in the current relaxation epoch. A more explicit realization in the context of radiation is presented in Section 9.3.

4.6 Fermions, Bosons, and Spin

Particle statistics emerge from the topological structure of admissible projected configurations. Configurations requiring a 4π rotation to return to an equivalent projected description give rise to fermion-like behavior, while 2π-periodic configurations correspond to bosons. This distinction reflects a topological obstruction rather than a symmetry principle imposed at the fundamental level.

Spin as a Topological Property

Spin is not an intrinsic kinematic degree of freedom but a purely topological property of admissible projected configurations. Fermionic configurations require a 4π transformation in configuration space to return to an equivalent effective description, implying that the relevant configuration space admits a double covering with fundamental group

$$\pi_1(\mathcal{C}_{\text{eff}}) = \mathbb{Z}_2. \tag{25}$$

When an effective quantum description is applicable, a 2π transformation induces a sign change of the associated wavefunction,

$$\psi \longrightarrow -\psi, \tag{26}$$

while a 4π transformation restores the original state. This 4π-periodicity directly implies fermionic antisymmetry and the Pauli exclusion principle, as detailed in Section **??**.

Exchanging two identical fermionic excitations corresponds topologically to a 2π loop in the combined configuration space and induces a sign change, dynamically excluding symmetric configurations [24]. The spin–statistics connection thus admits a unified topological origin within the effective descriptive framework.

4.7 Charge as a Topological and Relaxational Property of χ

Unified Relaxation Budget for Mass and Charge

Both inertial mass and electric charge draw on the same finite relaxation capacity of χ. A localized excitation mobilizes capacity in two structurally distinct channels: a scalar inhibition channel associated with inertial response (mass), and an oriented or chiral channel associated with a net topological flux (charge). Admissible projected configurations satisfy a single combined bound

$$\mathcal{B}_m[\chi] + \mathcal{B}_e[\chi] \leq \mathcal{B}_{\max}, \tag{27}$$

where $\mathcal{B}_{\max}$ is fixed by the universal relaxation capacity constraint (Section 3.4). Effective mass and charge are therefore competing manifestations of a common substrate

resource, and the observed discreteness of particle masses may be approached as a classification of admissible stable configurations under a single saturation constraint.

Charge as a Directed and Conjugate Relaxation Mode

Charges arise only after projection, as stable invariants characterizing admissible projected configurations. Charge conjugation is reinterpreted as a transformation between *relationally conjugate* projected configurations: paired topological classes related by an internal reversal of relational organization, reflecting the internal duality of the projection fiber.

At the discrete level, the χ dynamics induces a bounded relaxation flux $\vec{J}_\chi \sim \nabla\chi$. Charge corresponds to the non-integrability of this flux around localized excitations: the resulting winding number defines an integer-valued topological invariant whose sign encodes chirality. Electric attraction and repulsion arise from the geometric compatibility or frustration between torsional flux patterns of neighboring excitations. The bounded nature of $\vec{J}_\chi$ implies a maximal admissible charge density and naturally removes short-distance singularities.

The robustness of this chiral–torsional invariant is tested in Appendix B.17.

CP Symmetry as Projective Chirality.

CP symmetry corresponds to a combined transformation acting on the orientation of the projection itself. When the projection is achiral, conjugate configurations are mapped symmetrically and CP is preserved. When the projection is chiral, CP is violated as a direct consequence of projective asymmetry, without introducing explicit CP-violating terms at the level of χ.

4.8 Antiparticles, Creation/Destruction, and CPT

Antiparticles as Relationally Conjugate Configurations

A particle and its antiparticle correspond to projected configurations belonging to distinct but conjugate topological classes within the space of admissible projected descriptions, related by an internal reversal of relational organization. Annihilation occurs when a particle-like configuration and its conjugate combine into a composite description that no longer supports localized structural constraints, redistributing relational structure into delocalized radiation-like excitations. This constitutes a process of *structural unknotting*: mass itself measures the degree of topological obstruction to relaxation.

Why Antimatter Does Not Require Time Reversal.

The monotonic ordering of χ defines an absolute arrow of admissible projection that cannot be inverted. Antiparticles correspond to topologically conjugate classes, not to reversed temporal trajectories. The apparent association between antimatter and time reversal in standard formalisms is a feature of the effective representation.

Matter–Antimatter Asymmetry without Fundamental CP Violation.

If the projection from χ to effective spacetime is chiral, conjugate classes need not be realized with equal stability or projectability. Matter–antimatter asymmetry emerges as a selection effect imposed by differential projectability, without requiring dynamical CP-breaking interactions.

Particle Creation and Destruction

Particle creation corresponds to a projected configuration acquiring sufficient structural organization to support a stable topological class. Particle destruction occurs when a configuration loses its topological admissibility and admits continuous deformation toward a delocalized effective description.

CPT as a Global Projective Property

C, P, and T are individually effective and representation-dependent. Their combined action corresponds to a full relational conjugation of projected descriptions, mapping any admissible effective configuration to another admissible configuration representing the same underlying χ structure. CPT invariance is therefore not a microscopic symmetry but a global projective consistency condition ensuring that the space of admissible descriptions is closed under full relational conjugation. Violations of CPT would signal a breakdown of projectability itself.

CPT as an Admissibility Consistency Condition

Certain projected configurations carry orientation-sensitive structural invariants (chirality, phase winding, relational orientation). Under admissible factorization, these signed invariants must be redistributed, possibly requiring paired localized excitations carrying opposite orientations—interpreted as particle–antiparticle pairs. CPT symmetry reflects the invariance of admissibility under a combined reversal of signed structural invariants, effective spatial orientation, and the effective ordering parameter. A technical formulation is provided in Appendix B.16.

Why CPT Survives Quantum Gravity.

CPT survives because it expresses the minimal requirement for a coherent physical projection. Quantum gravity may challenge locality, geometry, and the notion of time, but cannot violate CPT without undermining the possibility of a consistent emergent universe.

4.9 Neutrinos as Partially Projectable Modes

Neutrinos correspond to *partially projectable modes* of χ: configurations whose relational structure admits a stable projection in some degrees of freedom while remaining weakly or non-projectable in others. This partial projectability explains their extremely small effective masses, weak interaction strength, and sensitivity to global rather than local structural properties of the projection.

Dirac vs. Majorana Character.

A Dirac neutrino admits distinct conjugate projected realizations; a Majorana neutrino corresponds to a configuration whose partial projectability collapses the distinction between conjugate classes. The Dirac or Majorana character is not a fundamental choice but a manifestation of how fully the projection resolves relational conjugation. Lepton number conservation emerges only in regimes where conjugate configurations are distinguishable; when partial projectability erases this distinction, effective lepton number violation becomes admissible.

Neutrino Oscillations without Fundamental Mass Eigenstates.

Different flavors correspond to closely related partially projectable configurations whose internal relational structures overlap but are not identical. As projected descriptions evolve along the monotonic ordering of χ, the relative projectability of these configurations varies, leading to coherent transitions between flavor labels without invoking mass eigenstates as fundamental objects.

Stability of the Projection Boundary.

Neutrinos occupy an intermediate regime between fully localized particles and delocalized radiation. They act as carriers of marginal structural information, redistributing relational organization without inducing strong backreaction, thereby preventing abrupt transitions between projectable and non-projectable regimes. In strong-gravity or near-deprojection regimes, neutrinos remain among the last modes to retain partial projectability.

Why Neutrinos Are the Lightest Fermions.

Neutrino configurations reside closest to the boundary of projectability. Their absence of electromagnetic coupling and partial self-conjugacy prevent the formation of tightly bound projected structures. The smallness of neutrino masses is a structural necessity imposed by their role as marginally projectable modes.

Neutrinos as Probes of Pre-Geometric Structure.

Because neutrinos operate near the projection boundary, they provide a unique observational window into the pre-geometric structure of χ. Their weak localization allows them to sample relational structures inaccessible to fully projectable modes, and deviations in their phenomenology may encode signatures of pre-geometric ordering.

Failure of Absolute Localization.

Neutrinos cannot be fully confined within a bounded spacetime region without loss of admissibility, explaining their absence of sharply defined position operators and extremely small interaction cross-sections.

Limits of Effective Quantum Field Theory.

Neutrinos systematically probe the limits of local QFT assumptions. Their weak localization, extended coherence, and oscillatory behavior signal a breakdown of the

strict particle ontology. Standard QFT constructs (mass eigenstates, flavor mixing matrices) are understood as effective bookkeeping devices for marginally projectable configurations.

Experimental Signatures.

Potential signatures include small departures from standard oscillation patterns at ultra-long baselines, coherence and decoherence effects sensitive to global spacetime properties, constraints from neutrinoless double beta decay on the projective resolution of conjugate configurations, and cosmological neutrino backgrounds encoding information about the approach to the projection boundary.

Synthesis.

Neutrinos mark the transition between physics described by local quantum fields on spacetime and the pre-geometric relational dynamics of χ. They constitute the structural frontier of emergent spacetime, where effective geometry, quantum description, and pre-geometric ontology converge.

4.10 Spectral Stability and the Lamb Shift

The stability of charged particle-like excitations is governed not only by topological admissibility but also by the fine spectral structure induced by the coupling between localized modes and the global relaxation flow. While the linear effective description predicts degenerate energy levels for certain atomic configurations, this degeneracy is lifted once non-linear saturation effects and projectability constraints are taken into account.

In standard QED, the Lamb shift arises from radiative corrections requiring renormalization. In Cosmochrony, no vacuum degrees of freedom are introduced. Atomic bound states correspond to admissible localized relaxation modes. S-states ($\ell = 0$) probe finer scales of the projection fiber where Born–Infeld saturation and spectral frustration are maximal, whereas P-states ($\ell = 1$) remain less sensitive to these inner-core constraints.

The effective Born–Infeld dynamics induces a finite upward shift of the S-state energy:

$$\Delta E_{\mathrm{Lamb}} \sim \kappa\, \alpha^5 m_e c^2, \tag{28}$$

where α is the dimensionless ratio between the local relaxation flux and the maximal saturation flux c_χ, and κ is a numerical factor of order unity. Numerically, $\alpha^5 m_e c^2 \simeq 10^{-5}\,\mathrm{eV}$, corresponding to a frequency shift of order 1 GHz, in agreement with the observed $2S_{1/2}$–$2P_{1/2}$ splitting. This correction is intrinsically finite thanks to the maximal relaxation speed c_χ.

Hyperfine Structure.

The same spectral-probe logic extends to hyperfine structure. When the electron occupies an S-state, its non-vanishing density at the nucleus brings electronic and nuclear torsional cores into spectral proximity. Hyperfine splitting reflects the relative alignment of torsional fluxes: parallel alignments accumulate frustration and oppose

relaxation, while antiparallel alignments partially compensate torsion. Together with the Lamb shift, hyperfine structure emerges as a finite spectral correction governed by Born–Infeld saturation at different relational scales.

4.11 Summary

Particles arise as stable, localized projected configurations that resist admissible relaxation ordering. Mass is identified with the degree of effective resistance to χ relaxation, naturally yielding $E = mc^2$ as a kinematic identity. Spin and statistical behavior originate from topological obstructions: fermionic configurations exhibit 4π periodicity, providing a unified origin for spin-$\frac{1}{2}$ behavior, fermionic antisymmetry, and the Pauli exclusion principle [24, 25]. Electric charge is interpreted as a chiral–torsional invariant of the relaxation flux. Residual spectral splittings—such as the Lamb shift and hyperfine structure—arise as finite corrections induced by non-linear saturation and projectability constraints.

5 The Projection Fiber and Gauge Emergence

The projection fiber Π is a central structural element linking the pre-geometric substrate χ to effective spacetime descriptions. It encodes the admissible equivalence classes and internal degrees of freedom through which relational configurations of χ can be consistently projected into geometric and field-like representations.

Gauge interactions do not arise from fundamental interaction fields. They emerge as symmetry structures of the projection process itself, under local re-identification of equivalent representatives along the fiber. This section develops the geometry of the projection fiber and clarifies how distinct classes of gauge phenomena naturally emerge from its structure.

5.1 The Geometry of the Π Subspace

The relational substrate χ is not accessed in its full structural complexity but through admissible local projections onto a reduced projection fiber $\Pi \cong S^3$. Here Π denotes the projection *fiber*, i.e. the space of admissible internal representatives associated with a projected configuration, not the projection map itself.

The identification $\Pi \cong S^3$ is not imposed *a priori* but follows from the minimal compact geometry (in dimension and connectivity) required to support non-injective yet stable projections. Its associated Hopf fibration naturally induces an effective $SU(2) \times U(1)$ symmetry structure, which emerges as an invariance of the projection process.

The metric on Π is dynamically induced by the local density of relational connections encoded in the underlying relational graph G, used as a numerical and representational support, not as a physical discretization. The mapping from the global graph Laplacian Δ_G to the effective projected Laplacian Δ_Π is

$$\Delta_\Pi = P^\dagger \Delta_G P, \tag{29}$$

where P denotes the projection operator onto the admissible spectral subspace. The smooth three-sphere geometry corresponds to a large-N spectral coarse-graining limit of the discrete relational structure.

5.2 Gauges as Relaxation Transmittance

Gauge interactions are reinterpreted as degrees of freedom of the relaxation flow within the projection fiber Π, encoding how locally admissible projections are coherently related despite non-injectivity.

- **Electromagnetism ($U(1)$):** Corresponds to the phase degree of freedom of the relaxation flow along the fibers of the Hopf fibration of $\Pi \cong S^3$. This emergent geometric parameter reflects the freedom to locally re-identify projected descriptions without altering global relational consistency. The fine-structure constant α characterizes the *transmittance* of the relaxation flow through the fiber: the stability of admissible projective re-identifications along the fiber.

- **Weak Interaction ($SU(2)$):** Emerges from the rotational degrees of freedom of the S^3 projection fiber itself. These encode non-abelian modes of relaxation transmittance, corresponding to shear-like distortions of admissible projections. The massive character of the $W^{\pm}$ and Z^0 bosons follows from a non-zero spectral gap associated with these modes, interpretable as spectral drag or torsion intrinsic to the fiber geometry.
- **Strong Interaction ($SU(3)$):** Associated with topological constraints arising from non-trivial winding structures of projected configurations. The effective $SU(3)$-like symmetry reflects the threefold (triality) structure of the minimal self-intersecting stable soliton, identified with the trefoil knot ($w = 3$). Color symmetry emerges as a geometric consequence of topological stability classes within the projection fiber.

5.3 Topological Constraints and Invariants

The stability of localized physical descriptions within Π is governed by the conservation of topological invariants. When an excitation of χ admits a closed, non-contractible configuration within Π, it forms a persistent topological obstruction to complete relaxation. Such configurations cannot be eliminated by smooth deformation without violating admissibility constraints.

These obstructions are described in terms of knot-like (non-contractible loop and self-linking) topological structures within the projection fiber. Once formed, they impose global constraints on the relaxation process and give rise to long-lived, localized projected configurations. Particles correspond to stable topological defects of the projection.

The winding number w constitutes the primary invariant characterizing these obstructions. It labels distinct equivalence classes of admissible projected configurations and plays a central role in the organization of the mass spectrum (Section **??**). The energetic cost required to maintain a non-trivial winding against the global pressure of relaxation is perceived, at the effective level, as rest energy (mc^2). Mass emerges as a spectral and topological consequence of persistent non-contractible structures within the projection fiber.

5.4 The Vacuum State as a Minimal Surface

In the absence of localized excitations, the projection fiber Π relaxes toward a configuration of minimal spectral tension: the smoothest admissible projected configuration compatible with global relaxation constraints. Geometrically, the vacuum corresponds to a minimal surface in a purely spectral sense (not a spatial embedding): curvature, torsion, and winding modes are simultaneously minimized within Π. In this state, the relaxation flow encounters no topological obstruction and propagates uniformly across the fiber. Any deviation—localized curvature, torsional distortion, or non-trivial winding—manifests as the presence of effective fields or particles.

The usual notion of field quantization is replaced by the quantization of admissible topological modes within a finite-volume projection fiber. Only a discrete set of deviations from the minimal surface is compatible with stability and projectability constraints, leading naturally to a discrete spectrum of excitations.

Vacuum energy is neither divergent nor arbitrary. It is intrinsically bounded by the spectral cutoff imposed by the relational graph underlying Π. The finiteness of vacuum energy reflects the finiteness of admissible spectral deformations of the minimal configuration, rather than the summation of zero-point energies of independent field modes.

Part III
Gravitation and Cosmology

6 Gravity as a Collective Effect of Particle Excitations

6.1 Local Slowdown of Relaxation Ordering

Gravitation emerges from the collective influence of localized projected configurations on admissible relaxation ordering. When particle-like configurations are present in significant number, their combined effect leads to a macroscopic reduction of the admissible ordering rate. In an effective spacetime parametrization, this may be expressed as

$$\mathcal{D}_{\text{eff}}\,\chi_{\text{eff}} \;\simeq\; c\,(1-\alpha\,\rho)\,, \tag{30}$$

where ρ denotes the effective density of localized projected configurations and α encodes their average contribution to relaxation resistance. This first-order approximation is valid when localized constraints are dilute and weakly overlapping.

The coupling parameter α is emergent and scales as $\alpha \propto G/c^2$ in terms of effective inertial mass densities. The collective slowdown manifests as gravitational time dilation and curvature effects, without introducing any independent gravitational force or mediator.

6.2 Collective Gravitational Coupling and Operational Geometry

The collective reduction of admissible relaxation ordering modulates how efficiently structural variations can be correlated between different effective locations. In regions where projected descriptions are nearly homogeneous, the effective coupling approaches a uniform value; localized configurations weaken it by introducing structural constraints.

Spatial separation is defined operationally: two effective regions are close if structural variations can be efficiently correlated between them. In the continuum and weak-constraint regime, this operational notion admits a compact description in terms of an effective spatial metric summarizing the collective response to relative variations. Spacetime curvature emerges as a descriptive manifestation of how localized configurations modulate collective ordering and correlation structure.

A more explicit relational construction of the coupling mechanism is presented in Appendix D.1.

6.3 Emergent Curvature

Spatial variations in admissible relaxation ordering lead to non-uniform correlation patterns within projected descriptions. When a smooth geometric parametrization is applicable, these non-uniformities are summarized by gradients of an emergent metric structure, reproducing the phenomenology traditionally attributed to curved spacetime: gravitational time dilation, geodesic deviation, and lensing effects.

Einstein's Equations as a Structural Equilibrium Principle.

When projected configurations admit a smooth, locally injective geometric description, their collective structural constraints can be summarized by an effective metric $g_{\mu\nu}$. Einstein's equations emerge *necessarily* as the unique consistency condition relating curvature to the effective distribution of relaxation-resistant configurations. The Einstein

tensor encodes a geometric identity constraining admissible macroscopic descriptions; the stress–energy tensor summarizes how localized configurations resist relaxation ordering. Einstein's equations therefore express a balance condition between geometry and physical structure.

This interpretation explains the extraordinary universality of general relativity: as long as a smooth spacetime description exists and relaxation ordering is monotonic, bounded, and weakly inhomogeneous, the same geometric relations must hold, independently of the microscopic nature of the underlying substrate. General relativity thus plays a role analogous to thermodynamics—exact within its domain, silent outside it.

When projection ceases to be locally injective, Einstein's equations do not break down; they simply no longer apply, because the concept of spacetime has not yet emerged.

6.4 Recovery of the Schwarzschild Metric

For a static, approximately spherically symmetric distribution of localized projected configurations, the collective reduction of admissible relaxation ordering admits a simple effective description.

Operational potential from χ-relaxation slowdown.

The dimensionless lapse-like factor is

$$N(r) \;\equiv\; \frac{D^{\chi}_{\mathrm{loc}}(r)}{D^{\chi}_{0}}, \qquad 0 < N(r) \leq 1, \tag{31}$$

with the weak-field identification

$$\frac{D^{\chi}_{\mathrm{loc}}}{D^{\chi}_{0}} \;\simeq\; 1 + \frac{\Phi}{c^2}, \qquad \left|\frac{\Phi}{c^2}\right| \ll 1. \tag{32}$$

Poisson-like equation and exterior solution.

In the weak-structure regime:

$$\nabla^2 \Phi \;\simeq\; 4\pi G_{\mathrm{eff}}\, \rho, \tag{33}$$

yielding, for an isolated spherical source of mass M:

$$\Phi(r) \;\simeq\; -\frac{G_{\mathrm{eff}} M}{r}. \tag{34}$$

Metric components from Φ.

The static spherically symmetric ansatz reads

$$ds^2 = -N(r)^2 c^2 dt^2 + N(r)^{-2} dr^2 + r^2 d\Omega^2. \tag{35}$$

In the weak-field limit:

$$g_{tt} \simeq -\left(1 + 2\frac{\Phi}{c^2}\right), \tag{36}$$

$$g_{rr} \simeq \left(1 + 2\frac{\Phi}{c^2}\right)^{-1} \simeq 1 - 2\frac{\Phi}{c^2}, \tag{37}$$

coinciding with the standard Schwarzschild weak-field expansion:

$$g_{tt} \simeq -\left(1 - \frac{2G_{\text{eff}}M}{c^2 r}\right), \quad g_{rr} \simeq \left(1 - \frac{2G_{\text{eff}}M}{c^2 r}\right)^{-1}. \tag{38}$$

Comparison to classic observational tests.
Gravitational redshift follows directly from g_{tt}:

$$\frac{\nu_{\text{obs}}}{\nu_{\text{emit}}} \simeq 1 + \frac{\Phi(r_{\text{emit}}) - \Phi(r_{\text{obs}})}{c^2}. \tag{39}$$

Light deflection yields the standard angle

$$\alpha \simeq \frac{4G_{\text{eff}}M}{bc^2}, \tag{40}$$

with b the impact parameter.

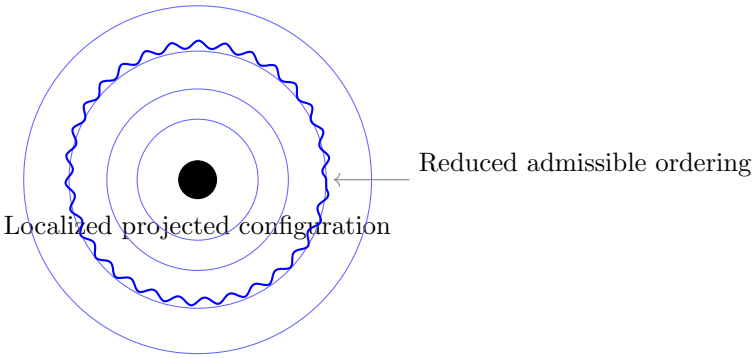

Fig. 5 Emergence of Schwarzschild-like behavior. A localized projected configuration induces a spatially varying reduction of admissible relaxation ordering, manifesting as differential proper-time accumulation and emergent metric curvature.

6.5 Equivalence Principle

All admissible localized projected configurations constrain relaxation ordering in the same universal manner. Their internal composition plays no role in how they affect or respond to the admissible ordering environment. Inertial resistance and gravitational

response are two effective manifestations of the same underlying constraint, and the equivalence principle arises as an emergent symmetry of admissible projected descriptions.

6.6 Gravitational Waves

Time-dependent variations in the distribution of localized projected configurations induce collective and transient modulations of admissible relaxation ordering. These modulations propagate at the maximal admissible ordering speed c and are described, in an effective spacetime language, as gravitational waves. Unlike electromagnetic radiation, they represent collective variations of the admissible ordering and correlation structure itself.

The standard properties—propagation at speed c, transverse polarization, and energy transport—are recovered as effective features of collective ordering dynamics. Gravitational-wave descriptions remain valid only within regimes where projection onto an effective spacetime remains well defined; in strong-gravity environments approaching the deprojection threshold (Section 6.7), such modulations may become attenuated or lose a clear spacetime interpretation.

6.7 Strong Gravity and Black Holes

Projectable	$\rightarrow$	**Horizon**	$\rightarrow$	**Non-projectable**
Gravitational Waves		Boundary of Projection		Deprojected Regime
Effective Modulations		Π non-injective		No spacetime Representation

Fig. 6 Conceptual regimes of projection in Cosmochrony. Black holes mark the boundary beyond which spacetime representations cease to be injective.

In regions of sufficiently high density of localized projected configurations, admissible relaxation ordering becomes strongly constrained, defining an effective horizon. Black holes correspond to domains where physical processes become asymptotically inaccessible due to the loss of injectivity of spacetime projection. This naturally accounts for extreme time dilation without requiring divergent curvature invariants.

Because admissible ordering is bounded, configurations corresponding to infinite curvature or density cannot be physically realized. Apparent singularities signal the breakdown of spacetime representability, not genuine divergences of the underlying relational structure.

Black Holes, Deprojection, and Vacuum Reprojection

In strong-gravity regimes, the projection $\Pi : \mathcal{C}_{\text{rel}} \longrightarrow \mathcal{M}$ loses injectivity: multiple inequivalent relational configurations correspond to the same effective spacetime event. This *deprojection* does not destroy information. Relational information ceases to be

expressible in spatiotemporal form but remains encoded structurally and is in principle reprojectable once projectability is restored. Reprojection manifests as radiation-like excitations or particle–antiparticle pairs.

Black Hole Entropy as Relaxation Saturation

Black hole entropy measures the saturation of relaxation capacity at the horizon. Near the boundary where the effective temporal ordering ceases to be resolvable, a large multiplicity of distinct χ micro-configurations become indistinguishable at the level of the effective metric:

$$S_{\mathrm{BH}} \;\sim\; \log \left|\Pi^{-1}(g_H)\right|, \tag{41}$$

where g_H denotes the saturated horizon geometry. The area law follows from the fact that saturation occurs at the boundary between projectable and non-projectable regimes. Hawking thermality arises from the coarse-grained statistics of discrete reprojection events at the saturation interface.

The numerical factor $1/4$ in $S = A/4$ arises from the fourfold degeneracy in the stability spectrum of χ excitations, linked to the intrinsic 4π periodicity discussed in Section 4.2.

6.8 Black Hole Evaporation and the Information Problem

Black hole evaporation is an effective process arising from the gradual restoration of projectability near the boundary separating projectable and non-projectable domains. The apparent information loss identified by Hawking [26] arises from applying a spacetime-based description beyond its domain of validity. In Cosmochrony, information is encoded in the global relational configuration independently of its spacetime projection.

Horizon Reprojection Equation

The energy flux emerging from the horizon is a sum over discrete reprojection events:

$$\Phi_\chi \equiv \frac{dE}{dt} = \sum_k \delta(t - t_k)\, \hbar_\chi\, \nu_k(L_{\mathrm{sol}}).$$

Here $\hbar_\chi$ is the fundamental quantum of reprojection, the $\nu_k(L_{\mathrm{sol}})$ are resonance frequencies of the stability operator at the horizon, and t_k label the instants at which local configurations reach the projection threshold.

Emergent Temperature and Relaxation Gradient

The apparent Hawking temperature is determined by the gradient of effective χ relaxation normal to the horizon:

$$k_B T_\chi = \frac{\hbar_\chi c}{2\pi}\, \left|\nabla_\perp \chi_{\mathrm{eff}}\right|_H .$$

For more massive black holes, the relaxation gradient is distributed over a larger area, reducing the frequency of reprojection events and explaining the inverse mass–temperature relation without invoking vacuum particle creation.

Information Conservation and Spectral Encoding

During deprojection, information is stored in the nonlinear degrees of freedom of χ within the projection fiber. During reprojection, each emitted quantum carries the spectral imprint of the eigenmodes governing the χ configuration, ensuring global information conservation.

Entropy as a Projection Saturation Limit

The Bekenstein–Hawking area law

$$S = \frac{A}{4} \tag{42}$$

is reinterpreted as the informational capacity of the projection map at the horizon boundary. Entropy quantifies hidden relational structure—the structural multiplicity of χ configurations no longer distinguishable at the metric level—rather than thermal ignorance.

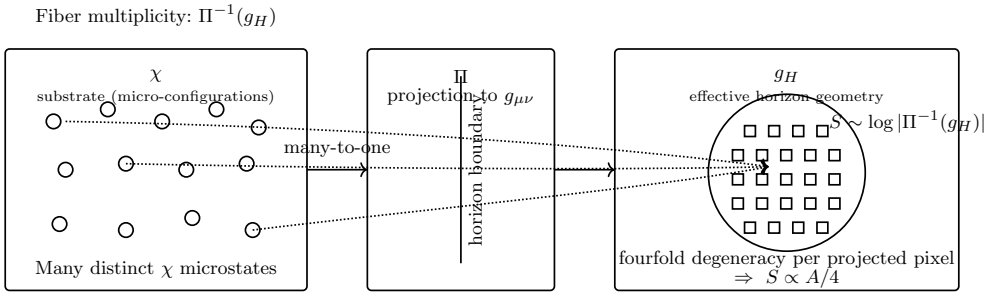

Fig. 7 Saturation of the projection map at the horizon. Multiple micro-configurations of χ collapse onto the same effective horizon geometry g_H. Entropy measures the structural multiplicity of the fiber $\Pi^{-1}(g_H)$.

Prediction: Spectral Granularity

If Hawking radiation is fundamentally discrete, it cannot be a perfect black-body continuum. The spectral line width of a reprojected quantum is

$$\Delta\nu_k \approx \frac{1}{\tau_\chi}\sqrt{\alpha}\,\ln(Q), \tag{43}$$

where τ_χ is the characteristic relaxation time near the horizon, $\alpha \simeq 3 \times 10^{-7}$ is the spectral packing fraction, and Q is the topological charge of the emitted configuration.

The ratio between line width and line spacing is universally governed by α:

$$\frac{\Delta\nu}{\delta\nu} \propto \alpha. \tag{44}$$

Observational Prospects

In the late stages of evaporation, the spectral spacing may enter the sensitivity bands of next-generation interferometers (LISA, Einstein Telescope). The universal relation $\Delta\nu/\delta\nu \simeq \alpha$ should also apply to analogue gravity systems, where current experiments in Bose–Einstein condensates approach the required spectral resolution ($\delta f/f \sim 10^{-5}$), making near-term tests feasible.

6.9 Unified Origin of Gravitational and Electromagnetic Effects

Gravitational and electromagnetic phenomena arise as complementary effective manifestations of the same relational substrate. Gravitational effects correspond to sustained, quasi-static constraints on admissible relaxation ordering induced by persistent localized configurations. Electromagnetic phenomena arise from time-dependent, phase-structured patterns within admissible projected descriptions, admitting an effective formulation in terms of propagating oscillatory modes. The familiar distinction between the two interactions emerges at the level of effective descriptions rather than from fundamentally separate fields.

An explicit derivation of Maxwell-like equations within the Cosmochrony framework is provided in Appendix A.11.

6.10 Effective Gravitational Lensing

In the weak-field and thin-lens regimes, the lens equation is

$$\boldsymbol{\beta} = \boldsymbol{\theta} - \frac{D_{ls}}{D_s}\,\nabla_{\boldsymbol{\theta}}\psi(\boldsymbol{\theta}), \tag{45}$$

with the lensing potential

$$\psi(\boldsymbol{\theta}) = \frac{2D_{ls}}{c^2 D_l D_s}\int \Phi_{\rm eff}(D_l\boldsymbol{\theta}, z)\; dz. \tag{46}$$

The effective potential $\Phi_{\rm eff}$ is a geometric descriptor encoding collective constraints of the projected χ-substrate. All observable lensing quantities (convergence, shear, magnification, caustics) follow in the usual way. No additional dark matter component is required: lensing directly probes the emergent geometry.

6.11 Summary

Gravity emerges as a macroscopic consequence of localized projected configurations collectively constraining admissible relaxation ordering. Classical gravitational

phenomena—time dilation, curvature, gravitational waves, and black holes—are recovered as distinct descriptive regimes of this collective constraint. In extreme regimes, the spectral structure of horizon-associated phenomena encodes direct information about the relaxation dynamics and projection topology of the underlying substrate.

7 Cosmological Implications

7.1 The Big Bang as a Maximal Constraint Regime of the χ Substrate

The Big Bang is interpreted as the boundary of applicability of effective spacetime descriptions. In this regime, the density of structural and topological constraints within χ exceeds the threshold required for stable geometric projection: effective notions of spatial distance, temporal duration, and causal ordering cease to be well-defined. The apparent singular behavior of standard cosmological models reflects the extrapolation of geometric descriptions beyond their domain of validity.

Cosmological evolution is therefore described as the progressive relaxation of this maximal constraint regime. The Big Bang marks not the origin of spacetime, but the transition beyond which spacetime becomes an appropriate effective framework. The arrow of time arises from the intrinsic monotonic ordering of χ configurations (Section 2.6).

7.2 Cosmological Cycles of Constraint and Reprojection

The maximally constrained regime is not confined to the early universe. It may be locally reapproached whenever structural constraints saturate, most notably in black holes. Deprojection does not destroy information but renders it inaccessible to spacetime descriptions. Reprojection is the restoration of descriptive projectability once relational consistency conditions are satisfied.

Phenomena commonly associated with the quantum vacuum reflect the persistent presence of reprojectable relational structures within χ. The vacuum represents a regime of minimal yet non-vanishing projectability. Cosmological evolution involves a continuous interplay between global relaxation, local reconfinement, deprojection, and reprojection across scales.

7.3 Cosmic Expansion Without Inflation

In standard cosmology, an inflationary phase resolves the horizon problem [27, 28]. In Cosmochrony, large-scale homogeneity and isotropy reflect the global relational coherence of the χ substrate in the maximally constrained regime, rather than the outcome of a rapid expansion of spacetime. Prior to the emergence of a stable geometric projection, notions such as distance, light cones, and causal disconnection are undefined. The horizon problem therefore does not arise.

7.4 Cosmic Expansion as χ Relaxation

Cosmic expansion reflects the progressive relaxation of the relational substrate [29]. As the ordering parameter increases monotonically, projected descriptions admit an ever broader range of mutually distinguishable relational configurations. Expansion is not driven by an external energy component but is an intrinsic consequence of the relaxation ordering. Localized matter configurations act as persistent structural

constraints, leading to spatially inhomogeneous unfolding that later manifests as large-scale structure.

7.5 Emergent Hubble Law

In homogeneous regimes, the relaxation ordering is uniform and admits the linear representation

$$\chi(t) = \chi_0 + c\,t. \tag{47}$$

Identifying effective spatial scales with accumulated relational differentiation yields a Hubble-like law [30, 31] with

$$H(t) \equiv \frac{1}{\chi}\,\frac{d\chi}{dt}, \tag{48}$$

where H_0 quantifies the current state of global relaxation.

Observational discriminant: Cosmochrony predicts a $\sim 5\%$ higher $H(z)$ at $z \sim 1$ compared to ΛCDM, testable with DESI/Euclid (Section **??**).

Cosmic Acceleration Without Dark Energy.

The observed late-time acceleration does not require a cosmological constant. As structure formation proceeds, localized configurations increasingly constrain local relaxation, introducing growing spatial inhomogeneities. When interpreted within homogeneous and isotropic models, these inhomogeneities manifest as apparent acceleration. Cosmic acceleration is an emergent interpretative effect arising from progressively uneven relaxation across cosmic scales.

7.6 Cosmic Microwave Background

The CMB reflects the imprint of early relaxation and reprojection processes as the substrate transitioned toward a regime admitting stable geometric descriptions. Large-scale correlations arise from the global relational coherence of χ prior to geometric differentiation, rather than from superluminal expansion. Acoustic features are interpreted as resonance patterns arising once the standard photon–baryon plasma description becomes applicable [32–34].

Effective closure: primordial spectrum.

The standard Boltzmann transfer functions remain unchanged. Cosmochrony modifies the CMB spectra only through the primordial curvature spectrum:

$$C_\ell^{XY} = 4\pi \int_0^\infty \frac{dk}{k}\, P_\zeta(k)\, \Delta_\ell^X(k)\, \Delta_\ell^Y(k), \tag{49}$$

with a projectability-induced infrared filter and emergent tilt:

$$P_\zeta(k) = A_s \left(\frac{k}{k_*}\right)^{n_\chi - 1} C^2\!\left(\frac{k}{k_p}\right), \qquad C(x) \xrightarrow{x\ll 1} 0, \quad C(x) \xrightarrow{x\gg 1} 1. \tag{50}$$

Relational spectral scales and angular multipoles.

The admissibility cutoff can be expressed in terms of the low-lying spectrum of the relational operator L_χ (Section 2.4):

$$k_n \;\propto\; \sqrt{\lambda_n(\lambda_*)}, \qquad \ell_n \;\approx\; k_n\, D_A(z_*), \tag{51}$$

yielding the robust ratio constraint

$$\frac{\ell_n}{\ell_1} \;\approx\; \sqrt{\frac{\lambda_n}{\lambda_1}}. \tag{52}$$

Numerical relaxation experiments (Appendix D.7) indicate $\lambda_2/\lambda_1 \simeq 8/3$, implying $\ell_2/\ell_1 \approx 1.63$, searchable as a scale-independent modulation signature in the low-ℓ sector. These ℓ_n characterize relational angular modulations associated with admissibility, not the acoustic peak indices of the photon–baryon plasma.

7.7 Dark Matter as Residual Relaxation Effects

Dark matter phenomena correspond to configurations of χ that resist relaxation while failing the projectability conditions required for Standard Model interactions. These **non-projected spectral modes** possess inertial mass and contribute to gravitational curvature while remaining invisible to electromagnetic or electroweak probes.

Galactic Rotation and Effective Spectral Stiffness.

The flattening of rotation curves is interpreted as a spatial variation of G_{eff} induced by the local relaxation state. At large radii, a transition in the effective spectral stiffness leads to a logarithmic gravitational potential, reproducing MOND-like behavior without invoking a modification of gravity or a universal acceleration scale. Unlike the universal constant a_0 in MOND, the transition threshold $\mathcal{K}_c$ is local and environment-dependent, naturally explaining the observed variation of the apparent dark matter fraction among galaxies.

Gravitational Lensing and Substrate Memory.

Lensing phenomena (e.g. the Bullet Cluster) are manifestations of **relaxation lag**: the projective geometry associated with mass-solitons persists after baryonic gas has lost coherence. Light deflection is treated as effective refraction within the spectral gradient of the projected χ geometry.

Predictive Distinction from Particulate Dark Matter.

Cosmochrony predicts non-local correlations between gravitational mass discrepancies and the global spectral age of a system, the absence of sharp central cusps, a minimum smoothing scale imposed by the spectral response, and **spectral echoes**—faint gravitational signatures in regions where matter was previously present.

7.8 Entropy and the Arrow of Time

The arrow of time is a fundamental structural feature arising from the intrinsic monotonic relaxation ordering of χ, not a derived statistical phenomenon. Entropy increase emerges only at the level of effective spacetime descriptions, providing a statistical summary of how macroscopic degrees of freedom evolve under the irreversible relaxation of χ. Entropy growth does not explain the arrow of time; it reflects the underlying temporal asymmetry already present in the substrate.

This reverses the standard explanatory hierarchy: time asymmetry is imposed intrinsically by the relaxation structure, not attributed to special initial conditions. Processes involving deprojection do not correspond to entropy decrease or temporal reversal but represent a transition to a level of description where thermodynamic notions no longer apply.

7.9 Cosmic Voids as Maximal Relaxation Probes

Cosmic voids are regions where the relaxation of χ is least frustrated by localized excitations. Within the effective description (Section 3.4), near-maximal substrate relaxation produces enhanced geodesic defocusing, leading to a negative gravitational lensing signal and non-linear peculiar velocity outflows at void boundaries—effects absent or suppressed in ΛCDM.

Connection to local H_0 determinations.

Enhanced outward peculiar velocities at void boundaries can bias low-redshift distance–redshift inferences toward higher locally inferred expansion rates. A decisive test is the cross-correlation between void lensing profiles and locally inferred H_0 maps.

Phenomenological void parametrization.

Observable void signals are modeled as a ΛCDM baseline plus a saturating correction controlled by a single dimensionless amplitude $\beta_{\rm void}$:

$$\kappa_{\rm obs}(R) = \kappa_{\Lambda\rm CDM}(R)\left[1 + \beta_{\rm void}\,\mathcal{S}\big(\mathcal{A}(R)\big)\right], \tag{53}$$

$$v_{\rm obs}(r) = v_{\Lambda\rm CDM}(r)\left[1 + \beta_{\rm void}\,\mathcal{S}\big(\mathcal{B}(r)\big)\right], \tag{54}$$

with $\mathcal{S}(x) = x/\sqrt{1+x^2}$ interpolating between linear and saturated regimes.

7.10 The Hubble Tension

The discrepancy between early- and late-universe determinations of H_0 is well established [34–37]. In Cosmochrony, different observational probes access different regimes of effective projectability. Early-universe measurements probe a regime close to the transition from maximal constraint to geometric projectability; late-time measurements probe a more weakly constrained regime where effective spacetime descriptions are more fully developed. The tension arises from using a single spacetime-based parametrization to describe observations sampling distinct stages of relational relaxation.

The Hubble Tension as a Diagnostic of Topological Decoherence

The effective Hubble parameter may be expressed as

$$H_{\text{eff}}(\mathbf{x}, t) \sim \frac{1}{\tau_\chi(\mathbf{x}, t)}, \tag{55}$$

where τ_χ is an effective relaxation timescale. Regions of high structural complexity (clusters, filaments) correspond to topologically frustrated configurations in which the relaxation timescale acquires a spatial dependence:

$$\tau_\chi(\mathbf{x}) = \tau_\chi^{(0)} \left[1 + \epsilon\, \mathcal{T}(\mathbf{x})\right], \tag{56}$$

where $\mathcal{T}(\mathbf{x})$ encodes local topological density. The tension reflects a non-commutativity between cosmological averaging and local projection.

Cosmochrony predicts that locally inferred values of H_0 should exhibit weak but systematic correlations with the surrounding topological environment. Quantitative estimates are provided in Section 11.1 and Appendix C.3.

7.11 Large-Angle Temperature Anomalies

Large-angle CMB anomalies—low-multipole power suppression and unexpected large-scale alignments—remain only partially explained within ΛCDM [38]. In Cosmochrony, these features are residual relational correlations inherited from the pre-geometric regime of χ.

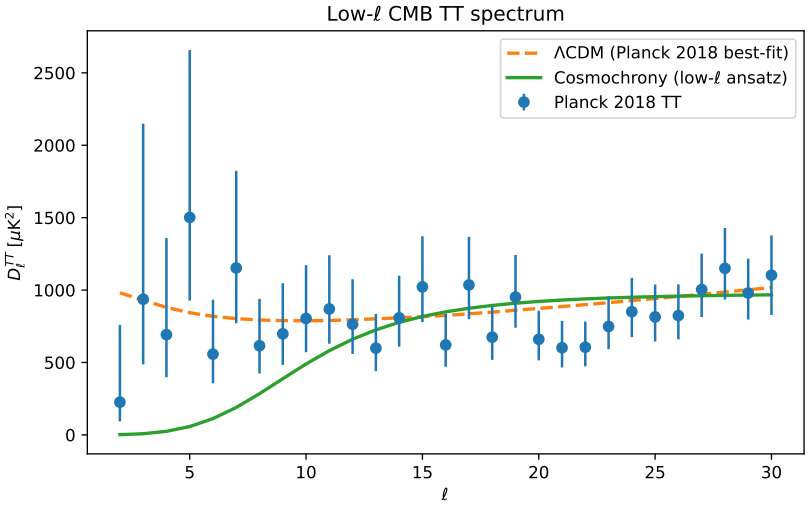

Fig. 8 Low-ℓ CMB TT power spectrum comparison. The Cosmochrony ansatz (green) shows natural suppression of power at large angular scales ($\ell < 10$) compared to ΛCDM (dashed orange).

Structural Admissibility and Low-ℓ Suppression

The primordial spectrum is modulated by an admissibility filter:

$$P_{\rm obs}(k,t) = \mathcal{A}^2(k,t)\, P_0(k), \tag{57}$$

with a natural phenomenological form

$$\mathcal{A}(k,t) = \exp\left[-\left(\frac{k_c(t)}{k}\right)^p\right], \tag{58}$$

where $k_c(t)$ is the coherence scale associated with the maximal size of projectively admissible configurations. For $k \ll k_c(t)$, power suppression arises from the structural impossibility of supporting such global modes within the available relational complexity. The scale $k_c(t)$ admits a graph-theoretic interpretation through the spectral gap $\lambda_2(t)$ of the effective connectivity graph.

Testable Predictions

A. Correlated Suppression Across TT, TE, and EE Spectra.

The coherence scale k_c should be consistent across temperature and polarization spectra. Future high-precision measurements (e.g. *LiteBIRD*) provide a decisive test.

B. Absence of Primordial Non-Gaussianities.

The framework predicts an exceptionally small $f_{\rm NL}$. A significant detection would falsify this scenario.

C. Scale-Dependent Spectral Tilt Near the Cutoff.

A mild running of n_s localized near k_c is expected. A detailed treatment is provided in Appendix C.1.

7.12 Effective Potential for Galactic Dynamics from χ-Relaxation Saturation

Operational status.

The effective potential is defined only through observable kinematics:

$$g_{\rm eff}(r) \equiv -\frac{d\Phi_{\rm eff}}{dr}, \qquad v^2(r) = r\,\frac{d\Phi_{\rm eff}}{dr}. \tag{59}$$

Emergent acceleration scale.

The nonlinear χ-relaxation constraint induces an effective background kinematic scale

$$a_0(t) \sim c\,H(t), \tag{60}$$

weakly time-dependent, with a projection efficiency factor $\eta = O(0.1)$ for galactic dynamics.

Aspect	ΛCDM	MOND	Cosmochrony
Ontology	Non-baryonic halo	Modified dynamics	Relaxation properties of χ
Flat rotation curves	Invisible mass	$g \simeq \sqrt{g_N a_0}$	Saturation: $g \simeq \sqrt{g_N a_0(t)}$
Key scale	Halo profile parameters	Universal a_0	Emergent $a_0(t) \sim cH(t)$
Tully–Fisher	Formation models	$v^4 \propto GM_b a_0$	$v^4 \propto GM_b a_0(t)$
Discriminating signature	Cusps vs. cores	Strict universality	Slow evolution of $a_0(t)$

Table 1 Conceptual comparison of flat-rotation-curve explanations.

Asymptotic regimes and flat rotation curves.

Let $g_N(r) = GM_b(r)/r^2$. In the high-acceleration regime ($g_N \gg a_0$), $g_{\rm eff} \simeq g_N$. In the low-acceleration regime ($g_N \ll a_0$), saturation yields

$$g_{\rm eff}(r) \simeq \sqrt{g_N(r)\, a_0(t)}, \tag{61}$$

implying

$$\Phi_{\rm eff}(r) \simeq \sqrt{GM_b\, a_0(t)}\, \ln\!\left(\frac{r}{r_s}\right) + \text{const.}, \tag{62}$$

a logarithmic potential producing asymptotically flat rotation curves. The transition radius is $r_s(t) = \sqrt{GM_b/a_0(t)}$.

Minimal smooth interpolation.

A parsimonious operational fit function is

$$g_{\rm eff}(r) = \sqrt{g_N(r)^2 + a_0(t)\, g_N(r)}. \tag{63}$$

Baryonic Tully–Fisher scaling.

In the deep-saturation regime:

$$v_\infty^4 \simeq G\, M_b\, a_0(t), \tag{64}$$

with a mild redshift dependence through $a_0(t) \sim cH(t)$.

Observed rotation curves: multi-galaxy test

The Cosmochrony prediction is confronted with observed rotation curves of NGC 3198 (flat), NGC 2403 (rising), and NGC 5055 (mildly declining). No dark matter halo is introduced. Baryonic contributions are taken from the literature; the only fitted parameter is the stellar mass-to-light ratio $\Upsilon_\star$. The acceleration scale is fixed by $a_0(t_0) \sim cH(t_0)$.

7.13 Summary

Cosmological phenomena emerge from the global relaxation ordering of χ. Cosmic expansion, large-scale homogeneity, late-time acceleration, and the arrow of time

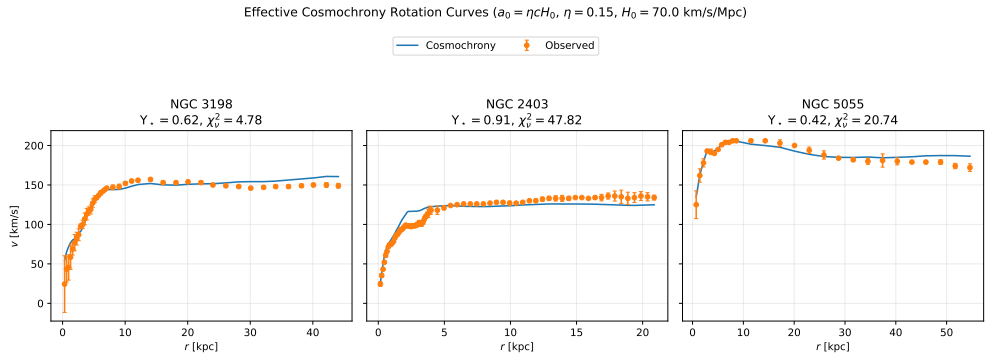

Fig. 9 Observed rotation curves compared with the Cosmochrony saturation prediction. Left: NGC 3198. Center: NGC 2403. Right: NGC 5055. See Appendix D.8 for data sources.

arise naturally from the relaxation process, without invoking an inflationary phase, dark energy, or an initial spacetime singularity. The Big Bang is a limiting regime of maximal constraint; black holes represent localized reapproaches to the same descriptive boundary. At the effective level, the framework reproduces the Hubble law, CMB structure, and large-scale gravitational behavior as emergent consequences of a single relational relaxation process.

Part IV
Quantum Mechanics

8 Quantum Phenomena and Entanglement

Building on the non-injectivity of the projection Π (Section 2.4), this section shows how entanglement, nonlocal correlations, measurement statistics, and the formal apparatus of quantum mechanics emerge without introducing additional ontological degrees of freedom. The framework adopts **ontological monism**: there is a single ontological substrate χ, while apparent multiplicity and spatial separation are properties of the projected description.

8.1 Non-Factorizable Projected Descriptions and Quantum Correlations

A single admissible configuration of χ may correspond to multiple distinct effective degrees of freedom. What appear as separate particles or subsystems are multiple projective manifestations of a single underlying ontological configuration. Effective degrees of freedom cannot be assigned independent states; any admissible description must be globally consistent with the underlying χ configuration, leading to persistent correlations that do not rely on signal exchange or spacetime proximity.

Ontological Monism and the Shared Projection Hypothesis

A single connected excitation in χ can be represented as several spatially separated effective excitations. The observed separation is a property of the projected metric representation, not a fundamental separation of the underlying entity.

Shared Fiber Phase and Spin Correlations.

Spin correlations can be read as correlations of a *shared* internal degree of freedom of the projection fiber. A measurement at one location selects a locally stable reprojection of that shared fiber degree of freedom; the correlated statistics at the distant location reflect the restricted set of reprojections still compatible with the same underlying configuration.

8.2 Nonlocality and the Holistic Character of Projected Descriptions

Quantum nonlocality does not arise from superluminal interactions but reflects the intrinsically non-factorizable character of certain admissible projected descriptions [39]. Entangled systems correspond to single projected configurations that cannot be decomposed into independent subsystems without loss of admissibility.

8.3 Nonlocal Correlations Without Superluminality

Correlated outcomes arise because spacelike separated measurements correspond to different local reprojections of a single non-factorizable description. The factorization assumptions underlying Bell-type inequalities are violated, while dynamical locality and relativistic causality remain intact (see Appendix **??**). The correlations are *ontological*—fixed by the non-injective global relational structure—rather than *dynamical*.

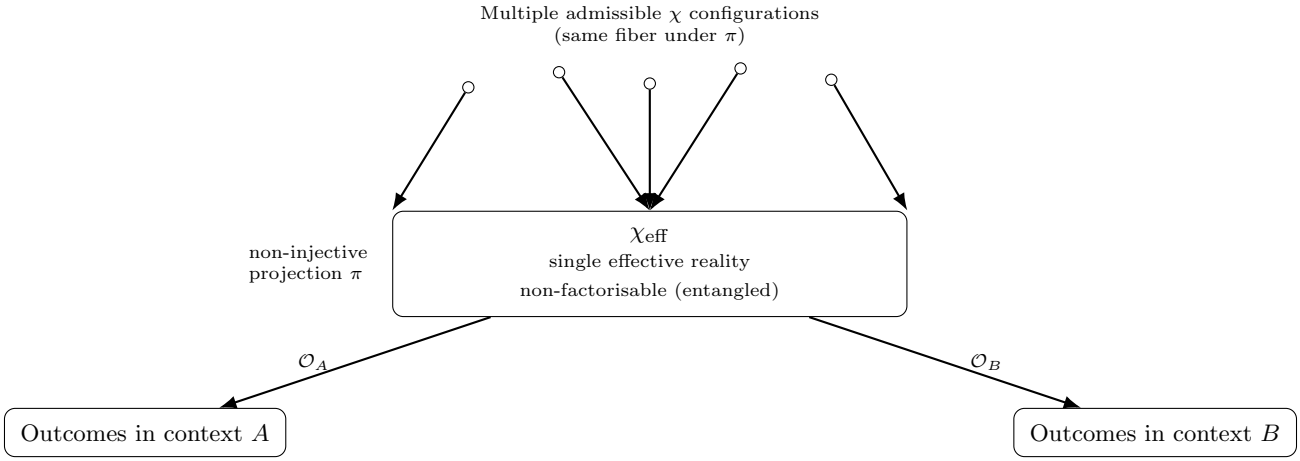

Fig. 10 Entangled (non-factorisable) regime. Multiple underlying χ configurations map to the same χ_{eff}. Different measurement contexts define distinct operational projections producing correlated outcomes without introducing multiple effective realities.

Attosecond-resolved measurements have demonstrated that quantum correlations become experimentally accessible on timescales far shorter than any interaction-based mechanism [40]. Within Cosmochrony, the observed timescale corresponds to the resolution time of the effective projection Π, not to a physical propagation time: it probes projective accessibility rather than dynamical formation of correlations.

8.4 Temporal Ordering and Relativistic Consistency

Temporal ordering arises only at the effective level. Different observers may assign different orderings to spacelike separated events; such differences reflect observer-dependence of spacetime slicing and have no impact on the relational consistency of admissible descriptions. Relativistic covariance is preserved by the invariance of the underlying non-injective relational configuration across all admissible projected descriptions.

8.5 Relation to Bell Inequalities

Bell's theorem [39] rules out any ontological completion of quantum mechanics based on factorizable hidden-variable models. Cosmochrony fully accepts Bell's theorem and identifies the ontological assumption that fails: the factorization hypothesis $P(a, b|x, y, \lambda) = P(a|x, \lambda)\, P(b|y, \lambda)$.

Because the projection Π is generically non-injective, admissible projected states are not associated with independent ontic pre-images for their subsystems. The factorization hypothesis is not merely violated but *ill-defined* within the space of admissible projected descriptions.

Bell-type violations arise in an intermediate regime of projective compression: the effective description is sufficiently coarse-grained to permit subsystem separation, yet

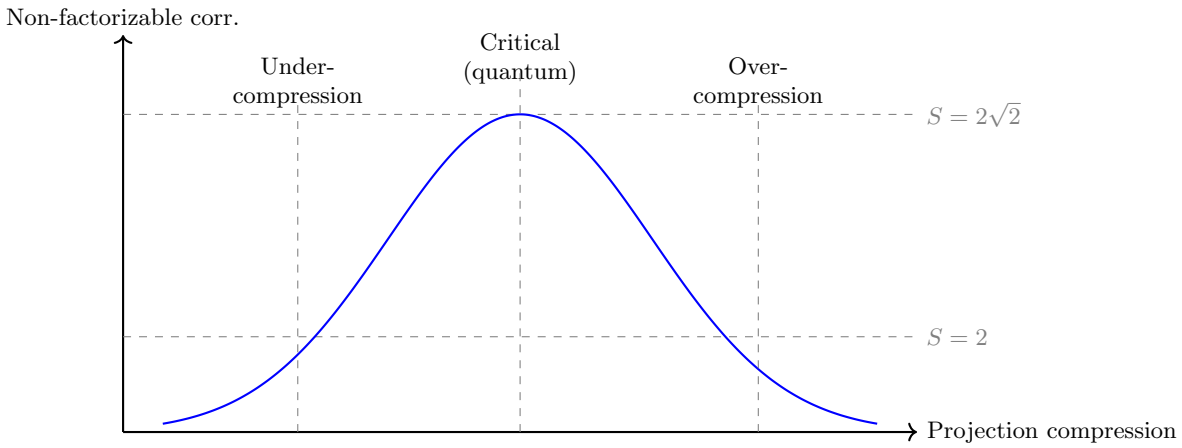

Fig. 11 Bell inequality violations as a function of the compression induced by Π. Non-factorizable correlations emerge in an intermediate regime.

retains enough global relational structure to prevent factorization. In the limit of extreme coarse-graining, projected descriptions become effectively classical.

No hidden variables and no superluminal influence are introduced. Quantum nonlocality is ontological rather than dynamical: the failure of Bell-type factorizability arises from the structure of admissible projected descriptions, not from nonlocal interaction.

8.6 Measurement, Decoherence, and Apparent Collapse

Quantum measurement does not involve fundamental wavefunction collapse. Measurement corresponds to the transition from a non-factorizable admissible projected description to a set of effectively factorized local projections. Decoherence suppresses interference between incompatible descriptive branches by rendering their relative phase information inaccessible within spacetime representations [41]. The underlying relational structure remains globally well defined. The apparent collapse is the effective manifestation of a non-injective relational structure becoming only partially projectable into spacetime.

8.7 Limits of Entanglement and Environmental Effects

Entanglement arises only within restricted regimes in which a non-factorizable global description remains jointly projectable. Environmental coupling progressively restricts the set of admissible projected descriptions to locally stable, approximately factorizable regimes. Entanglement is most robust for effectively isolated systems and becomes increasingly fragile in macroscopic environments. Classical behavior emerges when only factorized projected descriptions remain admissible, without requiring any modification of the underlying relational structure.

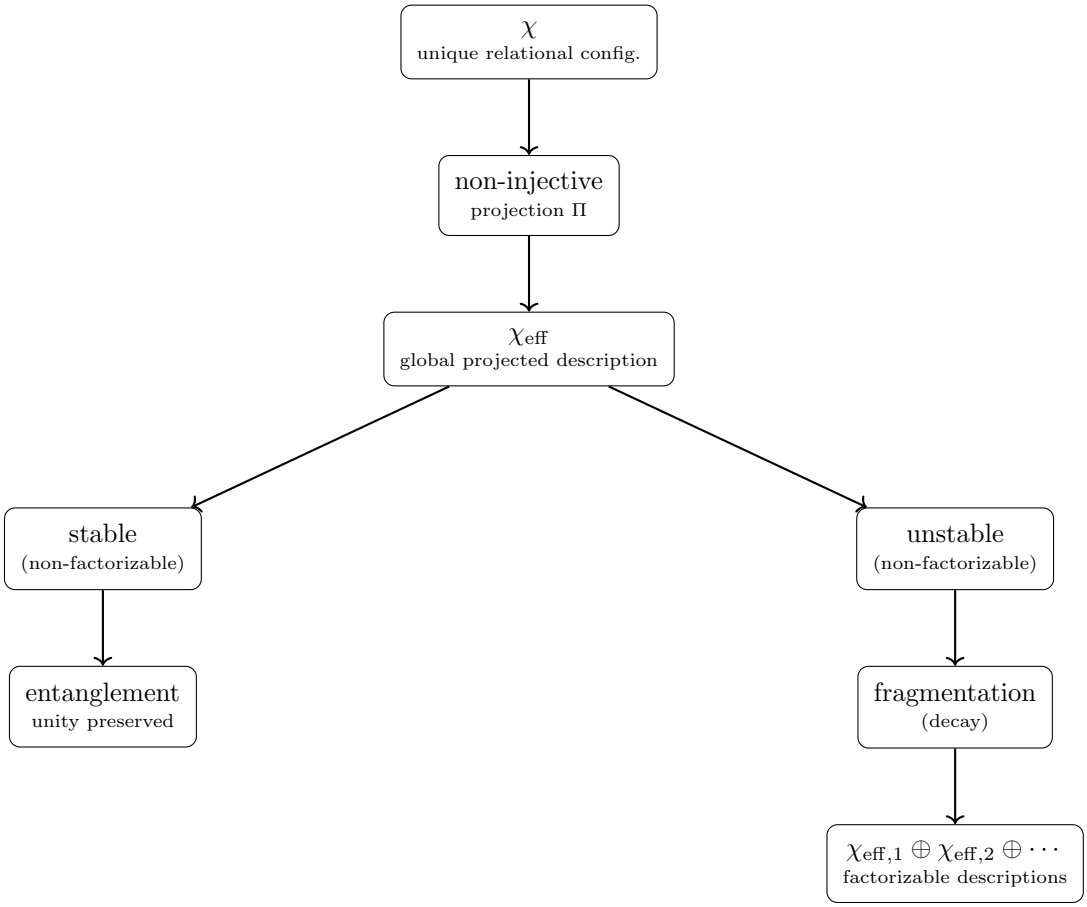

Fig. 12 Conceptual branching induced by non-injective projection. Stable non-factorizable descriptions manifest as entanglement; unstable ones fragment into localized factorizable descriptions (particle decay).

8.8 Structural Stability of Projected Descriptions

Entanglement, measurement, and decay correspond to distinct stability regimes of projected descriptions. Entanglement corresponds to the regime in which a non-factorizable projected description remains structurally stable. Measurement and decoherence correspond to selective stabilization: interaction with an environment amplifies certain relational features while rendering alternative descriptions inadmissible. Particle decay represents the regime in which the non-factorizable description becomes unstable, and stability is recovered through factorization into several localized configurations.

A technical analysis is provided in Appendix B.14.

8.9 Entanglement as a Critical Regime of Projective Compression

Quantum entanglement arises as a structural consequence of the non-injective projection $\Pi : \chi \to \chi_{\text{eff}}$. The projection reduces a high-dimensional relational configuration to a lower-dimensional effective description; the resulting fiber $\Pi^{-1}(\chi_{\text{eff}})$ constitutes an information-theoretic channel whose bandwidth depends on unresolved modes of χ.

Non-factorizable correlations emerge only in an intermediate *critical* regime of projective compression: the effective description is sufficiently coarse-grained to permit subsystem identification, yet retains enough global relational structure to prevent full factorization. Increased compression (environmental coupling, decoherence) suppresses correlations, yielding classical behavior; decreased compression breaks subsystem separation. The critical regime may be intermittent, with correlations appearing during specific spectral reconfiguration events (Appendix D).

8.10 Implications for Quantum Computation

Effective resources exploited in quantum computation may be reinterpreted as manifestations of structural non-injectivity and global consistency constraints. Multiple underlying relational configurations may correspond to the same effective observable state, providing a natural origin for effective parallelism without explicit information exchange. Part of the computational advantage may reflect general properties of non-factorizable descriptive mappings rather than exclusively quantum dynamical effects.

8.11 Integration with the Standard Model: A Spectral Interpretation

Weak Boson Masses from Spectral Geometry

The masses of $W^{\pm}$ and Z^0 emerge from the spectral properties of the Hodge Laplacian Δ_1 acting on 1-forms of the fiber bundle Π. The space of 1-forms decomposes into gauge-invariant subspaces $\Omega^1_{SU(2)}$ and $\Omega^1_{U(1)}$. Effective masses are

$$m_W \propto \sqrt{\lambda_{1,SU(2)}}, \qquad m_Z \propto \sqrt{\lambda_{1,U(1)}},$$

with the mass ratio governed by the metric anisotropy and curvature structure of the χ-induced geometry on Π.

Emergent Gauge Couplings

Gauge couplings are defined through normalized heat-kernel traces:

$$g^2 = 4\pi \left[\widehat{\mathrm{Tr}}_{SU(2)}\big(e^{-t_0 \Delta_{SU(2)}}\big) - \widehat{\mathrm{Tr}}_{U(1)}\big(e^{-t_0 \Delta_{U(1)}}\big) \right],$$

$$g'^2 = 4\pi\, \widehat{\mathrm{Tr}}_{U(1)}\big(e^{-t_0 \Delta_{U(1)}}\big),$$

with $t_0 = L^2_{\text{fiber}}$. The Weinberg angle follows from spectral asymmetry:

$$\tan^2 \theta_W = \frac{\widehat{\text{Tr}}_{U(1)}(e^{-t_0 \Delta_{U(1)}})}{\widehat{\text{Tr}}_{SU(2)}(e^{-t_0 \Delta_{SU(2)}})}.$$

Geometric Phase Transition and Mass Generation

Mass generation is a geometric phase transition of the χ substrate. Below a critical spectral density χ_{crit}, only massless modes are supported. Above it, spectral weight condenses into specific invariant subspaces, generating discrete non-zero eigenvalues $m_n \propto \sqrt{\lambda_n}$.

Strong Sector: Topological Confinement and Color

Color charge maps to the three fundamental degrees of freedom of the proton's trefoil topology ($Q = 3$). Topological confinement: separating components of a $Q = 3$ soliton requires linear energy increase exceeding the pair-creation threshold. Asymptotic freedom: at short distances the global topological constraint is not yet engaged, rendering the interaction effectively weaker.

The Origin of Mass: Spectral Overlap

Fermion masses are emergent quantities determined by the resonance between internal stability spectra and the global relaxation flux:

$$m_{\text{eff}} \propto \int_{\text{Fiber}} \mathcal{S}(\phi_n) \cdot \mathcal{R}(\chi)\, d\Pi. \tag{65}$$

Multiple fermion generations correspond to distinct stable topological classes of solitonic χ-configurations. The mass hierarchy $m_e \ll m_\mu \ll m_\tau$ arises from the ordered spectrum of L_{sol}:

$$m_n \sim \text{Spec}(L_{\text{sol}})_n. \tag{66}$$

Mixing matrices (CKM, PMNS) encode the misalignment between the mass basis (eigenvectors of L_{sol}) and the interaction basis (principal axes of Π). CP violation originates from non-trivial topological torsion of the projection fiber.

8.12 Relation to Quantum Formalism

The formal apparatus of quantum mechanics arises as an effective framework organizing admissible projected descriptions in regimes where localization, linearity, and approximate factorization hold. Quantum mechanics is not replaced but reinterpreted as an effective theory whose validity is restricted to regimes admitting a stable, approximately linear, spacetime-based description.

Status of the Wavefunction.

The wavefunction ψ is not a fundamental physical entity but a statistical encoding of admissible local reprojections compatible with a given non-factorizable projected

configuration. Its complex phase encodes relational constraints between alternative local descriptions; its modulus determines the statistical weight of accessible reprojections.

Emergence of Hilbert Space Structure.

In regimes where relational constraints are weak and approximately factorizable, distinct admissible descriptions can be combined, giving rise to approximate linear structure. Superposition reflects the formal coexistence of compatible descriptive alternatives. The inner product encodes mutual compatibility; orthogonality corresponds to mutually exclusive descriptive regimes. Unitary evolution is a consistency-preserving transformation valid as long as projectability and factorizability remain intact.

Emergence of the Schrödinger Equation.

In the non-relativistic regime, separating a rapidly varying rest-energy phase from a slowly varying envelope yields

$$i\hbar\,\partial_t\psi = -\frac{\hbar^2}{2m}\nabla^2\psi + V(x)\psi. \tag{67}$$

Operators and Non-Commutativity.

The canonical commutation relation $[\hat{x}, \hat{p}] = i\hbar_{\text{eff}}$ expresses the non-commutativity of geometric measurements induced by projection from the pre-geometric substrate. The uncertainty principle emerges as a geometric consistency condition on admissible effective descriptions.

Origin of Quantization.

Only a restricted class of localized projected configurations admits long-lived, internally consistent descriptions. Admissible configurations form discrete equivalence classes, yielding effective energy quantization. Planck's constant emerges as a universal conversion factor characterizing the minimal structural scale at which projected descriptions remain stable.

Measurement and the Born Rule.

Measurement outcomes correspond to effective reprojections onto mutually exclusive descriptive regimes. The Born rule emerges as the unique stable measure on the space of admissible projected descriptions that remains invariant under loss of phase coherence, coarse-graining, and environmental coupling.

Entanglement and Nonlocal Correlations.

Entangled systems arise when a unified relational configuration admits an effective projection onto spatially separated degrees of freedom. Correlations are fully compatible with relativistic causality (Appendix **??**).

Spin and Statistics.

Spin emerges as a topological property of admissible projected configurations. 4π-periodic configurations correspond to fermionic behavior; 2π-periodic ones to bosonic

behavior. The spin–statistics connection follows from the same topological constraints (Appendix B.4).

Orbital Geometry as Probabilistic Visibility.

Atomic orbitals correspond to effective probabilistic visibility patterns of admissible projected descriptions. Regions of high probability correspond to domains where consistent reprojection is most robust; nodal regions correspond to incompatible descriptive regimes.

Scope and Limitations.

All standard quantum-mechanical formalisms remain valid and unchanged within their domains. Cosmochrony provides an interpretative and unificatory account of the structural origin of quantum phenomena without introducing new degrees of freedom or hidden variables. A complete formal correspondence between the relational substrate and the operator-based structures of quantum theory is left for future work.

8.13 Summary

Gauge interactions emerge as admissible modes of the projection process. The photon corresponds to scalar transmission modes; $W^{\pm}$ and Z^0 bosons arise as shear-like spectral modes whose masses reflect the spectral rigidity of the projection fiber. Strong interactions and confinement are reinterpreted through topological stability of knotted solitonic configurations. Mass emerges from spectral overlap between localized configurations and the global relaxation flux. Entanglement and nonlocal correlations reflect the persistence of non-factorizable admissible projected descriptions. Quantum mechanics appears as an effective statistical framework describing the limits of local projectability imposed by a globally non-injective relational structure. Classical behavior emerges as the limiting case in which only locally stable, factorizable projected descriptions remain admissible.

Part V
Predictions, Discussion, and Conclusion

9 Radiation and Quantization

9.1 Radiation as χ–Matter Interaction

Radiation arises when a localized, relaxation-resistant configuration undergoes a transition toward a less constrained state. The excess relational content ceases to admit a particle-like projected description and becomes expressible only through delocalized projected modes. In effective spacetime descriptions, this redistribution appears as radiative emission—a transfer of descriptive weight from particle-like configurations to propagating field-like descriptions, without invoking discrete objects or stochastic processes.

9.2 Emergence of Photons

Photons are not fundamental entities. Prior to emission or detection, no photon exists as an independent object. A reconfiguration of relational structure within χ ceases to admit a localized projection and becomes expressible only through extended, delocalized effective modes—represented in spacetime as electromagnetic waves.

Photon-like events emerge only at interaction: when a delocalized projective mode becomes locally constrained by interaction with a localized excitation, the projection resolves into a discrete transfer of relaxation capacity. Quantization is a property of interaction and local reprojection, not of propagation. Wave–particle duality reflects a duality of description rather than of underlying ontology. Interference phenomena arise from the coherence of delocalized projective modes; individual detection events correspond to localized reprojections.

9.3 Geometric Origin of $E = h\nu$

Building on Section 4.5, the Planck relation

$$E = h\nu \tag{68}$$

acquires a geometric interpretation in the context of radiative processes. The energy E measures the relaxation potential redistributed during a reprojection event; the frequency ν characterizes the minimal temporal resolution required for a coherent effective description of this redistribution. The constant h is the effective projection of the fundamental substrate invariant $\hbar_\chi \equiv c^3/(K_{0,\mathrm{bare}}\,\chi_{c,\mathrm{bare}})$ (Section D.6), acting as a universal conversion factor between structural relaxation capacity and temporal projective resolution.

In the photoelectric effect, the threshold frequency ν_0 corresponds to the minimal projective resolution required to destabilize a bound electronic soliton. Quantization of radiative energy arises not from discretized propagation but from the discrete nature of local reprojection events, which impose a minimal unit of effective relaxation transfer determined by the spectral graininess $\hbar_\chi$.

9.4 Vacuum Fluctuations and the Casimir Effect

Vacuum fluctuations reflect the intrinsic structural indeterminacy of χ in regimes where no stable localized excitations are present. The relaxation admits a wide range of locally compatible projective descriptions; these fluctuations represent variability of effective descriptions rather than physical energy stored in the vacuum.

When material boundaries impose structural constraints on local projectability, certain effective descriptions become incompatible with the boundary conditions, reducing the set of admissible projective configurations between the boundaries. The Casimir effect arises from this asymmetry: a difference in the density of admissible effective reprojections, manifesting as a pressure on the confining surfaces. No fundamental vacuum energy density or propagating vacuum modes are required.

9.5 Weakly Interacting Radiation

Weakly interacting radiation corresponds to delocalized projective regimes whose structural contrast is insufficient to efficiently induce localized reprojection upon encountering matter. Low-frequency or weakly coupled modes are characterized by smooth, slowly varying relational structure, strongly suppressing the probability of stable localized energy transfer. Small interaction cross sections reflect the low likelihood that a given projective configuration satisfies the geometric and topological conditions required for localized reprojection.

9.6 Summary

Radiation and quantization arise from interactions between localized matter excitations and the χ substrate. Photon-like events emerge only during interaction-induced reprojection. Quantization reflects geometric and topological constraints of the relaxation dynamics at the level of projection: discrete energy transfer occurs when continuous projective descriptions satisfy the conditions required for localized reprojection.

10 Spectral Mass Spectrum and Hierarchy

10.1 Spectral Stability and the Unit of Mass

Rest mass is a spectral invariant associated with the stability of admissible projected configurations. It is identified with the fundamental eigenmode of the scalar Laplacian $\Delta_G^{(0)}$ acting on the projection fiber Π, subject to topological constraints $\mathcal{T}$:

$$m^2c^2 \;=\; \lambda_{\mathcal{T}} \;\equiv\; \mathrm{Eig}\Big(\Delta_G^{(0)}\Big)\,\Big|_{\mathcal{T}}. \tag{69}$$

Here $\lambda_{\mathcal{T}}$ encodes the minimal energetic cost required to maintain the configuration against the global relaxation of χ. Mass therefore quantifies resistance to relaxation.

The electron mass m_e corresponds to the lowest non-trivial admissible eigenmode λ_1, representing the fundamental resonance of χ within the finite-volume geometry $\Pi \cong S^3$. The conversion to physical mass units is

$$m \;=\; m_e\sqrt{\frac{\lambda_{\mathcal{T}}}{\lambda_1}}. \tag{70}$$

10.2 Non-Commutativity as a Source of Mass

Torsion acts as a dynamical constraint that competes with relaxation transport through the projection fiber.

Inhibition of Relaxation

Let Ω_w be the effective torsion operator associated with winding number w. For the fundamental lepton configuration ($w = 1$), relaxation and torsion are spectrally compatible:

$$[\Delta_G^{(0)}, \Omega_1] = 0. \tag{71}$$

For higher-winding configurations ($w \geq 2$), torsional constraints become spectrally frustrated:

$$[\Delta_G^{(0)}, \Omega_w] \neq 0 \qquad (w \geq 2). \tag{72}$$

This non-commutativity inhibits uniform relaxation across the fiber and induces irreducible spectral compression, manifesting as amplified inertial mass. The torsional action is a purely spectral invariant:

$$\mathcal{A}(w) \;\equiv\; \frac{1}{2}\ln\left(\frac{\det\Big(\Delta_G^{(0)} + \Omega_w\Big)}{\det\Big(\Delta_G^{(0)}\Big)}\right), \tag{73}$$

where the determinant is understood in the zeta-regularized sense.

The Pisano Ratio as a Stability Fixed Point

For $w = 2$, the projection fiber ceases to be spectrally isotropic and splits into competing sectors $\Pi = \Pi_{\parallel} \oplus \Pi_{\perp}$. Dynamical stability selects the most irrational admissible ratio

between their spectral frequencies, in analogy with KAM-type criteria:

$$\frac{\lambda_{\parallel}}{\lambda_{\perp}} = \varphi \qquad \Longrightarrow \qquad \beta \equiv \frac{1}{\varphi}, \tag{74}$$

where $\varphi = (1+\sqrt{5})/2$ is the golden ratio.

Leptonic Spectrum Synthesis

For the muon, non-commutative torsion yields the parameter-free prediction

$$\boxed{\frac{m_\mu}{m_e} = \sqrt{\frac{\lambda_2}{\lambda_1}} \cdot \frac{3}{2\alpha} \cdot \frac{1}{\varphi}} \qquad \text{with} \qquad \frac{\lambda_2}{\lambda_1} = \frac{8}{3}. \tag{75}$$

The robustness of the ratio $\lambda_2/\lambda_1 = 8/3$ is demonstrated independently in Appendix D.7.

10.3 Gravitational Shadows and the Spectral Wake

The torsional constraint Ω_w induces an extended spectral deformation of the surrounding substrate—a persistent modification of the local spectral density of relaxation modes, referred to as a *spectral wake* or gravitational shadow. This shadow does not correspond to additional matter or propagating degrees of freedom, but to a long-lived redistribution of relaxation capacity induced by the topological obstruction. It provides an ontological basis for phenomena usually attributed to dark matter without introducing new particles.

Two characteristic features emerge. *Elastic remanence*: the deformation persists under displacement of the baryonic configuration, accounting for the observed offsets in systems such as the Bullet Cluster. *Non-local susceptibility*: when the local gradient falls below $a_0 \sim cH_0$, the substrate response transitions from linear to non-linear, recovering MOND-like phenomenology as an emergent phase of spectral response. Dark matter effects are thus reinterpreted as manifestations of persistent spectral memory in the relational substrate.

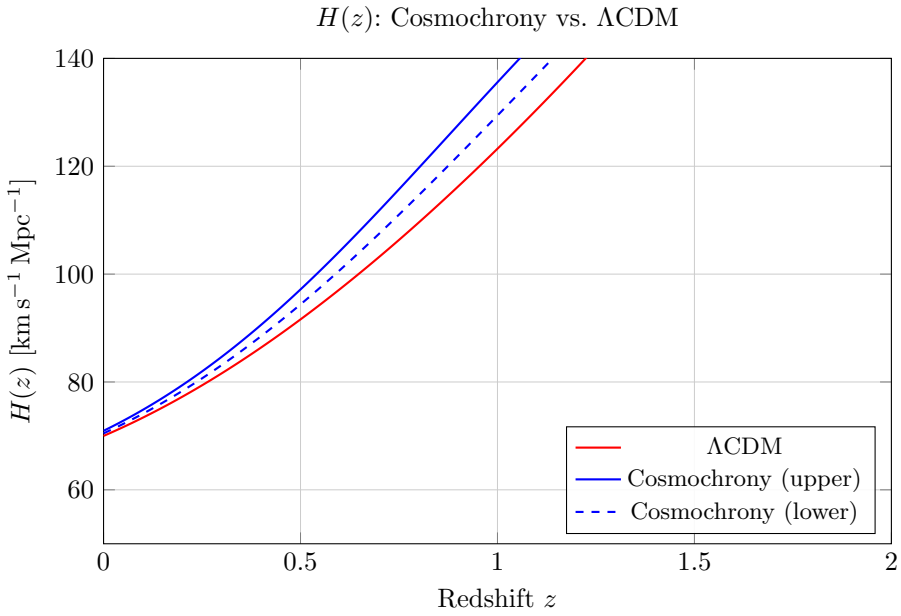

Fig. 13 Schematic comparison of $H(z)$. Cosmochrony predicts a mild enhancement at intermediate redshifts due to relaxation inhomogeneities.

11 Testable Predictions and Observational Signatures

Numerical estimates presented below are order-of-magnitude consistency estimates derived from the geometric coupling between the χ substrate and the effective relaxation fraction Ω_χ. Their role is to demonstrate that the framework operates within a phenomenologically relevant regime.

11.1 Hubble Constant from χ Dynamics

The Hubble parameter arises as an effective quantity:

$$H(t) = \frac{\dot{\chi}}{\chi}. \tag{76}$$

Assuming $\dot{\chi}_{\text{eff}} \simeq c$, the present-day value is $H_0 \simeq c/\chi(t_0)$. Early- and late-universe probes sample χ at different relaxation stages, naturally leading to systematically different inferred values of H_0 without invoking additional cosmological components.

Resolution of the Hubble tension.

The effective $H(z)$ acquires a mild redshift dependence departing from ΛCDM at intermediate redshifts ($0.1 \lesssim z \lesssim 10$), testable through upcoming BAO and supernova surveys.

11.2 Redshift Drift

Monotonic relaxation dynamics implies a slowly evolving cosmological redshift. The effective drift rate is

$$\dot{z}_{\text{eff}} \;\sim\; H_0(1+z) - \frac{c}{\chi(t)}, \tag{77}$$

corresponding to a secular variation of order $\Delta z \sim 10^{-10}\,\text{yr}^{-1}$ at $z \sim 1$, differing from ΛCDM at the $\sim 10\%$ level. Future extremely large telescopes equipped with ultra-stable spectrographs may probe this effect.

11.3 Gravitational Wave Propagation

In regions of high excitation density near compact objects, local suppression of χ relaxation modifies the persistence and coherence of gravitational-wave projective descriptions, inducing frequency-dependent phase shifts or dispersion-like behavior rather than dissipative losses.

LISA signature: a $\sim 10\%$ effective reduction of coherent gravitational-wave amplitudes near black holes, distinct from general relativity's purely propagative behavior.

The relative amplitude reduction scales as

$$\frac{\Delta A}{A} \sim \left(\frac{r_s}{r}\right)^2,$$

yielding $\Delta A/A \sim 10^{-2}$ for propagation at $r \approx 10\,r_s$. This effect should manifest most clearly during the late-time ringdown phase of binary black hole mergers, appearing as frequency-dependent deviations from general relativistic ringdown templates. Future space-based observatories (LISA) with signal-to-noise ratios exceeding ~ 100 may provide sufficient sensitivity.

11.4 Galaxy Rotation Curves from Structural Relaxation

Persistent relaxation gradients in the χ-substrate modify the effective inertial response of orbiting matter, producing approximately flat rotation curves without introducing dark matter components (Section 7.12). Observable consequences include a correlation between rotation curve flattening and indicators of structural relaxation activity, deviations from baryonic scaling relations in dynamically young galaxies, and a reduced need for fine-tuned dark matter profiles in low-surface-brightness systems.

11.5 Spin and Topological Signatures

If spin originates from topologically nontrivial configurations of χ (Section 4.6), ultra-high-precision interference experiments sensitive to 4π rotational symmetry may probe deviations associated with the internal topology of localized projectable configurations. Such deviations would appear as extremely small phase shifts under closed 2π versus 4π rotational cycles. These signatures are expected to be strongly suppressed and lie beyond current experimental resolution.

11.6 Absence of Dark Energy Signatures

Because cosmic acceleration emerges as a geometric consequence of global relaxation, no independent dark energy component is introduced. The framework predicts the absence of signatures associated with dynamical dark energy: no evolving equation of state, no clustering, no additional propagating degrees of freedom. The combined absence of these features, together with suppressed low-ℓ CMB power, specific angular correlations, and the absence of an inflationary tensor imprint at large angular scales, provides a potential observational discriminator.

11.7 CMB Polarization Signatures (Outlook)

Residual large-scale projective correlations inherited from the pre-geometric relaxation of χ are expected to imprint scale-dependent signatures on the CMB (Section 7.6). The observed $\sim 10\%$ suppression of the CMB quadrupole power relative to ΛCDM arises naturally from these relaxation dynamics [42]. Appendix C.1 provides quantitative estimates.

The* $8/3$ *Scaling in CMB Polarization.

The fundamental ratio $\lambda_2/\lambda_1 = 8/3$ is expected to leave a structural signature in the polarization sector. The bare geometric tensor-to-scalar ratio is

$$r_0 = \frac{\Delta_t^2}{\Delta_s^2} = \frac{\lambda_{\text{base}}}{\lambda_{\text{fiber}}} = \frac{3}{8} \simeq 0.375. \tag{78}$$

The observed ratio undergoes topological decoherence:

$$r_{\text{obs}}(t) = r_0 \cdot \exp\left(-\zeta \frac{\tau_\chi}{t}\right), \tag{79}$$

providing a structural explanation for the low observed $r < 0.036$ without invoking slow-roll dynamics.

11.8 Neutrino-Mediated Relaxation and Decay Signatures

Particle decay and neutrino emission are manifestations of structural reorganization (Sections 4.4, 4.9). Neutrino-like excitations act as non-local relaxation channels, contributing to irreversible smoothing of admissible configurations.

Environmental Modulation of Particle Stability

11.9 Environmental Modulation of Particle Lifetimes

Particle stability may exhibit a weak environmental dependence. At leading order:

$$\frac{\delta\Gamma}{\Gamma} \simeq \beta \frac{\Delta U}{c^2}, \tag{80}$$

where $\beta \lesssim 10^{-6}$ (from local position invariance constraints) and $\Delta U/c^2 \sim 10^{-7}$–$10^{-6}$ for typical galactic environments, yielding

$$\frac{\delta\tau}{\tau} \sim 10^{-13}\text{–}10^{-12}, \tag{81}$$

well below current sensitivities but conceptually distinct from standard effects. The cleanest experimental target is leptonic weak decay; the most amplified interferometric target is neutral-meson mixing. Near compact objects ($\Delta U/c^2 \sim 10^{-4}$), the effect rises to $\delta\tau/\tau \sim 10^{-10}$, manifesting as environment-correlated spectral biases in hadronic cascades.

11.10 Strong Gravitational Lensing

The effective lensing potential decomposes as $\Phi_{\rm eff} = \Phi_{\rm bar} + \Phi_\chi$, with convergence

$$\kappa(\boldsymbol{\theta}) = \frac{D_l D_{ls}}{c^2 D_s} \int \nabla_\perp^2 \Phi_{\rm eff}(D_l\boldsymbol{\theta}, z)\, dz, \tag{82}$$

yielding $\kappa = \kappa_{\rm bar} + \kappa_\chi$. The emergent contribution is parametrized as

$$\Phi_\chi(\mathbf{x}) = \frac{c^2}{2} \ln\!\left(\frac{K(\bar{\chi}(\mathbf{x}))}{K_\infty}\right). \tag{83}$$

Testable signatures include partial decorrelation between baryonic mass and lensing strength, enhanced sensitivity to cluster morphology, strong lensing without dark matter substructure, and redshift dependence tracing relaxation rather than mass accretion history.

Early Massive Structures in the JWST Era

Massive galaxies and strong lensing at $z \gtrsim 8$ are naturally accommodated: effective mass reflects localized resistance to relaxation associated with spectrally robust projected configurations, rather than requiring rapid hierarchical assembly.

"Impossibly Early" Galaxies

Their large effective masses encode strong resistance to relaxation rather than cumulative accretion. Cosmochrony predicts that such galaxies should exhibit relatively stable effective masses over extended redshift intervals, contrasting with the rapid growth required in hierarchical scenarios.

Qualitative Predictions

Massive galaxies at $z \gtrsim 8$ should persist with only moderate mass evolution. Early strong-lensing configurations should display weak redshift evolution of their effective convergence, with an early onset followed by moderate evolution.

Strong Gravitational Lensing in Abell-1689

The emergent convergence is isolated as

$$\kappa_\chi(\boldsymbol{\theta}) = \kappa_{\rm eff}(\boldsymbol{\theta}) - \kappa_{\rm bar}(\boldsymbol{\theta}), \tag{84}$$

with the emergent lensing potential obtained from $\nabla^2_{\boldsymbol{\theta}}\psi_\chi = 2\kappa_\chi$. In Cosmochrony, κ_χ is emergent geometric focusing from collective χ-substrate constraints, not additional dark matter.

11.11 Experimental Outlook and Discriminating Signatures

Particle creation is reinterpreted as a universal dissipation channel activated whenever directional relaxation approaches its maximal transport capacity. This unifies several high-energy phenomena:

Astrophysical Jets.

Relativistic jets are dynamically selected channels through which excess substrate tension is discharged by continuous structure creation. A predicted *saturation clamping* near the horizon—a non-linear relation between near-horizon stress and plasma density—is testable with Event Horizon Telescope observations.

Primordial Cosmology.

Matter production emerges as a byproduct of relaxation-driven expansion. Cosmochrony predicts that primordial fluctuations may carry imprints of discrete nucleation events, suggesting specific non-Gaussianity and phase correlations at large angular scales.

Ultra-High-Energy Cosmic Rays.

UHECRs exceeding the GZK threshold may be locally produced during transient saturation spikes near compact objects. A predicted strong anisotropy correlated with nearby compact objects and multimessenger correlations would provide a decisive signature.

Multi-Scale Falsification Program.

The framework suggests a hierarchy of tests: precision atomic physics (Section 4.10), Schwinger threshold in ultra-intense lasers, saturation clamping in relativistic jets, and large-scale CMB anomalies as relics of discrete primordial nucleation.

11.12 Summary

Cosmochrony yields observationally testable signatures spanning cosmology, gravitation, galactic dynamics, and particle phenomena. All arise from non-injective projection and structural relaxation. Predicted deviations from ΛCDM at the percent level include suppression of low-ℓ CMB power, a mild redshift-dependent modulation of $H(z)$, and coherence-modifying effects in gravitational-wave propagation near compact objects. These signatures define a coherent phenomenological pattern from a single underlying mechanism—the irreversible relaxation and partial projectability of the χ substrate.

12 Discussion and Comparison with Existing Frameworks

12.1 Relation to General Relativity

Spacetime curvature in Cosmochrony is an emergent descriptive construct (Section 6.3). No *a priori* metric dynamics is postulated; instead, an effective geometry emerges from variations in local relaxation dynamics. Matter configurations locally constrain the relaxation of χ, leading to differential rates of effective proper-time evolution that are reinterpreted as effective metric deformations. In the weak-field regime, Newtonian gravity is reproduced; in the strong-field limit, Schwarzschild-like solutions emerge. General Relativity is recovered as the appropriate effective theory within its empirically validated domain.

12.2 Relation to Quantum Formalism

Cosmochrony does not treat quantization or wave dynamics as fundamental [43]. Particles correspond to localized, topologically stable configurations; discrete observables arise from boundary conditions, topological constraints, and interaction-induced reprojection. The Planck relation $E = h\nu$ is a geometric correspondence between redistributed relaxation potential and minimal projective resolution. Entanglement reflects a shared, non-factorizable χ configuration persisting only within a finite critical regime of projection, while decoherence reflects irreversible loss of relational accessibility.

12.3 Analogy with Collective Phenomena in QCD

A useful structural analogy may be drawn with low-energy QCD [44], where fundamental degrees of freedom (quarks, gluons) do not appear as isolated entities. Similarly, Cosmochrony formulates fundamental dynamics solely in terms of χ and its relaxation; observable quantities arise only after projection into regimes admitting stable effective descriptions. What appear as elementary constituents at a given effective level may represent stable, regime-dependent invariants of the underlying dynamics, in direct analogy with QCD confinement.

12.4 Comparison with ΛCDM Cosmology

ΛCDM introduces cold dark matter, dark energy, and inflation as effective postulates [9, 45]. In Cosmochrony, cosmic expansion follows from monotonic relaxation of the substrate, with $H(t) = \dot{\chi}/\chi$ and $H_0 \sim c/\chi(t_0)$. Dark energy is reinterpreted as the large-scale relaxation dynamics; cosmic acceleration reflects cumulative relaxation over cosmological timescales. The coincidence problem and the Hubble tension may admit interpretations in terms of epoch-dependent relaxation dynamics rather than new fundamental constituents. Low-ℓ CMB suppression is explored as a structural consequence of relaxation constraints rather than a statistical fluctuation.

Table **??** summarizes the conceptual differences between Cosmochrony, ΛCDM, and Loop Quantum Gravity.

12.5 Historical Admissibility of Projected Degrees of Freedom

The set of effective degrees of freedom depends on the admissibility conditions imposed by the relaxation state. In the early Universe, only highly coherent, low-complexity global configurations were admissible. As relaxation proceeds, the admissible space progressively enlarges, enabling increasingly localized invariants described as particles, fields, and interactions. The particle spectrum is therefore a historically conditioned outcome of relaxation dynamics, not a timeless feature. This perspective reconciles the emergence of complexity with monotonic entropy increase: the early Universe is characterized by both low entropy and low admissible complexity. Low-ℓ CMB anomalies may be interpreted as relics of this early regime of restricted admissibility.

12.6 Inflation, Horizon Problems, and Initial Conditions

Because χ describes a global relaxation process rather than metric expansion, causal connectivity is not defined in terms of spacetime lightcones at the fundamental level. Large-scale coherence arises from initial relational smoothness and subsequent monotonic relaxation, without requiring an inflationary phase. The horizon problem is rendered inoperative by the absence of an initially fragmented causal structure at the pre-geometric level. A detailed quantitative treatment of primordial perturbations and their CMB imprint remains an open direction for future work.

12.7 Conceptual Implications and Open Challenges

Temporal ordering arises from the monotonic relaxation of χ; energy quantifies residual capacity to resist this relaxation; irreversibility reflects its progressive exhaustion. Time, energy, and irreversibility are not independent axioms but complementary effective descriptions of the same relational dynamics.

Open challenges include the quantitative reconstruction of CMB anisotropies from early-time χ dynamics, the detailed treatment of non-equilibrium decoherence and reprojection, the emergence of gauge symmetries from topological features, and the long-term stability of solitonic configurations under extreme conditions. Progress will require large-scale simulations of χ dynamics, discretized lattice realizations, and targeted experimental tests.

12.8 Ontological Parsimony and the Metric

Cosmochrony achieves genuine ontological simplification rather than relabeling. In GR, the metric $g_{\mu\nu}$ is a fundamental tensor field with ten independent components; matter and energy are conceptually distinct from geometry. In Cosmochrony, only χ is fundamental; the metric carries no independent ontological status; matter, energy, and geometry correspond to distinct regimes of the same relational structure.

The frameworks are operationally distinct: GR propagates two tensorial gravitational-wave polarizations from the metric; Cosmochrony has no independent geometric degrees of freedom. Singularities signal breakdown of effective geometric descriptions while χ remains well-defined. Quantization applies only to effective

excitations within projectable regimes, not to χ itself [46].

$$\text{Standard:} \quad g_{\mu\nu} \text{ (geometry)} + \psi \text{ (matter)} + \Lambda \text{ (dark energy)}, \tag{85}$$

$$\text{Cosmochrony:} \quad \chi \text{ (single substrate)} \longrightarrow \{\text{spacetime, matter, expansion}\}. \tag{86}$$

12.9 Relation to the Higgs Mechanism: Emergence from χ Dynamics

The Higgs field and its VEV are reinterpreted as effective low-energy descriptors of a specific projective regime of χ.

Structural Transition

Below a critical scale χ_c (homogeneous regime), only massless globally coherent configurations are admissible. Above χ_c (structured regime), localized relaxation-resistant configurations stabilize as massive excitations. The electroweak scale is related through

$$\langle \phi_H \rangle \;\propto\; \frac{\hbar_{\text{eff}}\, c}{\chi_c}, \tag{87}$$

naturally recovering the observed scale for $\chi_c \sim 10^{-18}\,\text{m}$.

Mass Generation as Solitonic Stabilization

Fermion masses scale as $m_f \propto y_f\, \hbar_{\text{eff}}/\chi_c$; gauge boson masses as $m_W \propto g\, \hbar_{\text{eff}}/\chi_c$. These relations reproduce standard Higgs-generated mass terms at the effective level.

Phenomenological Status

No deviation from established collider results is implied at accessible energies. Departures may arise only in extreme regimes. Open challenges include deriving the detailed mapping between χ soliton spectra and the full Standard Model mass spectrum.

12.10 Structural Interpretation: Projective Thermodynamics

Physical observables arise through a generically non-injective projection $\Pi : \Omega \to O$. In saturation regimes, the resulting loss of distinguishability induces a structural entropy:

$$S_\Pi = -\sum_{o \in O} \mu(\Pi^{-1}(o)) \log \mu(\Pi^{-1}(o)), \tag{88}$$

which is an objective property of the projection.

Effective parameters such as temperature or metric curvature emerge as Lagrange multipliers absorbing unresolved relational complexity. High effective temperatures or anomalous geometric features reflect the compression of a bounded relational flux into a reduced observable description, not excess local energy density. The bounded character of substratic relaxation ensures that projection-induced quantities remain

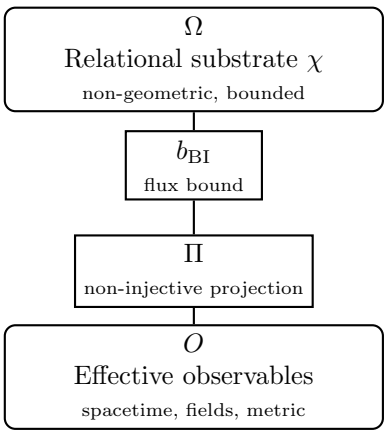

Fig. 14 Projective regimes in Cosmochrony. The substrate Ω undergoes bounded relaxation (b_{BI}). Observables arise through non-injective projection Π.

finite, rendering the framework predictive despite the non-injective nature of the projection.

12.11 Bounds on Projective Resolvability Across Scales

Saturation phenomena across scales—gravitational response in low-density environments, accessibility of quantum correlations—reflect a common limitation on the projective resolvability of relational structure: the rate at which global relational structure encoded in χ can be rendered operationally accessible within emergent spacetime descriptions. Attosecond chronoscopy experiments illustrate this notion: measured delays reflect the minimal temporal resolution required for a non-factorizable projected description to become resolvable, not a dynamical buildup of correlations [40].

The bound manifests as an effective inequality:

$$\left| \frac{\partial \mathcal{O}_{\mathrm{eff}}}{\partial \tau} \right| \leq b\, \mathcal{S}_{\Pi},$$

where b is the fundamental resolvability bound and $\mathcal{S}_{\Pi}$ characterizes the structural complexity of the non-injective projection.

Its phenomenological manifestations are:

$$a_\star \approx \eta_G\, b\, c, \tag{89}$$

for gravitational saturation, and

$$B_{\Pi}(\mathcal{M}) = \eta_{\mathcal{M}}\, b\, \mathcal{S}_{\Pi}, \tag{90}$$

for the operational projective bandwidth associated with a measurement protocol $\mathcal{M}$. These are distinct dimensional expressions of the same underlying bound. A modification

of the fundamental resolvability of the $\chi \to \Pi$ mapping would induce correlated shifts in both galactic saturation scales and quantum chronoscopy timescales.

12.12 Projective Non-Termination and the Condition of Temporal Ordering

Time is identified with the ordering of distinguishable projected states: $\Delta\tau \sim \mathrm{dist}(U_n, U_{n+1})$. A hypothetical terminal state U_0 satisfying $\Pi(\chi + \delta\chi) = U_0$ for all admissible $\delta\chi$ would imply $\Delta\tau \to 0$ for all internal observers.

The inaccessibility of absolute zero emerges as a projective necessity: zero-point fluctuations are reinterpreted as the minimal projective bandwidth required to prevent collapse of the observable description into a stationary state. Time ceases only when the projection becomes stationary—a regime structurally forbidden by the existence of a finite bound on projective resolvability.

13 Conclusion and Outlook

Cosmochrony reduces the fundamental assumptions of physics to a single dynamical origin: the irreversible relaxation of a pre-geometric relational substrate χ. From this substrate, time, spacetime geometry, and a wide spectrum of physical phenomena emerge as effective descriptions.

A central result is the *ab initio* derivation of the effective dynamical laws: the Born–Infeld-like Lagrangian is the unique functional compatible with causal saturation of relaxation fluxes at c_χ. The speed limit c_χ and Planck's constant h appear as complementary bounds on projectability, respectively limiting the maximal propagation rate and the minimal resolvable granularity. General Relativity is recovered as a thermodynamic limit of the underlying relational dynamics.

The framework provides a unified geometric origin for the Standard Model: gauge interactions emerge as projection dynamics; matter and mass arise from topological obstructions and spectral frustration; the dark sector is reinterpreted as non-projected spectral density (dark matter) and global relaxation flux (dark energy). Quantum entanglement arises when a single relational configuration admits multiple admissible effective realizations under non-injective projection, persisting only within a finite critical regime.

At cosmological scales, expansion and the arrow of time follow from the diminishing tempo of relaxation. At galactic scales, saturation of the relaxation constraint produces flat rotation curves without dark matter halos. In strong-gravity regimes, black hole evaporation is reinterpreted as discrete reprojection ensuring information preservation.

The space of admissible projected configurations evolves as relaxation proceeds: the particle content of the Universe is a historically conditioned outcome, not a timeless input.

Conceptual Shift and Outlook

Cosmochrony represents a shift from a "matter-on-spacetime" paradigm to a "relaxation-of-substrate" ontology. Immediate falsifiable research directions include: cosmological signatures (low-ℓ CMB anomalies from finite relaxation capacity), galactic phenomenology (dark matter effects correlated with local relaxation gradients), and fundamental-scale effects (environment-dependent variations in decay rates or couplings in extreme regimes). Future work will focus on the systematic derivation of the Standard Model spectrum as a hierarchy of topological frustration modes within the relaxation dynamics.

Part VI
Appendices

A Mathematical Foundations of Cosmochrony

This appendix provides a rigorous mathematical formulation of the χ-field dynamics: effective Lagrangian and hydrodynamic limit, stability analyses, analytical solutions, relational foundations of emergent geometry, and the Born–Infeld derivation. All results are derived from the fundamental postulates without assuming a pre-existing spacetime metric.

A.1 Effective Lagrangian Description as a Hydrodynamic Limit

In regimes where χ varies smoothly, a continuum approximation provides contact with standard geometric formulations. Distances are defined through the resistance to relaxation propagation, leading to an effective line element

$$g_{\mu\nu}\, dx^\mu dx^\nu \;\sim \sum_{(u,v)\in \mathrm{path}} \frac{1}{K_{uv}}.$$

To reproduce the continuum evolution equations (Equation 242), one introduces an effective Lagrangian density:

$$\mathcal{L}_{\mathrm{eff}} = \frac{1}{16\pi G_{\mathrm{eff}}}\, F(\chi)\, R - \Lambda_{\mathrm{flow}}^4\, \chi + \cdots$$

where R is the Ricci scalar of the effective metric and $F(\chi)$ parametrizes how relaxation dynamics maps onto the geometric description. This Lagrangian is purely representational; it does not define the fundamental dynamics, has no ontological status, and should not be quantized. Einstein-like field equations emerge as universal geometric descriptions of slowly varying collective phenomena.

A.2 Stability Analysis of the χ-Field Dynamics

The effective relaxation dynamics in a smooth geometric regime is

$$\partial_t \chi = c\sqrt{1 - \frac{|\nabla\chi|^2}{c^2}}. \tag{91}$$

Consider a homogeneous background $\chi_0(t) = c\,t + \chi_{0,0}$ with perturbation $\delta\chi(x,t)$, $|\nabla\delta\chi| \ll c$. Expanding:

$$\partial_t \delta\chi = -\frac{1}{2c}\,|\nabla\delta\chi|^2 + \mathcal{O}(|\nabla\delta\chi|^4). \tag{92}$$

No linear term appears: homogeneous relaxation is marginally stable at linear order. The leading nonlinear correction is strictly negative, so spatial inhomogeneities reduce the local relaxation rate and are dynamically suppressed. The functional $E[\delta\chi] = \frac{1}{2}\int |\nabla\delta\chi|^2\, d^3x$ is non-increasing, establishing nonlinear stability. Planar perturbations are progressively flattened; spherical perturbations decay monotonically.

A.3 Analytical Solutions of the χ-Field Dynamics

Explicit solutions of the effective relaxation equation:

$$\partial_t \chi = c\sqrt{1 - \frac{|\nabla\chi|^2}{c^2}}. \tag{93}$$

Homogeneous relaxation.

$\nabla\chi = 0$ gives $\partial_t\chi = c$, hence $\chi(t) = \chi_0 + c\,t$. This underlies emergent cosmological expansion (Section 3.7).

Gradient-saturated profiles.

Spherically symmetric configurations with $|\partial_r\chi| = c$ satisfy $\partial_t\chi = 0$ (local freezing), taking the form $\chi(r) = \chi_0 \pm c\,r$. These model horizons as boundaries where spacetime notions cease to be operationally meaningful.

Linear relaxation fronts.

$\chi(x,t) = \chi_0 + c\,t \pm v\,x$ with $|v| < c$ are exact solutions describing kinematic boundaries, not propagating waves.

Absence of linear wave solutions.

Small perturbations do not propagate as oscillatory modes (Section A.2). Apparent wave-like phenomena arise only at the effective level through collective excitations.

A.4 Coupling with Matter: Effective Source Term $S[\chi, \rho]$

In an emergent spacetime description, the influence of localized excitations on relaxation is summarized by:

$$\Box_{\text{eff}}\chi = S[\chi, \rho]. \tag{94}$$

The source $S[\chi, \rho]$ encodes the effective resistance of localized excitations to global relaxation.

Weak-field regime.

$$S[\chi, \rho] \;\simeq\; -\,\alpha\,\rho, \tag{95}$$

with $\alpha \sim G/c^2$. This reproduces the Poisson equation and Schwarzschild solutions at leading order.

Strong-field regimes.

Nonlinear corrections:

$$S[\chi, \rho] = -\,\alpha\,\rho\,F\left(\frac{\rho}{\rho_c},\,\chi\right), \tag{96}$$

where F is bounded and ρ_c is a saturation density scale. These prevent unphysical halting of relaxation and encode departures from classical gravity in strong-field regimes.

A.5 Strong-Field Constitutive Coupling Near a Schwarzschild Black Hole

The effective constitutive relation encoding relaxation suppression:

$$K_{\text{eff}} = K_0 \exp\left(-\frac{(\Delta\chi)^2}{\chi_c^2}\right). \tag{97}$$

The dimensionless lapse-like factor:

$$N(r) \equiv \frac{\mathcal{D}_{\text{loc}}\chi(r)}{\mathcal{D}_0\chi}, \qquad 0 < N(r) \leq 1. \tag{98}$$

Matching to Schwarzschild phenomenology:

$$ds^2 = -f(r)c^2dt^2 + f(r)^{-1}dr^2 + r^2d\Omega^2, \quad f(r) = 1 - \frac{r_s}{r}, \tag{99}$$

implies

$$N(r)^2 = f(r) = 1 - \frac{r_s}{r}. \tag{100}$$

Identifying $K_{\text{eff}}(r)/K_0 \equiv N(r)^2$ yields:

$$K_{\text{eff}}(r) = K_0\left(1 - \frac{r_s}{r}\right), \quad r > r_s. \tag{101}$$

Inverting the constitutive relation:

$$\frac{(\Delta\chi(r))^2}{\chi_c^2} = -\ln\left(1 - \frac{r_s}{r}\right). \tag{102}$$

As $r \to r_s^+$:

$$\Delta\chi(r) \sim \chi_c\sqrt{-\ln\left(1 - \frac{r_s}{r}\right)}. \tag{103}$$

This divergence signals breakdown of the hydrodynamic parametrization, not a physical singularity. A Schwarzschild horizon corresponds to vanishing relaxation conductivity, $K_{\text{eff}} \to 0$.

A.6 Minimal Kinematic Constraint

In its saturated form, the universal kinematic bound reads:

$$(\partial_t\chi)^2 + |\nabla\chi|^2 = c^2, \tag{104}$$

with inequality for unsaturated configurations. This does not presuppose a spacetime metric or Lorentzian structure; it expresses a purely kinematic admissibility condition at the pre-geometric level. The constant c is the effective manifestation of the invariant bound c_χ (Section 2.11).

Lorentz symmetry arises *a posteriori* as a property of saturated relaxation. In homogeneous regimes, the constraint enforces $\partial_t \chi = c$, yielding linear growth of χ_{eff} and effective cosmic expansion. In inhomogeneous regimes, partial saturation manifests as gravitational time dilation and curvature.

At Planck-scale resolution, the continuum gradient must be replaced by finite differences on the underlying relational graph. A fully discrete formulation is deferred to future work.

A.7 Effective Evolution Equation

Once a stable geometric description has emerged, ordering relations between projected configurations take the schematic form $\Box_{\text{eff}} \chi = S[\chi, \rho]$, where $\Box_{\text{eff}}$ is the emergent-metric d'Alembertian and ρ represents the effective density of relaxation-resistant configurations. In the weak-field regime, $S[\chi, \rho] \simeq -\alpha\rho$ with $\alpha \sim G/c^2$, reproducing the Poisson equation and Schwarzschild-like solutions. In strong-field regimes, nonlinear corrections encode saturation effects imposed by $\partial_t \chi \leq c$ and mark the limits of the hydrodynamic approximation.

A.8 Relational Foundation and Emergent Geometry

The continuous representation of χ is a pragmatic strategy for contact with established formalisms. At a more fundamental level, Cosmochrony can be formulated in purely relational terms, without *a priori* spacetime points, distances, or metric. Temporal ordering arises from the monotonic relaxation ordering; spatial relations are reconstructed from patterns of correlation and connectivity within χ. A concrete realization is developed in Appendix **??**, where the metric appears only as a derived object encoding relational properties.

A.9 Energy and Curvature

Energy emerges as an effective measure of resistance to global relaxation. The diagnostic functional

$$\mathcal{E}_\chi^{\text{eff}} \;=\; \frac{1}{2}\left[(\partial_t \chi)^2 + (\nabla \chi)^2\right] \tag{105}$$

provides a coarse-grained measure of temporal and spatial deformation. Regions of large $\mathcal{E}_\chi^{\text{eff}}$ correspond to strong internal gradients and are identified with particle-like excitations.

The energetic ordering of atomic orbitals reflects the structural cost of sustaining increasingly extended and oscillatory χ configurations. This is independent of the geometric visibility discussed in Appendix A.10. Effective spacetime curvature characterizes internal deformation and its modulation of relaxation propagation; it arises secondarily as a macroscopic descriptor.

A.10 Level Sets, Projections, and Apparent Orbital Geometry

For a continuous scalar field $\phi : \mathbb{R}^3 \to \mathbb{R}$, the level set

$$\mathcal{L}_c = \{\mathbf{x} \in \mathbb{R}^3 \mid \phi(\mathbf{x}) = c\}. \tag{106}$$

may consist of disconnected components without implying discontinuity of ϕ. The projected set

$$P_c = \{z \in \mathbb{R} \mid \exists (x, y) \text{ s.t. } \phi(x, y, z) \geq c\} \tag{107}$$

typically consists of disjoint intervals, and the envelope function

$$f(z) = \max_{x,y} \phi(x, y, z) \tag{108}$$

gives $P_c = \{z \mid f(z) \geq c\}$. Fragmentation is a geometric consequence of thresholding, not fundamental discontinuity. Orbital-like patterns, nodal structures, and visibility regions are emergent manifestations of an underlying continuous field.

A.11 Emergent Electrodynamics from χ Dynamics

In the weak-field limit, the variational formulation yields a linearized wave equation admitting propagating collective modes. The spatial gradient of χ decomposes as $\nabla\chi = -\nabla\phi + \mathbf{A}_{\mathrm{T}}$ with $\nabla \cdot \mathbf{A}_{\mathrm{T}} = 0$ (Helmholtz projection induced by solitonic topology).

Charge as Transverse Torsion

The bounded canonical current

$$\mathbf{J}_\chi \;\propto\; \frac{\nabla\chi}{\sqrt{1 - |\nabla\chi|^2/c^2}}$$

saturates as $|\nabla\chi| \to c$. A localized excitation carries effective charge if

$$q \;\equiv\; \kappa \oint_\gamma \mathbf{A}_T \cdot d\boldsymbol{\ell} \;=\; \kappa \int_S (\nabla \times \mathbf{A}_T) \cdot d\mathbf{S}. \tag{109}$$

Sign reflects chirality of the transverse torsion; stability follows from topological character.

Emergent Electromagnetic Fields

Defining $\mathbf{E} = -\nabla\phi - \frac{1}{c}\partial_t \mathbf{A}_{\mathrm{T}}$ and $\mathbf{B} = \nabla \times \mathbf{A}_{\mathrm{T}}$, these satisfy Maxwell-like relations:

$$\nabla \cdot \mathbf{E} = 4\pi G_{\mathrm{eff}} \rho_{\mathrm{em}}, \tag{110}$$

$$\nabla \times \mathbf{E} + \tfrac{1}{c}\partial_t \mathbf{B} = 0, \tag{111}$$

$$\nabla \cdot \mathbf{B} = 0, \tag{112}$$

$$\nabla \times \mathbf{B} - \tfrac{1}{c}\partial_t \mathbf{E} = \tfrac{4\pi G_{\mathrm{eff}}}{c} \mathbf{J}_{\mathrm{em}}. \tag{113}$$

Gauge transformations $\phi \to \phi - \frac{1}{c}\partial_t \Lambda$, $\mathbf{A}_{\mathrm{T}} \to \mathbf{A}_{\mathrm{T}} + \nabla\Lambda$ leave $\mathbf{E}$, $\mathbf{B}$ invariant. This emergent $U(1)$ symmetry reflects the relational nature of χ.

A.12 Relational Consistency of the Effective Lagrangian

The Born–Infeld-like Lagrangian is constructed as a canonical representation of the relational dynamics (Section 3).

Step 1: Relational Constraint

$$\mathcal{C}_i[\chi] \equiv \sum_j K_{ij}(\chi_i - \chi_j)^2 \leq \chi_c^2, \tag{114}$$

enforcing bounded relative variations as a structural causality condition.

Step 2: Variational Formulation

$$S[\{\chi_i\}, \{\mu_i\}] = \int d\lambda \left[\sum_i \frac{1}{2} \left(\frac{d\chi_i}{d\lambda} \right)^2 - U[\{\chi_i\}] - \sum_i \mu_i(\lambda)(\mathcal{C}_i[\chi] - \chi_c^2) \right], \tag{115}$$

with KKT conditions ensuring $\mu_i \geq 0$ and complementary slackness.

Step 3: Continuum Limit

The discrete constraint maps to

$$|\nabla\chi|^2 \leq c^2, \tag{116}$$

with $c^2 \equiv a^2\chi_c^2/K_0$. The canonical representation satisfying boundedness, monotonicity, saturation, and regularity is:

$$f(x) = -c^2\sqrt{1-x}, \tag{117}$$

yielding:

$$\mathcal{L}_{\text{eff}} = -c^2\sqrt{1 - \frac{|\nabla\chi|^2}{c^2}} + \partial_t\chi. \tag{118}$$

Step 4: Role of the Potential

In the continuum limit, $U[\{\chi_i\}] \to \int d^3x\, V(\chi)$.

Step 5: Connection to Emergent Geometry

The effective metric is defined via the Hessian:

$$g_{\mu\nu}^{\text{eff}} \propto \frac{\partial^2 \mathcal{L}_{\text{eff}}}{\partial(\partial_\mu\chi)\partial(\partial_\nu\chi)}, \tag{119}$$

up to conformal rescalings.

Continuum Limit and Laplace–Beltrami Operator

With scaling $K_{ij} = V_i^{-1} w(d_{ij}/\varepsilon)$, the discrete sum converges to

$$\int_{\mathcal{M}} g^{ab}\, \partial_a \chi\, \partial_b \chi\, \sqrt{|g|}\, d^n x.$$

The metric g_{ab} arises as the continuum encoding of microscopic connectivity.

Necessity of the Born–Infeld Structure

A quadratic action permits unbounded gradients, violating the maximal relaxation speed c_χ. The Born–Infeld structure is the minimal non-polynomial functional enforcing strict saturation, finite energy density, and self-regularizing behavior. The saturation constant b relates to the speed of light through microscopic coupling density K_0, with $c \leq b$ ensuring no projected perturbation propagates faster than the substrate can relax.

B Conceptual Extensions of Cosmochrony

This appendix develops conceptual and phenomenological extensions: the ontological status of χ, particles as topological solitons, emergence of classical limits, perspectives on deriving mass spectra, and structural origins of quantum correlations, CPT symmetry, and CP asymmetry.

B.1 Interpretative Status of the χ Field

This appendix supplements the primary definition of χ given in Section 2.1. It does not introduce new postulates, but provides interpretative clarifications to prevent common misreadings suggested by conventional field-theoretic language.

In the main text, χ is often written in the form $\chi(x^\mu)$ and manipulated using continuous differential operators. This notation should not be taken to imply that χ is a physical field propagating *within* a pre-existing spacetime manifold. Rather, spacetime coordinates serve only as convenient labels for organizing relational information in regimes where a stable geometric description has emerged.

Fundamentally, χ encodes a **non-energetic relational scale of relaxation** from which notions such as duration, distance, and causal ordering are reconstructed. The apparent embedding of χ in spacetime is therefore representational, not ontological. The manifold description is a secondary construct, introduced only after the relaxation dynamics of χ has reached sufficient regularity to admit a geometric interpretation.

This distinction mirrors the use of continuum variables in hydrodynamics or elasticity theory. Just as a velocity field does not exist independently of the underlying molecular interactions, $\chi(x^\mu)$ does not represent a fundamental spacetime field. It summarizes collective relational properties of the substrate once coarse graining becomes meaningful, **without implying an underlying differentiable structure at the fundamental level**.

In this sense, χ should not be interpreted as:

- a matter field living on spacetime,
- a dynamical scalar coupled to a pre-existing metric,
- or a hidden-variable replacement for the quantum wavefunction.

Instead, χ constitutes the pre-geometric quantity from which spacetime structure, effective fields, and physical observables emerge through projection and coarse graining. The use of continuous fields, Lagrangians, and differential equations throughout this work reflects practical representational choices rather than fundamental ontological or kinematical commitments.

This interpretative clarification is particularly important for understanding the role of localized excitations, solitonic structures, and effective fields discussed in the remainder of this appendix. These constructions should be read as regime-dependent invariants of the underlying χ dynamics, not as evidence that χ itself decomposes into independently propagating physical entities.

In summary, the χ field is not a field *in* spacetime. Spacetime is an emergent bookkeeping structure *for* χ once its relational dynamics becomes sufficiently regular.

This asymmetry is essential to the ontological parsimony of the Cosmochrony framework and underlies its reinterpretation of geometry, matter, and quantum phenomena.

B.2 Topological Configurations of the χ Field: Solitons as Particles

This appendix provides effective geometric representations of the topological stability principles introduced in Section 4.2.

Status and scope of this construction.

The solitonic configurations discussed in this appendix are not introduced as fundamental degrees of freedom of Cosmochrony. They are *effective geometric representations* intended to illustrate how particle-like properties may arise from stable, localized configurations of the χ field *once a smooth, orientable geometric projection becomes applicable*.

At the fundamental level, Cosmochrony does not assume a pre-existing spatial manifold, metric, or differential structure. The scalar field χ is not defined *in* spacetime; rather, spacetime emerges as an effective description of relational regimes of χ. A fully relational and pre-geometric formulation is presented in Appendix **??**.

Throughout this appendix, all geometric notions (distance, rotation, circulation, surface integrals) refer exclusively to an *effective projected field* χ_{eff}, obtained once a stable projective regime is reached. None of the figures or constructions below should be interpreted as depicting the fundamental χ field itself.

Within this effective regime, particles are interpreted as **topologically stabilized solitonic configurations** of χ_{eff}, within the effective descriptive regime only. Their apparent properties—such as **mass, spin, and charge**—do not correspond to independent fundamental quantum numbers, but emerge from the **structural organization and relaxation constraints** induced by these configurations.

Charge as Oriented Relaxation Asymmetry of χ_{eff}

In Cosmochrony, electric charge is not associated with a fundamental gauge field, local symmetry, or conserved Noether current. Instead, it emerges as an *oriented asymmetry in the relaxation structure* of the effective projected field χ_{eff}, once a stable geometric description becomes applicable.

A localized solitonic configuration may deform the surrounding χ_{eff} profile in one of two qualitatively distinct ways:

- A **positive effective charge** corresponds to a **local excess** of χ_{eff} relative to its asymptotic background value $\chi_{\text{eff},0}$. Such configurations locally resist relaxation and generate repulsive interaction tendencies with similarly oriented deformations.
- A **negative effective charge** corresponds to a **local deficit** of χ_{eff} relative to $\chi_{\text{eff},0}$, favoring compensating relaxation and attractive interactions with oppositely oriented configurations.

This polarity does not reflect an intrinsic sign of the fundamental χ substrate—which remains a scalar relational quantity without charge— but rather the orientation of the deformation with respect to the background relaxation flow in the projective regime.

From structural asymmetry to observable charge.

Within an effective geometric description, the magnitude of the charge associated with a solitonic excitation is controlled by the *net relaxation imbalance* induced by the configuration.

A convenient coarse-grained diagnostic of this imbalance is given by a Gauss-like flux integral,

$$q_{\text{eff}} \;\propto\; \oint_{\Sigma} \nabla\chi_{\text{eff}} \cdot d\mathbf{S},$$

where Σ denotes a closed surface surrounding the localized configuration in effective space. This expression does not define a fundamental conserved quantity; it merely quantifies the oriented relaxation asymmetry encoded in the projected gradient structure of χ_{eff}.

In three effective spatial dimensions, the geometric dilution of these gradients naturally leads to inverse-square interaction profiles. Coulomb-like behavior therefore arises as a collective geometric response of χ_{eff}, without introducing a fundamental electromagnetic field, potential, or gauge symmetry.

Coulomb-like interaction as frustration minimization.

Crucially, the effective interaction between two charged configurations is *not imposed as a force law*. It emerges from the minimization of projected geometric frustration.

In the projective regime, the leading diagnostic of this frustration is the Dirichlet-like functional

$$\mathcal{F}[\chi_{\text{eff}}] \;\equiv\; \frac{1}{2}\int |\nabla\chi_{\text{eff}}|^2 \, d^3x,$$

which encodes the local cost of relaxation gradients. Two localized oriented deformations interact because their combined configuration may either lower or increase $\mathcal{F}$ relative to the sum of isolated profiles. Attraction and repulsion are therefore not additional dynamical postulates, but direct signatures of the gradient of frustration in configuration space.

In this sense, Coulomb's law appears as a far-field consequence of frustration minimization under geometric dilution constraints, and not as an independently coded interaction.

This mechanism is implemented directly at the numerical level through the bounded relaxation algorithms described in Appendix D.4, where no explicit interaction law is introduced and all effective forces arise from the minimization of projected relaxation gradients.

Scope and limitations.

The present construction accounts for electrostatic-like interactions within the projective regime. Dynamical electromagnetic phenomena (such as radiation or magnetic induction) are not assumed here and would require additional projective modes beyond scalar relaxation asymmetry.

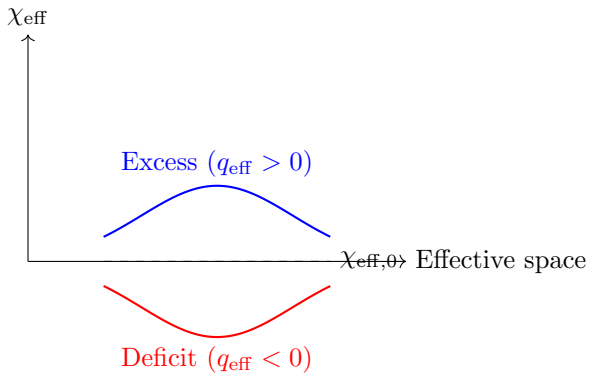

Fig. 15 Schematic illustration of oriented deformations of the effective projected field χ_{eff}. An excess or deficit relative to the background value $\chi_{\text{eff},0}$ determines the polarity of the effective charge. This diagram is purely illustrative and does not represent a solution of the fundamental χ dynamics.

Vortical Configurations and Integer-Spin Excitations

In the projectable regime, certain solitonic configurations of χ_{eff} admit cyclic internal organization patterns that can be described using an effective phase. When these patterns exhibit non-trivial circulation, the configuration may be modeled as a *vortical soliton*.

An effective winding number n may be defined as

$$n = \frac{1}{2\pi} \oint \nabla \arg(\chi_{\text{eff}}) \cdot d\mathbf{l},$$

where all quantities refer to the emergent geometric representation. This winding number is not fundamental and has no meaning outside the projective regime.

The integer n characterizes:

- the orientation of the relaxation asymmetry (sign of the effective charge),
- the topological robustness of the configuration,
- and the effective spin of the excitation, with integer values corresponding to bosonic behavior.

The energetic cost of such configurations increases with their internal structural complexity, leading to an effective mass scaling with $|n|^2$ in minimal models.

Skyrmion-Like Configurations and Spin-$\frac{1}{2}$ Excitations

More complex solitonic configurations arise when the internal organization of χ_{eff} involves non-trivial mappings between internal orientation space and effective physical space. Such configurations may be modeled using skyrmion-like constructions.

An effective topological index Q can be defined as

$$Q = \frac{1}{4\pi} \int \mathbf{n} \cdot (\partial_x \mathbf{n} \times \partial_y \mathbf{n})\, dx\, dy, \quad \mathbf{n} = \frac{\chi_{\text{eff}}}{|\chi_{\text{eff}}|}.$$

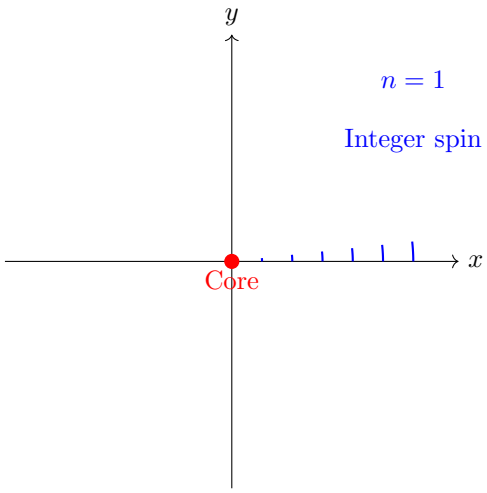

Fig. 16 Illustrative vortical configuration of the effective field χ_{eff} with winding number $n = 1$. The circulation represents a cyclic relaxation pattern associated with integer spin. This figure is schematic and purely conceptual.

where $n\mathbf{n}n$ denotes an effective orientation field constructed from χ_{eff}, not a fundamental vector degree of freedom.

Configurations with $Q = \pm 1$ exhibit a characteristic **4π-periodicity** under rotations. A 2π rotation does not return the configuration to an equivalent state, while a 4π rotation does. This topological property provides a geometric origin for spin-$\frac{1}{2}$ behavior and fermionic statistics within the projective regime.

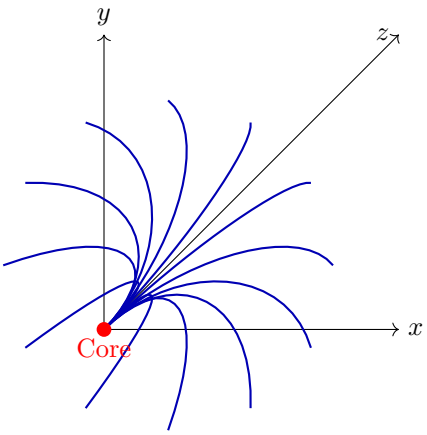

Fig. 17 Conceptual skyrmion-like configuration of χ_{eff}, illustrating a spin-$\frac{1}{2}$ excitation. The nontrivial internal mapping accounts for fermionic rotational behavior. This representation is purely illustrative.

Summary: Topology, Charge, and Spin

Table 2 Effective Solitonic Configurations and Emergent Particle Properties

Configuration	**Topological Index**	χ_{eff} **Asymmetry**	**Emergent Properties**
Vortical soliton	Winding number n	Excess / deficit	Charge $\propto n$, integer spin
Skyrmion-like soliton	Index $Q = \pm 1$	Oriented deformation	Charge $\propto Q$, spin-$\frac{1}{2}$

These constructions are not intended as a particle classification scheme nor as a replacement for the Standard Model. Their role is conceptual: to demonstrate how charge, mass, and spin may emerge coherently from the structural and topological organization of a single scalar substrate, without introducing additional fundamental fields, symmetries, or quantization postulates.

Coulomb-like interaction as frustration minimization (simulation link).

In Cosmochrony, the code does not implement a Coulomb law. It implements a bounded relaxation that systematically reduces projected geometric tension. In a projectable regime, the leading diagnostic of this tension is the Dirichlet-like functional

$$\mathcal{F}[\chi_{\text{eff}}] \equiv \frac{1}{2} \int |\nabla \chi_{\text{eff}}|^2 \, d^3x,$$

which emerges as the continuum encoding of the underlying relational constraint. Two localized oriented deformations interact because the combined configuration can either *lower* or *raise* $\mathcal{F}$ relative to the sum of isolated profiles. Attraction and repulsion are therefore not additional rules: they are the sign of the net frustration gradient in configuration space.

In three effective spatial dimensions, the far-field solution that minimizes $\mathcal{F}$ under a fixed flux constraint yields a $1/r^2$ dilution of the projected relaxation gradients, so Coulomb-like scaling appears as an emergent geometric response, not as a postulated force law.

B.3 Soliton Energy and Structural Mass Scaling

Status and scope of this analysis.

This subsection presents a *quantitative but non-numerical* analysis of the effective mass associated with localized solitonic configurations arising in the *projectable regime* of Cosmochrony. The objective is not to reproduce the observed particle mass spectrum, but to identify robust scaling relations, hierarchy constraints, and structural dependencies that emerge independently of microscopic details.

No claim is made that the expressions introduced below define a fundamental Hamiltonian or Lagrangian for the χ field. A fully predictive derivation of particle

masses would require a complete effective theory incorporating projection dynamics, interaction channels, and renormalization effects, which lies beyond the scope of the present work.

All energetic and spectral quantities discussed in this section refer exclusively to the effective projected field χ_{eff}. The fundamental χ field itself does not admit an energy functional or mass interpretation.

Mass as integrated resistance to relaxation.

Within Cosmochrony, the mass of a localized excitation is interpreted as a measure of the total *resistance to relaxation* imposed by the configuration on the surrounding χ_{eff} field.

Once an effective geometric description applies, this resistance can be summarized by an effective diagnostic functional

$$M_{\text{eff}} \;\propto\; \int_{\mathcal{V}} \left[\mathcal{T}(\nabla\chi_{\text{eff}}) + \mathcal{U}(\chi_{\text{eff}})\right] \, d^3x, \tag{120}$$

where:

- $\mathcal{T}$ encodes gradient-induced resistance associated with spatial inhomogeneities of χ_{eff},
- $\mathcal{U}$ represents effective nonlinear stabilization terms arising from collective relaxation constraints.

This expression should be understood as a *coarse-grained measure* of structural complexity rather than as a fundamental energy density. It quantifies how strongly a localized configuration delays or distorts the global relaxation of the projected field.

Scaling with soliton size and internal structure.

Consider a localized solitonic configuration characterized by:

- a typical spatial extent ℓ,
- a characteristic deformation amplitude $\Delta\chi_{\text{eff}}$.

Dimensional analysis then yields the generic scaling

$$M_{\text{eff}} \;\sim\; \ell^3 \left[\frac{(\Delta\chi_{\text{eff}})^2}{\ell^2} + V_{\text{eff}}(\Delta\chi_{\text{eff}})\right], \tag{121}$$

where V_{eff} denotes an effective nonlinear stabilization potential generated by projection and relaxation constraints.

For simple kink-like configurations, the balance between gradient resistance and nonlinear stabilization dynamically fixes the soliton width ξ. In this regime, the effective mass scale may be written schematically as

$$M_{\text{eff}} \;\sim\; \sqrt{\lambda_{\text{eff}}}\,\xi\,\chi_c^2, \tag{122}$$

where:

- χ_c denotes the characteristic local relaxation scale,
- λ_{eff} is an emergent, configuration-dependent stiffness parameter.

Neither χ_c nor λ_{eff} should be interpreted as fundamental constants. They summarize collective properties of the projected relaxation regime.

Structural stabilization and finite mass.

When stabilization arises from a balance between gradient-induced resistance and nonlinear relaxation constraints, the soliton size ℓ is dynamically fixed. This mechanism ensures that localized excitations possess a finite and stable effective mass without the need for fine-tuning.

Different classes of solitonic configurations (kinks, vortices, knotted or linked structures) involve distinct internal organizations of χ_{eff}. As a result, their effective masses exhibit different scaling behaviors with respect to ℓ and $\Delta\chi_{\text{eff}}$.

This implies that mass hierarchies arise *structurally* rather than through arbitrary parameter choices.

Topological classes and mass hierarchy.

The effective mass depends not only on the spatial extent of a soliton but also on its topological class. Configurations characterized by higher winding, linking, or covering indices necessarily involve increased internal gradients and more complex relaxation constraints.

Consequently, masses associated with different topological families obey ordering relations of the form

$$M_{n+1} \;>\; M_n, \tag{123}$$

where n labels an effective topological invariant. This establishes a natural mechanism for discrete mass hierarchies without introducing ad hoc mass parameters.

Spectral interpretation.

From a spectral perspective, localized excitations correspond to bound modes of the linearized relaxation operator around a solitonic background configuration of χ_{eff}.

The effective mass is then controlled by the lowest nontrivial eigenvalue of this operator,

$$M_{\text{eff}} \;\sim\; \lambda_{\text{min}}^{-1}, \tag{124}$$

where λ_{min} denotes the smallest positive eigenvalue governing the stability of the configuration.

This formulation emphasizes that mass is fundamentally a *spectral property* of the relaxation dynamics rather than an intrinsic attribute of a particle-like object.

Robustness and universality.

The scaling relations derived above depend only on generic features of the projected χ dynamics—locality, monotonic relaxation, and nonlinear stabilization—and are therefore expected to be robust against modifications of microscopic details.

While specific numerical values of particle masses cannot be fixed at this level, the existence of discrete, ordered, and stable mass scales emerges as a structural prediction of the framework.

Order-of-magnitude consistency.

Although the present analysis does not aim to reproduce the observed particle mass spectrum, it is instructive to examine whether the structural parameters entering the solitonic energy scale admit values compatible with known masses.

For a simple kink-like configuration with characteristic width $\lambda_{\text{eff}}^{-1}$ and amplitude set by the local relaxation scale χ_c, the effective rest energy scales as

$$E_{\text{sol}} \;\sim\; \chi_c^2 \lambda_{\text{eff}}, \tag{125}$$

up to dimensionless shape-dependent factors of order unity.

Identifying this energy with the electron rest mass, $E_{\text{sol}} \sim m_e c^2 \approx 0.511\,\text{MeV}$, and expressing all quantities in natural units ($\hbar = c = 1$), one finds that reproducing the electron mass requires

$$\lambda_{\text{eff}} \;\sim\; 10^{-44}, \tag{126}$$

for χ_c normalized near the Planck scale.

The appearance of such a small effective parameter should be viewed as a diagnostic indicator of deep scale separation rather than as evidence of fine-tuning, analogous to exponentially small gaps generated by collective or topological mechanisms in condensed-matter systems.

Such an extremely small value should not be interpreted as a fundamental coupling. Rather, it strongly suggests that λ_{eff} is dynamically generated through collective relaxation, projection effects, and topological constraints of the χ field.

Summary.

Localized solitonic configurations of the projected field χ_{eff} naturally possess finite effective masses determined by their size, internal organization, and topological class. Rather than predicting specific numerical values, Cosmochrony constrains the *scaling, ordering, and stability* of masses through geometric and spectral principles.

This structural quantitativity provides a coherent foundation for future extensions toward a fully predictive effective theory, without compromising the pre-geometric nature of the fundamental χ field.

B.4 Example: 4π-Periodic Soliton and Spinorial Behavior

This subsection provides an *explicit illustrative construction* supporting the topological interpretation of spin and statistics presented in Section 8.12. Its purpose is not to restate the phenomenological conclusions established there, but to demonstrate, through a minimal effective example, the *topological plausibility* of spinorial behavior emerging from localized scalar excitations.

The construction is intentionally minimal and purely effective. It does not constitute a microscopic derivation of fermions, nor does it introduce a fundamental spinor degree of freedom. Rather, it illustrates how 4π-periodic transformation behavior may arise from nontrivial topology in the configuration space of admissible projected descriptions once a projectable regime is reached.

All geometric notions used below refer exclusively to the effective projected field χ_{eff}. The fundamental χ field itself does not admit spatial localization, complex structure, or intrinsic phase.

Phase-Twisted Effective Solitonic Configuration

In the projectable regime, certain localized excitations of χ admit an effective internal organization that can be parametrized by an angular variable. For illustrative purposes only, such configurations may be represented using a complex-valued proxy field,

$$\chi_{\text{eff}}(x) = \eta \tanh(\kappa x)\, e^{i\theta(x)}, \tag{127}$$

where:

- the underlying physical field remains real,
- the complex phase does *not* represent an independent internal degree of freedom,
- the phase θ parametrizes the internal cyclic structure of the effective solitonic configuration.

Equivalently, this is an embedding of a cyclic internal label into a complex notation; no $U(1)$ symmetry or conserved phase current is assumed.

This representation should be understood purely as a convenient encoding of the internal organization of the excitation in effective space.

Choosing the effective rotation parameter α and defining

$$\theta(\alpha) = \frac{\alpha}{2}, \tag{128}$$

implies the 4π periodicity

$$\theta(\alpha + 4\pi) = \theta(\alpha) + 2\pi, \tag{129}$$

whereas a 2π cycle yields a globally inequivalent internal organization.

Topological Interpretation

The 4π periodicity does not originate from the introduction of a complex field or an intrinsic phase. It reflects a nontrivial topology of the configuration space of admissible projected configurations.

Although the spatial projection of the excitation may appear unchanged after a 2π rotation, the internal organization of the configuration is not. Only a 4π rotation restores full equivalence in the space of effective descriptions.

This behavior mirrors the double-cover structure $\mathrm{SU}(2) \to \mathrm{SO}(3)$ characteristic of spinorial representations. In the present framework, however, this structure arises from the topology of solitonic configurations of χ_{eff}, rather than from a fundamental spinor ontology.

Relation to Fermionic Transformation Properties

At the effective level, 4π-periodic excitations naturally acquire a sign change under 2π rotations. In multi-excitation configurations, this topological property implies that

the exchange of two identical excitations cannot be continuously deformed into the identity without crossing a topologically nontrivial sector.

This provides a geometric basis for fermion-like transformation behavior and fermion-like exchange phase (a sign change in the simplest sector). In full generality this requires the multi-excitation configuration space and its braid structure, which is beyond the scope of this illustrative example. The construction does not constitute a proof of the spin–statistics theorem; rather, it demonstrates that fermionic characteristics can emerge consistently from topologically constrained scalar-field excitations.

Explicit half-angle map and sign inversion.

To make the spin-$\frac{1}{2}$ correspondence explicit, let $\alpha \in [0, 2\pi]$ denote an *effective* rotation parameter acting on the localized configuration in the projectable regime. The defining topological feature is that the relevant loop in configuration space is non-contractible at 2π but becomes contractible at 4π.

A minimal way to encode this double-cover behavior is to introduce an effective spinorial descriptor $\psi(\alpha)$ whose phase advances by a *half-angle*:

$$\psi(\alpha) \;\equiv\; \psi_0\, e^{i\alpha/2}. \tag{130}$$

Then a 2π cycle produces a sign inversion,

$$\psi(\alpha + 2\pi) = \psi_0\, e^{i(\alpha+2\pi)/2} = -\,\psi_0\, e^{i\alpha/2} = -\psi(\alpha), \tag{131}$$

while a 4π cycle restores the original state,

$$\psi(\alpha + 4\pi) = \psi(\alpha). \tag{132}$$

$$\begin{aligned} &\alpha : 0 \to 2\pi \Rightarrow \text{nontrivial loop in } \mathcal{C}_{\text{eff}}\ (\mathbb{Z}_2) \Rightarrow \psi \mapsto -\psi, \\ &\alpha : 0 \to 4\pi \Rightarrow \text{trivial loop (homotopic to identity)} \Rightarrow \psi \mapsto \psi. \end{aligned} \tag{133}$$

In this construction, ψ is not a fundamental field: it is a compact *collective label* for the topological class of the solitonic configuration in the space of admissible projected descriptions. The sign change at 2π is therefore not imposed as a quantum postulate; it is an effective encoding of the $\mathbb{Z}_2$ obstruction associated with the 4π periodicity of the configuration.

(See Sec. B.6 for the configuration-space statement $\pi_1(\mathcal{C}_{\text{eff}}) = \mathbb{Z}_2$ and its effective implication $\psi \mapsto -\psi$ under a 2π loop.)

Conceptual Scope and Limitations

Conceptual Scope and Limitations

The purpose of this example is strictly illustrative. It demonstrates that:

- spinorial transformation behavior does not require a fundamental spinor field,
- 4π-periodicity may arise from topological obstructions in configuration space,

- fermion-like exchange behavior can emerge from scalar excitations with nontrivial topology.

No claim is made that this construction reproduces the full dynamics, interactions, or statistics of Standard Model fermions. It provides a concrete realization supporting the unified interpretation of spin and statistics developed in Section 8.12. A fully relational formulation of these topological properties, independent of any auxiliary geometric representation, is discussed in Appendix **??**.

B.5 Relation to Classical Limits

In Cosmochrony, the emergence of classical behavior does not correspond to the introduction of an independent theoretical layer. Instead, classical physics arises as a *dynamical regime* of the same underlying scalar structure, characterized by smoothness, dilution of localized excitations, and the suppression of topological and relational effects.

Weakly structured regime and effective linearization.

In regimes where the fundamental field χ admits a stable projective representation and where its effective projection χ_{eff} varies slowly over large scales, localized excitations become dilute and weakly interacting. Under these conditions, the dynamics of χ_{eff} can be linearized at the level of effective perturbations only around a quasi-homogeneous background configuration.

In this regime, small perturbations propagate as weak disturbances on an effectively flat geometric background. Superposition, approximate locality, and linear wave propagation emerge as effective properties of the coarse-grained relaxation dynamics. This reproduces the operational content of classical field theories and of free or weakly interacting quantum field theories formulated on Minkowski spacetime.

This correspondence should be understood as an *effective recovery* rather than as an ontological reduction. Cosmochrony does not reduce to standard quantum field theory; rather, standard field theories appear as limiting descriptions valid when relational structure becomes dynamically inert.

Suppression of relational and topological effects.

In the weakly structured regime, topological constraints associated with solitonic configurations are either absent or dynamically irrelevant. The configuration space effectively factorizes, and collective relaxation dominates over localized structural organization. As a result, particle-like excitations behave as approximately independent degrees of freedom, and classical intuition becomes applicable.

The classical limit therefore corresponds to a regime in which the relational content of χ is present but operationally inaccessible, masked by coarse-graining and scale separation.

Nonlinear regime and effective curvature.

Conversely, in regimes of strong spatial variation of χ_{eff} or high density of localized excitations, nonlinear effects dominate the dynamics. Large gradients locally constrain

relaxation, inducing effective curvature, time dilation, and horizon-like behavior in the emergent geometric description.

These regimes reproduce the phenomenology associated with curved spacetime, gravitational collapse, and strong-field effects, while remaining governed by the same underlying scalar dynamics. No additional gravitational degrees of freedom are introduced; curvature emerges as a collective response of the relaxation structure of χ_{eff}.

Meaning of the classical limit in Cosmochrony.

The classical limit in Cosmochrony is therefore not defined by $\hbar \to 0$, nor by the suppression of quantum postulates. It corresponds to a regime in which:

- the effective projection χ_{eff} is smooth and slowly varying,
- localized excitations are dilute and weakly correlated,
- topological and relational constraints are dynamically suppressed,
- coarse-graining yields stable geometric descriptions.

In this regime, classical spacetime and standard field dynamics emerge as reliable, approximate descriptions. Their validity reflects not fundamental structure, but the stability of a particular relaxation regime of the underlying χ field.

B.6 Status of the Formulation

The formulation presented in this work should be understood as a *minimal yet structurally complete* at the conceptual level theoretical framework. Its ontological commitments, dynamical principles, and interpretative structure are fully specified at the conceptual level, even though several technical developments remain open.

In particular, a fully covariant action principle formulated solely in terms of the fundamental χ dynamics, as well as a systematic quantization procedure, have not yet been derived in their final and definitive form. These missing elements should not be interpreted as conceptual deficiencies. Rather, they correspond to technical extensions required to interface a fundamentally relational and pre-geometric framework with conventional variational and quantum formalisms that presuppose spacetime structure.

Crucially, the absence of a finalized action or quantization scheme does not obstruct the recovery of known physical phenomenology at the level of qualitative structure and effective behavior. Throughout this work, general relativity and quantum field theory emerge as *effective, coarse-grained descriptions* valid within specific dynamical regimes of the projected field χ_{eff}. They are not introduced as independent axioms, but arise as stable limits of the underlying relaxation dynamics.

The present formulation therefore occupies a well-defined intermediate status. It is not intended as a closed or final theory, nor as a phenomenological model tuned to reproduce specific experimental data. Instead, it provides a coherent ontological and dynamical foundation from which both geometric and quantum structures can emerge, while remaining open to future refinements that may enhance its mathematical completeness, formal elegance, and predictive scope.

In this sense, Cosmochrony should be viewed as a foundational framework rather than as a fully developed effective field theory: its primary contribution lies in clarifying

what is fundamental and *how known physical structures can arise*, rather than in prescribing their final mathematical implementation.

B.7 Soliton and Particle Solutions

Within the Cosmochrony framework, elementary particles are interpreted as stable or metastable localized configurations arising in the *projectable regime* of the scalar field χ. These configurations, hereafter referred to as χ-solitons, emerge from nonlinear self-organization of the relaxation dynamics and persist as localized resistances to global relaxation.

This interpretation does not rely on the postulation of additional fundamental degrees of freedom. The only fundamental entity is the scalar field χ, which is not defined on spacetime. Spatial localization, energy, and particle-like persistence arise only once an effective geometric projection χ_{eff} becomes applicable.

While the fundamental field is scalar, certain solitonic configurations of χ_{eff} possess a nontrivial internal organization that cannot be faithfully encoded by a single real scalar variable. In particular, configurations characterized by internal cyclic structure, nontrivial winding, and 4π-periodicity exhibit transformation properties that require a double-valued representation under effective rotations.

In such cases, an effective spinorial description becomes unavoidable at the level of transformation properties and exchange behavior. This does not imply the existence of fundamental spinor fields. Rather, spinorial variables arise as *collective descriptors* encoding the internal topology and spectral structure of fermionic χ-solitons.

At the phenomenological level, these excitations admit a representation in terms of Dirac spinors. This representation should be understood as an emergent and coarse-grained description of the internal degrees of freedom of χ-solitons, not as an ontological extension of the theory. Within this regime, the Dirac equation appears as the minimal effective dynamical structure compatible with:

- approximate locality in the projected geometric description,
- effective relativistic covariance,
- and the topological constraints associated with 4π-periodic configurations.

in the absence of strong interactions or non-linear collective effects.

From this perspective, the Dirac structure does not introduce new fundamental entities. It provides a compact and universal encoding of the internal topology, spectral stability, and transformation behavior of fermionic solitons. Spin, fermionic statistics, and exclusion behavior arise as effective consequences of the nontrivial configuration space of these scalar-field excitations, rather than as independent postulates.

The existence and stability of χ-solitons impose structural constraints on the effective self-interaction functional governing the projected dynamics. Although the explicit form of this functional remains undetermined, it must satisfy the following minimal requirements:

1. the support of localized configurations with finite effective mass,
2. dynamical stability under small perturbations,

3. and the existence of topologically inequivalent sectors corresponding to distinct classes of particle-like excitations.

The detailed derivation of effective Dirac dynamics from fluctuations around χ-soliton backgrounds, as well as the emergence of a realistic mass spectrum, remains an open mathematical problem. These issues are addressed at a programmatic and illustrative level in Sections B.2–B.4 and further discussed in Appendix B.8.

B.8 Perspectives: Towards a Derivation of the Proton-to-Electron Mass Ratio

The proton-to-electron mass ratio is one of the most precisely measured dimensionless quantities in physics. Within the Cosmochrony framework, the purpose of this section is not to derive this value from first principles, but to clarify how such a ratio could emerge *structurally* from the spectral and topological organization of localized solitonic excitations of the projected field χ_{eff}.

The discussion should therefore be understood as a minimal and exploratory spectral ansatz. Its aim is to identify the relevant mechanisms, constraints, and scaling relations that any successful derivation would have to satisfy, rather than to provide a complete microscopic calculation.

Spectral Stability Hypothesis

Let χ_{sol} denote a stationary localized configuration arising in the projectable regime of the χ dynamics. Small perturbations $\delta\chi_{\text{eff}}$ around this background are governed, at the coarse-grained level, by a linear stability operator $\mathcal{L}_{\text{sol}}$, defined as the second variation of an effective localization functional.

Normal modes satisfy the eigenvalue problem

$$\mathcal{L}_{\text{sol}}\psi_n = \lambda_n \psi_n. \tag{134}$$

The eigenvalues λ_n characterize the resistance of the soliton to localized deformations. They encode intrinsic stiffness scales associated with the internal organization of the solitonic configuration.

Spectral mass scaling.

In regimes where an effective wave description applies, the normal modes exhibit characteristic oscillation frequencies

$$\omega_n = c\sqrt{\lambda_n}. \tag{135}$$

Identifying the lowest nontrivial frequency with the rest energy of the excitation leads to the effective scaling relation

$$m_n \;\propto\; \sqrt{\lambda_n}\,\chi_c, \tag{136}$$

where χ_c denotes a characteristic geometric scale associated with the spatial extension of the solitonic configuration in the projected regime.

This relation does not define a fundamental mass formula. It provides a coarse-grained link between spectral stability and inertial mass, consistent with the interpretation of mass as integrated resistance to relaxation.

Dimensional interpretation.

The eigenvalues λ_n carry dimensions of inverse length squared, reflecting the restoring stiffness of the soliton per unit deformation. The scale χ_c has dimensions of length and sets the geometric extension over which this stiffness is distributed.

The combination $\lambda_n \chi_c^2$ therefore defines a characteristic energy scale,

$$E_n \sim \lambda_n \chi_c^2, \tag{137}$$

which is identified with a rest energy through the effective relativistic matching $E = mc^2$ once a spacetime description becomes applicable.

This identification does not invoke a fundamental quantum constant and remains valid independently of the emergence of $\hbar_{\text{eff}}$.

Projection Scale and Effective Normalization

The fundamental description of the χ field is formulated in terms of relational relaxation rules rather than a spacetime action with fixed physical units. When a continuum approximation applies, an effective action for perturbations around a stable soliton may be introduced as a bookkeeping device.

In this regime, the effective action for perturbations $\delta\chi_{\text{eff}}$ may be written schematically as

$$S_{\text{eff}}[\delta\chi] = \int d^4x \, \frac{1}{2} \left(\frac{\chi_c}{c}\right)^2 \left[(\partial_t \delta\chi)^2 - c^2 (\nabla \delta\chi)^2\right]. \tag{138}$$

Expressing this action in emergent spacetime coordinates introduces a geometric rescaling factor linking χ-space and spacetime lengths. As a result, the canonical normalization of localized modes involves a quadratic scaling factor of the form

$$\left(\frac{\chi_c}{\ell_{\text{spacetime}}}\right)^2, \tag{139}$$

which controls the effective normalization of spectral quantities.

This factor reflects the geometric projection from the relational χ structure to emergent spacetime observables. It does not represent a fundamental coupling constant.

Energy Levels from Spectral Stability

The discrete energy levels associated with solitonic excitations follow from the spectral properties of the stability operator $\mathcal{L}_{\text{sol}}$, not from canonical quantization.

For a soliton labeled by n, the gradient contribution to the effective energy scales as

$$E_{\text{grad}}^{(n)} \sim c^2 \lambda_n \mathcal{N}_n, \tag{140}$$

where $\mathcal{N}_n$ denotes a normalization factor determined by the spatial profile of the mode.

In the spacetime-based description, this energy is identified with the rest-mass energy,

$$E_n \equiv m_n c^2. \tag{141}$$

The discretization of E_n arises from topological classification and spectral stability, not from postulated quantum operators. The role of $\hbar_{\text{eff}}$ appears only when matching this description to quantum observables.

Elementary versus Composite Spectral Structures

A key distinction must be drawn between elementary and composite solitonic excitations. Elementary particles, such as leptons, are expected to correspond to topologically elementary solitons whose inertial mass is dominated by a single lowest stability eigenvalue.

By contrast, baryonic excitations are composite configurations. Their mass reflects the combined contribution of several coupled stability modes associated with a bound structure. Mass ratios therefore take the schematic form

$$\frac{m_{\text{comp}}}{m_{\text{elem}}} \sim \frac{\sum_k \sqrt{\lambda_k^{(\text{comp})}}}{\sqrt{\lambda_0^{(\text{elem})}}}, \tag{142}$$

rather than the ratio of two isolated eigenvalues.

Ansatz for the Proton as a Composite Soliton

As an exploratory working hypothesis, the proton is modeled as a composite solitonic excitation. Specifically:

- the electron corresponds to a topologically elementary soliton with a fundamental stability eigenvalue λ_e,
- the proton corresponds to a bound configuration involving three such elementary solitons, supplemented by an additional collective binding mode with eigenvalue λ_{bind}.

The choice of a three-soliton composite is motivated by stability considerations observed in a wide class of nonlinear field theories admitting topological solitons, where three-body bound states often exhibit enhanced stability due to geometric phase locking [47]. This choice is not derived here from a classification of χ-soliton sectors and is not postulated as fundamental.

Skyrmion models in QCD provide an instructive analogy, but no dynamical equivalence is assumed. The relevance of this analogy lies in the universality of topological stabilization mechanisms, which do not depend on the presence of a non-Abelian gauge symmetry [48].

Mass Ratio from Spectral Scaling

Under these assumptions, the effective eigenvalue associated with the proton may be written schematically as

$$\lambda_p \;\approx\; \lambda_{\text{bind}} + 3\lambda_e, \tag{143}$$

leading to the mass ratio

$$\frac{m_p}{m_e} \;\approx\; \sqrt{\frac{\lambda_{\text{bind}} + 3\lambda_e}{\lambda_e}}. \tag{144}$$

In the binding-dominated regime $\lambda_{\text{bind}} \gg \lambda_e$, this reduces to

$$\frac{m_p}{m_e} \;\approx\; \sqrt{\frac{\lambda_{\text{bind}}}{\lambda_e}}. \tag{145}$$

Matching the observed ratio $m_p/m_e \simeq 1836$ therefore imposes the spectral constraint

$$\frac{\lambda_{\text{bind}}}{\lambda_e} \;\sim\; 3.4 \times 10^6. \tag{146}$$

This relation is not derived here. *The role of the empirical value is solely to delimit the scale of spectral separation required; the framework makes no claim that this separation is unique, minimal, or numerically rigid.* It is identified as a consistency condition constraining the relative spectral organization of elementary and composite solitonic sectors.

We interpret this large spectral hierarchy as defining a dimensionless *spectral packing fraction* α, characterizing the relative density of admissible stability modes in composite versus elementary solitonic sectors. Specifically, we define

$$\alpha \;\equiv\; \frac{\lambda_e}{\lambda_{\text{bind}}} \;\sim\; 3 \times 10^{-7}. \tag{147}$$

This quantity does not represent a coupling constant, but a structural measure of spectral compression induced by topological binding.

Topological Interpretation of the Spectral Hierarchy

Although the ratio $\lambda_{\text{bind}}/\lambda_e$ is introduced here as a spectral consistency condition, it is natural to seek a geometric or topological interpretation of this large hierarchy.

In particular, the composite nature of the proton ($Q = 3$) suggests that the associated binding modes may correspond to configurations of increased topological complexity. If the stability spectrum of L_{sol} is controlled by the effective multiplicity of internal configurations admitted under the non-injective projection Π, then λ_{bind} may be interpreted as a coarse-grained measure of the volume of the corresponding projection fiber.

From this perspective, the large ratio $\lambda_{\text{bind}}/\lambda_e \sim 10^6$ reflects not an arbitrary energy scale separation, but the rapid growth of internal configuration space associated with topologically composite solitons.

Indicative Geometric Scale

Although no explicit geometric or topological model is developed at this stage, it is useful to translate the observed spectral hierarchy into a characteristic dimensionless scale.

At a purely heuristic level, one may assume that the effective spectral weight of a composite soliton grows quadratically with a characteristic internal scale χ_c, so that

$$\frac{\lambda_{\text{bind}}}{\lambda_e} \sim \chi_c^2. \tag{148}$$

Under this assumption, the empirical constraint $\lambda_{\text{bind}}/\lambda_e \sim 3.4 \times 10^6$ corresponds to a scale of order

$$\chi_c \sim \mathcal{O}(10), \tag{149}$$

with a representative numerical value

$$\chi_c \approx 8.3. \tag{150}$$

Both expressions should be regarded as indicative rather than derived. They simply emphasize that the required spectral hierarchy corresponds to a modest geometric amplification, not to an extreme or finely tuned parameter choice. *No physical meaning should be attached to this numerical value in the absence of an explicit topological model.*

An Explicit Working Ansatz for $V(\chi)$

In the present appendix, the primary driver of mass hierarchies is the spectral organization of the solitonic stability operator. Nevertheless, turning this program into a falsifiable computational scheme requires an explicit *working* form for the effective potential $V(\chi)$, not as a fundamental source of masses, but as a controlled perturbation that: (i) stabilizes localized sectors, (ii) selects admissible core amplitudes, and (iii) produces fine splittings within a given topological class.

A minimal two-scale ansatz compatible with these roles is a *multi-well* (or weakly periodic) potential with a characteristic amplitude scale η and stiffness scale λ:

$$V(\chi) \;=\; \frac{\lambda}{4}\left(\chi^2 - \eta^2\right)^2 \;+\; \varepsilon\,\eta^4\Big[1 - \cos\Big(\frac{\chi}{\eta}\Big)\Big], \tag{151}$$

where $\varepsilon \ll 1$ is a dimensionless modulation parameter. The first term provides a robust double-well localization mechanism; the second term introduces a gentle quasi-periodic micro-structure capable of generating controlled intra-sector splittings without reparameterizing the global mass scale.

The interpretation in Cosmochrony is strictly *effective*: the coefficients in Eq. (151) are not fundamental constants, but phenomenological descriptors of how coarse-grained projectability constraints reshape the admissible configurations of χ_{eff}.

Linking (λ, η) to Observables Without Making Mass Fundamental

The parameters η and λ are introduced only to control the *shape* and *stiffness* of admissible localized sectors in the projected description. Their observable imprint is therefore indirect: they enter through how they shift the stability spectrum $\{\lambda_n\}$ of $\mathcal{L}_{\rm sol}$, and how robustly a given topological sector remains projectable under perturbations.

Dimensionless control combinations.

For a localized profile with characteristic extension χ_c, the potential introduces two natural dimensionless combinations,

$$g \;\equiv\; \lambda\,\chi_c^2\,\eta^2, \qquad u \;\equiv\; \varepsilon\,, \tag{152}$$

which govern (i) the curvature scale of $V(\chi)$ near admissible minima, and (ii) the magnitude of sub-structure corrections. The spectral hierarchy derived above is then phrased as the statement that the *ratio* m_p/m_e is predominantly controlled by topological/composite spectral packing, while (g, u) control the *stability* and *splittings* of the low-lying spectrum.

Matching strategy using the proton-to-electron ratio.

Denote by $\lambda_e(g, u)$ the fundamental stability eigenvalue of the $Q = 1$ sector, and by $\lambda_{\rm bind}(Q = 3; g, u)$ the characteristic binding-band scale of the composite sector. The empirical constraint $\lambda_{\rm bind}/\lambda_e \sim 3.4 \times 10^6$ derived in Eq. (the spectral constraint above) is then reinterpreted as a *feasibility condition*:

$$\exists\,(g, u) \text{ s.t.} \quad \frac{\lambda_{\rm bind}(Q = 3; g, u)}{\lambda_e(g, u)} \;\approx\; 3.4 \times 10^6, \tag{153}$$

while remaining stable under small variations of (g, u). In other words, (λ, η) are not tuned to *set* the mass ratio, but to ensure that the *topological spectral mechanism* can realize the required hierarchy in a broad basin of effective parameters.

The topological charge Q should not be interpreted as a linear mass multiplier. Its role is to constrain the admissible spectral organization of the soliton, from which the observed mass hierarchy emerges non-additively.

Secondary observables: fine splittings as diagnostics.

Once a viable region in (g, u) exists, the same potential ansatz predicts that small intra-sector differences (e.g. neutron–proton splitting, excited baryonic resonances, or generational splittings) arise from:

- perturbative eigenvalue shifts $\delta\lambda_n(g, u)$ induced by local curvature variations of V,
- weak breaking of idealized symmetries in composite sectors,
- environment-dependent dressing of the effective coefficients through projectability constraints.

These effects are conceptually aligned with the claim that $V(\chi)$ controls fine structure rather than the global mass scale.

Numerical Program: From $V(\chi)$ to Spectral Hierarchies

The numerical goal is not to simulate QCD, but to test a *structural* claim: whether bounded relaxation dynamics plus a controlled effective potential admits stable localized sectors whose stability spectra exhibit (i) a robust elementary mode λ_e, and (ii) a dense binding band λ_{bind} in a composite $Q = 3$ sector, separated by a large gap.

A minimal computational pipeline is:

1. **Dynamics and formation.** Implement the bounded relaxation update rule for χ in a discretized representation (spectral/finite-element basis or lattice proxy), including the effective potential term Eq. (151) as a controlled perturbation.
2. **Soliton harvesting.** Identify long-lived localized configurations and classify them by topological diagnostics (winding/charge proxies, knot-like invariants when available, or stability under deprojection/reprojection cycles).
3. **Stability operator extraction.** For each harvested configuration, compute the linearized stability operator $\mathcal{L}_{\text{sol}}$ (second variation of the effective localization functional) and extract its low-lying eigen-spectrum.
4. **Spectral ratio test.** Evaluate whether the emergent spectra support a regime where $\lambda_{\text{bind}}/\lambda_e \sim 10^6$ arises *without fine tuning*, and whether the ratio remains stable under moderate variation of (g, u).
5. **Fine-structure diagnostics.** Measure the sensitivity of subleading splittings $\delta\lambda_n$ to (g, u), providing a concrete handle for how $V(\chi)$ affects intra-sector structure while leaving the leading hierarchy topologically controlled.

This numerical program connects directly to the broader simulation framework described in the technical appendix on simulation algorithms and spectral extraction, and provides a clear set of falsifiable diagnostics: either large, robust spectral gaps appear generically in composite sectors, or the proposed topological-spectral mechanism fails to reproduce the required hierarchy.

Transition

The role of $V(\chi)$ is therefore operational: it stabilizes and perturbs admissible projected sectors while the *origin* of the mass hierarchy remains spectral and topological. This separation is developed further in the subsequent appendices on spectral ontology and on the secondary role of $V(\chi)$.

B.9 Spectral Scaling and the Projection Ontology

The preceding derivation of the mass ratio m_p/m_e rests on a fundamental shift in the ontology of mass. Within the Cosmochrony framework, inertial mass is no longer treated as an intrinsic "charge", but as a spectral signature of projection visibility.

Mass as Spectral Weight

The non-injective nature of the projection Π (see Section 2.10) implies that any effective particle in χ_{eff} corresponds to a large equivalence class of micro-configurations in the substrate χ. The stability eigenvalues λ_n of the operator L_{sol} can therefore be reinterpreted as a coarse-grained measure of this structural multiplicity, or *fiber weight*.

A configuration that requires a larger set of internal modes to remain stable and projectable manifests a higher resistance to global relaxation, and thus a higher inertial mass. This "fiber weight" interpretation is diagnostic: it does not claim a one-to-one equality between eigenvalue magnitude and microscopic degeneracy, but asserts that both track the same coarse-grained constraint— projectability under Π and resistance to relaxation.

Invariance of the Ratio

Since the ratio

$$\frac{m_p}{m_e} \approx \sqrt{\frac{\lambda_p}{\lambda_e}} \tag{154}$$

is independent of the absolute action scale $\hbar_\chi$, it is identified as a structurally protected invariant of the projection process itself. This is consistent with the observed universality of the proton-to-electron mass ratio to the extent that it is observationally constrained to be stable, regardless of the global relaxation state of χ.

The Spectral Packing Fraction (α)

The hierarchy between the composite sector (proton) and the elementary sector (electron) is encapsulated by the spectral packing fraction

$$\alpha \equiv \frac{\lambda_e}{\lambda_{\text{bind}}} \approx 3 \times 10^{-7}. \tag{155}$$

While introduced here via an empirical target, α represents the ratio of spectral transmittance under Π. The proton is heavy because its non-trivial topology ($Q = 3$) constrains the stability operator L_{sol} to exhibit a large internal spectral bandwidth. This topological constraint, often heuristically represented (as one possible representative) by a trefoil-like knot configuration, leads to a strong spectral gap between the binding modes λ_{bind} and the fundamental electronic mode λ_e.

Conclusion

While the precise numerical value $m_p/m_e \simeq 1836$ awaits a closed-form derivation from the spectral geometry of L_{sol} on topologically constrained effective manifolds / effective projected geometries, the Cosmochrony framework reformulates the mass-ratio problem in structural terms. The proton-to-electron mass ratio emerges as the macroscopic signature of a spectral gap dictated by the complexity of the substrate's excitations under projection, as schematically illustrated in Fig. 18, rather than as an arbitrary fundamental constant.

Summary and Outlook

Within the Cosmochrony framework, the proton-to-electron mass ratio is interpreted as an emergent constraint on the spectral and topological organization of solitonic excitations, not as a fundamental input parameter.

The analysis presented here provides a coherent toy model identifying the conditions under which such a ratio could arise. Whether the required spectral hierarchy can be

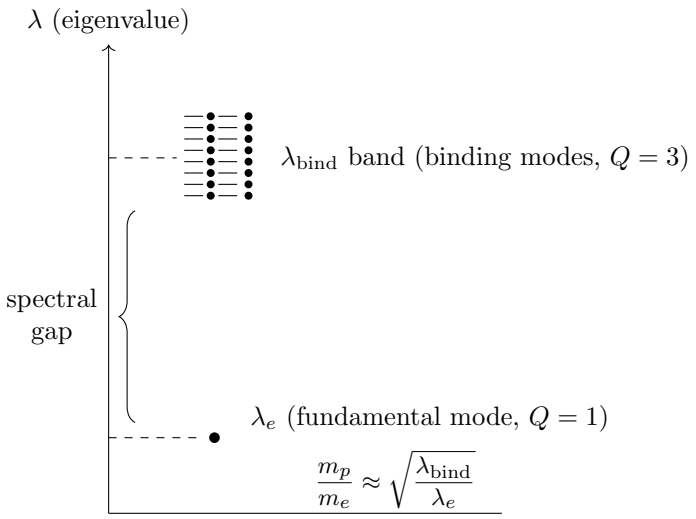

Fig. 18 Conceptual schematic of a spectral gap in the stability spectrum of $\mathcal{L}_{\text{sol}}$. The elementary mode λ_e is separated from a dense band of binding modes near λ_{bind}, illustrating the interpretation of m_p/m_e as a macroscopic signature of spectral organization rather than an intrinsic mass parameter.

generated dynamically from the χ relaxation dynamics remains an open problem, to be addressed through future analytical and numerical investigations.

B.10 Spectral Characterization of Mass and the Secondary Role of $V(\chi)$

This appendix clarifies the conceptual status of inertial mass in the Cosmochrony framework. Physically, mass originates from the resistance of localized configurations to the relaxation of the fundamental χ field. This resistance, however, admits a quantitative and structurally organized description in terms of the spectral properties of an associated stability operator defined in the projectable regime.

Spectral analysis therefore does not redefine the physical origin of inertial mass. Rather, it provides a coherent and potentially calculable characterization of how resistance to relaxation is distributed among stable and metastable configurations.

A central conjecture of Cosmochrony is that particle masses are not fundamental parameters encoded in the nonlinear potential $V(\chi)$. Instead, they emerge as spectral properties of a background-independent relaxation operator defined on a relational substrate, which may be represented, for calculational purposes, by a discrete graph structure.

The graph representation is not ontological but serves as a computational proxy for relational adjacency in the projectable regime.

Mass spectrum as eigenmodes of a relaxation operator.

Localized particle-like excitations are identified with normal modes of an effective relaxation operator $\Delta_G^{(0)}$, which may be represented as a Laplace–Beltrami operator

acting on a graph $G(V, E)$,

$$\Delta_G^{(0)} \psi_n = -\lambda_n \psi_n. \tag{156}$$

The eigenmodes ψ_n characterize the stability of localized solitonic configurations, while the eigenvalues λ_n encode their intrinsic resistance to deformation.

In regimes where an effective spacetime description applies, the inertial masses associated with these modes scale as

$$m_n c^2 \;\propto\; \sqrt{\lambda_n}\, \chi_c, \tag{157}$$

in agreement with the spectral relations introduced in Section B.8. This scaling reflects the fact that inertial mass measures the characteristic frequency associated with the resistance of a localized configuration to χ-field relaxation.

The situation is analogous to bounded elastic systems, where discrete vibrational frequencies arise from geometry and connectivity rather than from adjustable material parameters. Within Cosmochrony, mass hierarchies are therefore interpreted as geometric and topological properties of the underlying relational structure.

A decisive test of this conjecture would consist in computing the low-lying spectrum of $\Delta_G^{(0)}$ on large but finite networks with physically motivated connectivity rules. Even approximate agreement with observed mass ratios would strongly support the spectral origin of inertial mass and the non-fundamental role of $V(\chi)$.

Separation of descriptive levels.

To avoid circular dependencies between geometry, dynamics, and emergent particle properties, Cosmochrony distinguishes three conceptual levels.

At the fundamental level, inertial masses are associated with the spectral properties of a background-independent relaxation operator $\Delta_G^{(0)}$, defined solely by the intrinsic relational connectivity of the substrate. This operator is not tied to any spacetime geometry or instantaneous χ configuration and provides a stable spectral backbone.

At the emergent geometric level, coarse-grained configurations of χ_{eff} give rise to effective notions of spacetime, including curvature, gravitational time dilation, and cosmological expansion. These geometric effects influence propagation and interaction, but do not redefine the underlying spectral operator responsible for mass generation.

Finally, fast dynamical processes such as radiation, scattering, and decoherence correspond to interaction-induced redistributions of relaxation potential within the χ field. These processes affect observables without modifying the fundamental spectral structure.

Residual role of the potential $V(\chi)$***.***

Within this spectral picture, the nonlinear potential $V(\chi)$ plays a secondary and effective role. It does not set the overall mass scale. Instead, it provides a local coarse-grained description of nonlinear stabilization mechanisms associated with low-lying spectral modes.

The admissible form of $V(\chi)$ is constrained by the requirement that it support stable solitonic configurations compatible with the pre-existing spectral structure. It encodes neither an independent interaction nor a fundamental energy density.

Origin of the effective potential $V(\chi)$.

Characterizing $V(\chi)$ as secondary does not imply arbitrariness. Rather, $V(\chi)$ should be understood as an effective descriptor of the local nonlinear response of the relaxation dynamics in the vicinity of a stable configuration.

At the fundamental level, the dynamics of χ are governed by bounded relaxation rules and their associated spectral structure. When this dynamics is projected onto a reduced functional subspace associated with a localized soliton, nonlinear self-consistency constraints induce an effective local restoring structure. In this reduced description, these constraints may be summarized by an effective potential $V(\chi)$.

Different admissible forms of $V(\chi)$ correspond to different coarse-graining choices, while leaving invariant the underlying spectral origin of mass and stability.

Potential-induced corrections to stability eigenvalues.

To illustrate how $V(\chi)$ can modify stability eigenvalues without altering their spectral origin, consider the illustrative form

$$V(\chi) = \lambda \left(\chi^2 - \chi_c^2\right)^2 . \tag{158}$$

Expanding around the relaxed background $\chi = \chi_c$ yields a quadratic contribution for small fluctuations $\delta\chi$,

$$V(\chi_c + \delta\chi) \simeq \frac{1}{2} \left.\frac{d^2V}{d\chi^2}\right|_{\chi_c} (\delta\chi)^2 + \cdots , \tag{159}$$

with

$$\left.\frac{d^2V}{d\chi^2}\right|_{\chi_c} \propto \lambda\, \chi_c^2. \tag{160}$$

This term contributes additively to the linearized stability operator, shifting the eigenvalues as

$$\lambda_n \;\longrightarrow\; \lambda_n^{(0)} + \Delta\lambda_n^{(V)}. \tag{161}$$

For composite solitons, such corrections may differ slightly between closely related configurations (e.g., neutron versus proton), generating small mass splittings. By contrast, ratios dominated by topological organization (such as m_p/m_e) remain largely insensitive to the detailed form of $V(\chi)$.

Summary.

In Cosmochrony, inertial mass is fundamentally a spectral property of the relaxation dynamics of the χ field. The potential $V(\chi)$ serves as a derived, effective descriptor controlling fine structure, not as a primary source of mass. Extending this spectral characterization toward quantitative mass predictions requires specifying the relaxation operator and its boundary conditions, particularly for composite solitonic sectors.

B.11 Spectral Stability and the Emergence of $\hbar_{\text{eff}}$

In Cosmochrony, the effective Planck constant $\hbar_{\text{eff}}$ is not introduced as a fundamental quantum postulate. Instead, it emerges as a scaling parameter linking spectral stability of χ-field solitons to effective spacetime observables.

Fundamental scales of the χ dynamics

The χ field is characterized by three independent dynamical scales:

- K_0: maximal relaxation stiffness, with dimensions $[L^{-2}]$,
- χ_c: correlation length at which solitonic configurations stabilize,
- c: maximal relaxation speed.

From these, one may define a natural unit of action associated with the relaxation dynamics,

$$\hbar_\chi \equiv \frac{c^3}{K_0 \chi_c}, \tag{162}$$

which has the dimensions of action and is independent of the standard Planck constant. This quantity is introduced on dimensional grounds as the unique action scale constructible from the fundamental relaxation parameters.
Here and in the following, K_0 and χ_c denote the *bare substrate parameters*, i.e. universal invariants characterizing the rigidity and correlation capacity of the χ field. The scale-dependent values discussed in D arise only after coarse-graining and do not enter the definition of $\hbar_\chi$.

Spectral origin of effective quantization

Quantization in Cosmochrony follows from the discrete spectrum of the stability operator $\Delta_G^{(0)}$. For a solitonic excitation with eigenvalue λ_n, the characteristic frequency of small oscillations scales as

$$\nu_n \sim \frac{c}{\chi_c} \sqrt{\lambda_n} \mathcal{N}_n^{1/2}. \tag{163}$$

At the effective spacetime level, identifying the rest energy with the product of this frequency and an effective action scale yields

$$E_n = \hbar_{\text{eff}} \, \nu_n, \tag{164}$$

from which $\hbar_{\text{eff}}$ emerges as a geometric and spectral quantity, not as an independent constant.

Regime-dependent scaling

The effective value of $\hbar_{\text{eff}}$ depends on the scale at which the system is probed. In regimes where the characteristic spacetime scale $\ell_{\text{spacetime}}$ is comparable to χ_c,

$$\hbar_{\text{eff}} \approx \hbar_\chi, \tag{165}$$

recovering standard quantum behavior.

At macroscopic scales $\ell_{\text{spacetime}} \gg \chi_c$,

$$\hbar_{\text{eff}} \approx \hbar_\chi \left(\frac{\chi_c}{\ell_{\text{spacetime}}} \right)^2, \tag{166}$$

leading to a strong suppression of quantum effects and the emergence of classical behavior. This suppression reflects reduced spectral accessibility rather than decoherence or wavefunction collapse.

Consistency with quantum phenomenology

In the microscopic regime, where $\hbar_{\text{eff}} \approx \hbar$, standard quantization relations $E = \hbar\nu$ are recovered as effective descriptions. This agreement is not postulated but follows from the scaling behavior of $\hbar_{\text{eff}}$ once the projected regime matches laboratory scales.

Numerical constraints.

Reproducing particle-scale quantum behavior requires

$$K_0 \chi_c^2 \sim \hbar, \tag{167}$$

which constrains the admissible values of the relaxation stiffness and correlation length. These constraints are consistent with soliton stability and do not require fine tuning. This relation should be read as an order-of-magnitude consistency condition, not as an equality fixing independent parameters.

B.12 Renormalization of Substrate Parameters

To maintain consistency between the fundamental definition of $\hbar_\chi$ and the scale-dependent observations in Appendix D, we distinguish between:

- **Bare Parameters (K_0, χ_c):** Universal invariants of the χ substrate that determine the fundamental quantum of action $\hbar_\chi$.
- **Effective Parameters ($K_{\text{eff}}, \chi_{\text{eff}}$):** Environment-dependent values emerging from the coarse-graining of relaxation constraints, as detailed in Section D.

The universality of $\hbar$ and the spectral invariant α_{spec} (formerly α in Section B.9) stems from their dependence on the ratio of these bare quantities, which remains invariant under projective scaling *within a given relaxation epoch.*
In particular, dimensionless coupling constants such as the electromagnetic fine-structure constant α_{EM} do not inherit any arbitrariness from the substrate parameters (this statement concerns structural invariance, not a first-principles derivation of their numerical values). Within the Cosmochrony framework, the electric charge e is not treated as a free gauge parameter, but as a property of localized solitonic configurations. The associated transmittance is not an adjustable quantity but a geometric invariant of the soliton's spectral embedding relative to the projection fiber Π. As a result, the dependence on the substrate rigidity K_0 cancels out in dimensionless ratios,

ensuring their invariance within a fixed relaxation epoch up to higher-order projection corrections.

Summary.

Within Cosmochrony, both inertial mass and effective quantization emerge from the same spectral stability structure of the χ relaxation dynamics. The Planck constant appears not as a fundamental input, but as a scale-dependent effective parameter encoding the projection from relational dynamics to spacetime-based observables.

B.13 Structural Origin of Quantum Correlations and Non-Locality

This section provides a conceptual extension of the Cosmochrony framework, illustrating how quantum correlations and spin may be interpreted geometrically within a strictly monistic and non-injective projection ontology. The discussion is interpretative in nature and does not introduce additional dynamical postulates.

The non-injective nature of the projection operator Π, which maps the relational substrate χ onto the effective 4D manifold, provides a structural reinterpretation of quantum non-locality and entanglement. In this framework, EPR-type correlations are not viewed as the result of superluminal signaling, but as a direct consequence of the **shared ontological source** of projected observables. This shared source is relational rather than state-deterministic, and does not imply the existence of hidden spacetime-local variables.

Non-injectivity and Structural Identity.

Within Cosmochrony, what is effectively perceived as two spatially separated particles may correspond to a single, unified relational configuration in χ.

- **Geometric Separation vs. Relational Unity:** While the emergent metric $g_{\mu\nu}$ assigns a large spatial distance between two detectors, the underlying χ -excitation remains a single connected entity in the pre-geometric substrate.
- **The Shared Projection:** Entanglement is thus defined as the manifestation of a single χ -source through multiple, non-injective projective "images". The perceived "spooky action at a distance" is an artifact of the metric description, which fails to capture the underlying relational unity.

Torsional Conservation and the Origin of Spin Correlations.

This hypothesis extends naturally to the geometric origin of spin. If spin is interpreted as the projection of the internal degrees of freedom of the relational fiber (e.g., within the Hopf fibration $S^3 \to S^2$ [4]), then:

- A measurement at location A corresponds to a local stabilization of the projection's torsional phase.

[4] This reference is illustrative and does not imply that the substrate χ possesses a literal S^3 topology.

- Because the underlying configuration in χ is a unified structure, this local stabilization *structurally constrains* the admissible projective states available at any other location B originating from the same source.
- This mechanism ensures the conservation of global topological invariants across the shared projection without violating the causal bounds of the relaxation dynamics.

Relationship with Bell's Theorem.

Cosmochrony addresses the constraints of Bell's theorem by shifting the locus of reality. The framework remains **ontologically realist** at the level of the relational substrate, as the substrate χ possesses definite relational states, but it is **structurally non-local** with respect to the emergent spacetime. The violation of Bell inequalities is not seen as a failure of realism, but as a signature of **metric emergence**: the metric distance, used to define "locality" in the theorem, is not a fundamental property of the level where the correlations are established. Bell inequality violations are therefore attributed to the use of emergent metric locality in a context where the relevant degrees of freedom are defined prior to spacetime separation.

B.14 Metastability, Decay Channels, and Exponential Lifetimes

Diagnostic Structural Functional

We introduce a diagnostic functional $E_{\mathrm{struct}}[\chi_{\mathrm{eff}}]$, which quantifies the degree of structural constraint associated with a localized projected configuration. This functional should be understood as an effective measure of resistance to relaxation, consistent with the interpretation of mass developed in Section 6.3.

The explicit form of E_{struct} is not unique. For stability analysis, it may be constructed from quadratic variations of χ_{eff}, for instance

$$E_{\mathrm{struct}}[\chi_{\mathrm{eff}}] \sim \int_{\mathcal{V}} \left(|\nabla \chi_{\mathrm{eff}}|^2 + \mu^2 |\chi_{\mathrm{eff}}|^2 \right) \, d^3x, \tag{168}$$

where $\mathcal{V}$ denotes the effective localization region.

Admissible Factorization Channels

A decay channel is defined as an admissible factorization of a localized projected configuration into several localized configurations plus weakly structured modes,

$$\chi_{\mathrm{eff},A} \;\to\; \bigoplus_{i=1}^{N} \chi_{\mathrm{eff},i} \;\oplus\; \chi_{\mathrm{eff,rad}}. \tag{169}$$

Admissibility requires the preservation of global structural invariants,

$$Q(\chi_{\mathrm{eff},A}) = \sum_{i=1}^{N} Q(\chi_{\mathrm{eff},i}), \tag{170}$$

where Q denotes any topological or relational invariant associated with the projected description.

A channel is kinematically accessible if the total diagnostic structural functional satisfies

$$\Delta E_{\text{struct}} = E_{\text{struct}}[\chi_{\text{eff},A}] - \sum_i E_{\text{struct}}[\chi_{\text{eff},i}] - E_{\text{struct}}[\chi_{\text{eff,rad}}] > 0. \tag{171}$$

Exponential Lifetimes

Projected configurations explore nearby admissible micro-rearrangements due to intrinsic projective variability. Let Γ denote the effective rate at which such fluctuations reach an admissible factorization threshold.

If Γ is approximately constant over the relevant range of the effective ordering parameter τ, the survival probability satisfies

$$P(\tau) = \exp(-\Gamma\tau). \tag{172}$$

The decay width Γ decomposes into partial widths associated with distinct admissible channels,

$$\Gamma = \sum_c \Gamma_c. \tag{173}$$

This statistical description reproduces the phenomenology of quantum decay without postulating fundamental randomness or microscopic time evolution.

Structural Interpretation of Interaction Classes

Within this framework, different decay classes correspond to different degrees of constraint on admissible factorization paths. Strong decays involve direct and local reorganization of projected topology. Electromagnetic decays correspond to rearrangements preserving the core topological structure. Weak decays require deeper internal reconfiguration and therefore proceed through rarer admissible paths, resulting in longer lifetimes.

Non-Injective Projection and Structural Factorization

Let Π denote the projection operator from the χ-substrate to effective observable descriptions. This projection is generically non-injective: distinct relational configurations of χ may correspond to identical or indistinguishable effective observables, and conversely a single χ-configuration may give rise to multiple correlated effective observables.

Quantum entanglement corresponds to the case in which a single underlying χ-configuration χ_0 admits a non-factorizable projected description $\Pi(\chi_0)$. Although effective observables may be associated with spatially separated regions, the projected configuration cannot be written as a product of independent sub-configurations without violating admissibility.

Particle decay corresponds to a different regime of the same projection structure. In this case, the projected configuration $\Pi(\chi_0)$ becomes unstable under admissible

fluctuations. No single projected description remains admissible. Admissibility is recovered only through factorization,

$$\Pi(\chi_0) \longrightarrow \Pi(\chi_1) \oplus \Pi(\chi_2) \oplus \cdots, \tag{174}$$

where the χ_i are distinct relational configurations whose projections are individually admissible and localized.

The distinction between entanglement and decay is therefore not a distinction at the level of the χ-substrate, but a distinction in the stability properties of the projected description under non-injective projection.

B.15 Measurement, Temporal Ordering, and Antiparticle Emergence

Projective Selection and Measurement

Let Π denote the non-injective projection from the χ-substrate to effective observable descriptions. A given relational configuration χ_0 may admit multiple projected descriptions $\{\Pi_\alpha(\chi_0)\}$.

Measurement corresponds to the stabilization of a single projected description $\Pi_{\alpha^*}(\chi_0)$ under interaction with an environment. Alternative projected descriptions become inadmissible due to amplification-induced constraints.

Temporal Ordering from Admissibility

Let $\mathcal{A}$ denote the set of admissible projected configurations. Define a partial ordering $\prec$ such that

$$\Pi_a \prec \Pi_b$$

if Π_b can be obtained from Π_a by admissible relaxation or factorization, but not conversely.

Decay and measurement processes correspond to transitions toward configurations that are minimal with respect to $\prec$. This ordering induces an effective arrow of time without introducing a fundamental temporal parameter.

Structural Origin of Antiparticles

Assume that admissible projected configurations carry signed structural invariants $Q \in \mathbb{Z}$ or $Q \in \mathbb{Z}_2$, associated with orientation, chirality, or phase winding.

For a metastable configuration χ_A undergoing admissible factorization, invariance requires

$$Q(\chi_A) = \sum_i Q(\chi_i).$$

If $Q(\chi_A) = 0$ but factorization produces nonzero local contributions, admissibility requires the appearance of paired configurations with opposite signs,

$$Q(\chi_i) = +q, \quad Q(\chi_j) = -q.$$

These paired configurations are interpreted, at the effective level, as particle–antiparticle pairs. Their emergence reflects the necessity of preserving signed structural invariants under non-injective projection and factorization, rather than the creation of independent degrees of freedom.

B.16 Structural Interpretation of CPT Symmetry

Let Π denote the non-injective projection from the χ-substrate to effective descriptions. Projected configurations may carry signed invariants Q associated with relational orientation, chirality, or phase winding. These invariants are not defined at the fundamental level but emerge through projection.

Consider the combined transformation

$$(Q,\ \tau,\ \mathbf{x}) \ \longrightarrow\ (-Q,\ -\tau,\ -\mathbf{x}),$$

where τ denotes the effective ordering parameter and $\mathbf{x}$ the effective spatial localization. This transformation leaves the admissibility conditions invariant.

Under admissible factorization of a metastable configuration χ_A, conservation of signed invariants requires

$$Q(\chi_A) = \sum_i Q(\chi_i).$$

If local configurations carry nonzero signed contributions while the global invariant vanishes, admissibility enforces the appearance of pairs with opposite signs.

These paired configurations are interpreted as particle–antiparticle pairs. CPT symmetry thus emerges as an invariance of the admissible projection structure, rather than as a fundamental symmetry imposed on the χ-substrate.

B.17 CP Asymmetry and Chiral Selection

CPT versus CP as Admissibility Symmetries

Let projected configurations carry a set of signed structural invariants $\{Q_i\}$, associated with orientation, chirality, or phase winding. The admissibility conditions are invariant under the combined transformation

$$(Q_i,\ \tau,\ \mathbf{x}) \to (-Q_i,\ -\tau,\ -\mathbf{x}),$$

which defines an effective CPT symmetry.

In contrast, CP acts only on a subset of the invariants $\{Q_i\}$ and does not reverse the effective ordering parameter. As a result, CP is not, in general, an invariance of the admissibility conditions. Effective CP violation may therefore arise without violating CPT invariance.

Structural Bias and Matter–Antimatter Asymmetry

Assume that admissible projected configurations exhibit a slight asymmetry in relaxation efficiency with respect to the sign of a structural invariant Q. Let $\Gamma(Q)$ denote the effective stabilization rate.

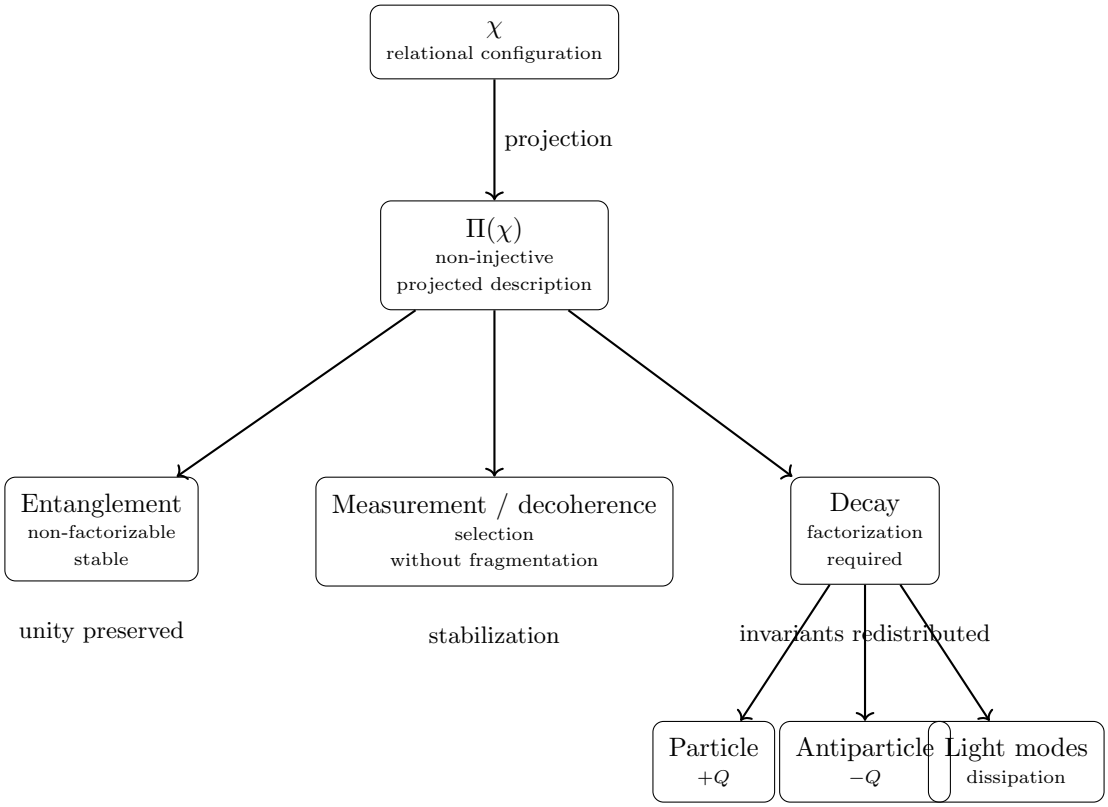

Fig. 19 Unified structural interpretation of quantum entanglement, measurement, and particle decay in Cosmochrony. All phenomena originate from the non-injective projection of a single relational configuration of χ. Antiparticles emerge when admissible factorization requires the redistribution of signed structural invariants.

If

$$\Gamma(Q) \neq \Gamma(-Q),$$

then configurations carrying one orientation will be statistically favored during relaxation, leading to an emergent matter–antimatter asymmetry without requiring explicit symmetry breaking at the fundamental level.

Chiral Filtering and Neutrino-Like Excitations

Consider weakly localized projected configurations carrying a chiral invariant $\chi_L = \pm 1$. Admissibility constraints may select only one sign of χ_L as compatible with stable relaxation.

Configurations of opposite chirality either fail to localize or decay rapidly. Neutrino-like excitations correspond to such minimally constrained configurations, which remain admissible only in one chiral sector and interact weakly with more structured excitations.

C Cosmological and Observational Implications of Cosmochrony

This appendix examines cosmological and observational implications: CMB spectrum and low-ℓ attenuation, horizon and flatness problems, the Hubble tension, observational estimates, phenomenological implications including MOND-like dynamics, and neutrino-mediated structural smoothing.

C.1 Low-ℓ CMB Power Suppression from Global χ Relaxation

This appendix provides a detailed phenomenological treatment of the low-ℓ CMB power suppression discussed in Sections 7.6 and 7.11.

One of the most persistent large-scale anomalies of the cosmic microwave background (CMB) concerns the suppression of temperature anisotropy power at the largest angular scales ($\ell \lesssim 30$), most notably in the quadrupole and octupole moments. Within the standard ΛCDM framework, such deviations are commonly attributed to cosmic variance, and no specific physical mechanism is associated with their occurrence.

Within the Cosmochrony framework, by contrast, the lowest multipoles probe global properties of the projected field χ_{eff} rather than independent local perturbations. Because the fundamental field χ evolves through a monotonic relaxation process constrained by finite connectivity and a maximal relaxation speed, the longest-wavelength modes correspond to collective configurations whose amplitudes are not freely adjustable.

Structural attenuation of global modes.

At very low multipoles, the associated angular modes span regions comparable to the full causal domain of the projected χ_{eff} configuration. As a result, these modes are subject to global relaxation constraints: their amplitude is systematically attenuated relative to the scale-invariant expectation.

This suppression is not the result of stochastic damping or fine-tuned initial conditions. It arises because the finite relaxation capacity of the χ field limits the degree to which globally coherent configurations can deviate from the relaxed background. The effect is deterministic in origin, while its detailed realization in any given universe remains statistical.

Cosmochrony therefore does not predict exact multipole amplitudes. Instead, it predicts a robust suppression tendency affecting the lowest ℓ-modes, whose precise pattern depends on the detailed global configuration of χ at last scattering.

Illustrative comparison with observations.

Figure 20 shows the observed CMB temperature power spectrum at low multipoles, displayed without aggressive smoothing, together with a schematic attenuation envelope representative of the Cosmochrony mechanism.

This comparison is intended to illustrate the qualitative structural deviation from scale invariance implied by global relaxation constraints. It does *not* constitute a multipole-by-multipole prediction, nor does it replace a full Boltzmann analysis.

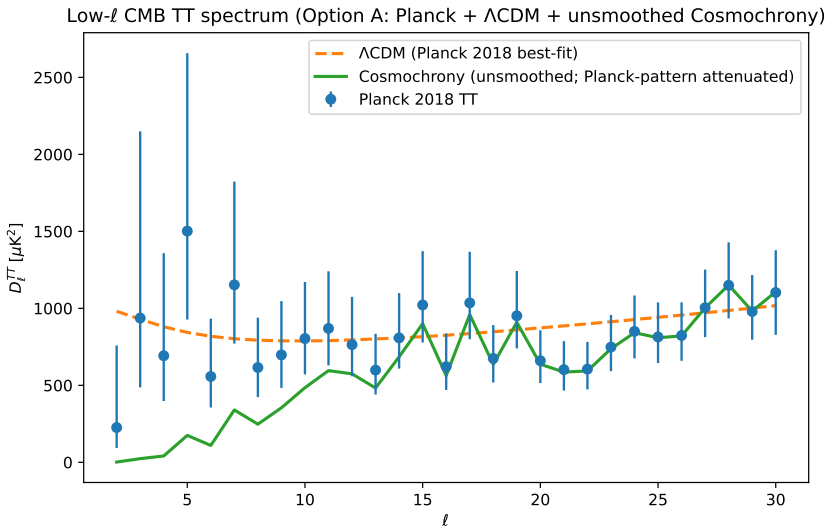

Fig. 20 Observed CMB temperature power spectrum at low multipoles ($\ell \lesssim 30$), shown without heavy smoothing. The shaded region illustrates a qualitative attenuation envelope expected from global relaxation constraints on the projected field $\chi_{\rm eff}$ in Cosmochrony. Unlike ΛCDM, where low-ℓ suppression is treated as a statistical accident, Cosmochrony interprets it as a structural consequence of the finite relaxation capacity of globally coherent configurations. The envelope may be summarized phenomenologically by Eq. (175).

Phenomenological parametrization.

To render this schematic attenuation minimally quantitative without introducing a full cosmological perturbation theory, we introduce a two-parameter phenomenological envelope in which the low-ℓ power is multiplicatively suppressed relative to the ΛCDM best-fit spectrum:

$$C_\ell^{\rm CC} = C_\ell^{\Lambda\rm CDM}\left[1 - \alpha \exp\left(-\frac{\ell}{\ell_0}\right)\right], \qquad \alpha \in [0,1], \quad \ell_0 > 0. \tag{175}$$

Equivalently, in terms of $D_\ell \equiv \ell(\ell+1)C_\ell/(2\pi)$,

$$D_\ell^{\rm CC} = D_\ell^{\Lambda\rm CDM}\left[1 - \alpha e^{-\ell/\ell_0}\right].$$

In this parametrization, α controls the overall amplitude of large-angle suppression, while ℓ_0 sets the angular scale beyond which the spectrum rapidly converges back to the standard ΛCDM behavior.

Indicative low-ℓ characterization.

An indicative estimate of (α, ℓ_0) may be obtained by fitting the ratio $R_\ell \equiv D_\ell^{\rm obs}/D_\ell^{\Lambda\rm CDM}$ over a restricted low-ℓ range (e.g. $\ell = 2\ldots30$), using cosmic-variance-dominated uncertainties $\sigma(R_\ell) \simeq \sqrt{2/(2\ell+1)}$.

This procedure is not intended as a detection claim. It provides a compact and reproducible summary of the suppression tendency, replacing heuristic hand-drawn envelopes by a controlled two-parameter characterization.

Conceptual distinction from ΛCDM.

In ΛCDM, low-ℓ deviations are interpreted *a posteriori* as statistical fluctuations around an ensemble mean defined by inflationary initial conditions. In Cosmochrony, the ensemble itself is constrained: the global relaxation dynamics of χ restrict the admissible configuration space for the longest-wavelength modes.

This leads to a qualitative physical distinction between large-scale and small-scale fluctuations. Small-scale modes probe local relaxation and behave approximately as independent perturbations, while large-scale modes encode global structural properties of the field.

Graph-theoretic origin of the admissibility filter.

Building on the concept of ontological poverty introduced in Section 2.9, the admissibility filter $\mathcal{A}(k,t)$ admits a natural graph-theoretic interpretation. At any effective cosmological time t, the relational substrate χ defines a connectivity graph $G(t)$ whose weighted Laplacian $L_G(t)$ encodes the admissible collective modes.

The spectrum of $L_G(t)$,

$$L_G(t)\,\psi_n = \lambda_n(t)\,\psi_n,$$

sets a minimal nonzero eigenvalue $\lambda_2(t)$ that characterizes the global connectivity of the relational structure. Modes with wavelengths exceeding the corresponding scale $k_c(t) \sim \sqrt{\lambda_2(t)}$ are structurally inadmissible.

The primordial power spectrum is therefore modulated by a structural admissibility filter,

$$\mathcal{A}(k,t) = \exp\left[-\left(\frac{\lambda_2(t)}{k^2}\right)^{p/2}\right],$$

reflecting the inability of an insufficiently connected relational graph to support large-scale coherent modes.

Scope and limitations.

The present analysis does not replace full Boltzmann calculations and does not aim to reproduce the entire angular power spectrum. Its purpose is to identify a robust qualitative signature of Cosmochrony: a systematic suppression tendency affecting the lowest CMB multipoles, arising from global relaxation constraints on the fundamental field.

Quantitative refinement of this effect, including detailed parameter inference and polarization observables, is deferred to future numerical studies of the χ dynamics.

C.2 Resolution of the Horizon and Flatness Problems Without Inflation

In standard cosmology, the horizon and flatness problems arise from extrapolating a spacetime-based notion of causality and geometry back to the earliest stages of cosmic

evolution. Within this framework, regions of the universe that appear widely separated today should not have been in causal contact, and the near-flatness of spatial geometry requires fine-tuned initial conditions. Inflation addresses these issues by postulating a brief phase of accelerated expansion in a pre-existing metric background.

Cosmochrony adopts a fundamentally different standpoint. Spacetime geometry, causal structure, and metric notions of distance are not assumed to be fundamental. They emerge only at a later stage, as effective descriptions of the relaxation dynamics of the scalar field χ. As a result, the assumptions underlying the horizon and flatness problems do not apply at the fundamental level.

Horizon problem: pre-geometric connectivity.

In Cosmochrony, large-scale correlations do not need to be established through signal propagation within spacetime. Instead, they originate from the fact that χ constitutes a single, globally connected dynamical substrate whose relaxation precedes the emergence of any effective spacetime description.

At early stages, before a metric notion of causality becomes meaningful, the configuration of χ is defined globally. Regions that later appear causally disconnected in the emergent spacetime may therefore share correlated configurations inherited from earlier phases of the relaxation process.

In this sense, Cosmochrony replaces inflationary causal contact with *pre-geometric connectivity*: correlations are established at the level of the fundamental field itself, rather than through superluminal expansion or specially prepared initial conditions on a metric background.

Flatness problem: relaxation toward geometric uniformity.

The flatness problem is addressed through the same underlying mechanism. In Cosmochrony, effective spatial curvature reflects large-scale gradients and inhomogeneities in the relaxation rate of the projected field χ_{eff}. As relaxation proceeds, configurations with large curvature gradients are dynamically disfavored, since they correspond to sustained resistance to global relaxation.

As a consequence, near-flat spatial geometry emerges as a natural attractor of the relaxation dynamics. Curvature dilution does not require exponential expansion or fine-tuning of initial curvature parameters. It reflects the tendency of the χ field to minimize large-scale geometric tension as it approaches a homogeneous relaxation state.

This mechanism operates independently of any inflationary phase and does not rely on a specific initial curvature value.

Implications for primordial correlations.

Because large-scale coherence arises from the global organization of χ rather than from the amplification of quantum vacuum fluctuations, Cosmochrony does not predict exact scale invariance at the largest wavelengths. Instead, the longest-wavelength modes are subject to global relaxation constraints, which may lead to deviations from scale invariance at the lowest multipoles of the cosmic microwave background.

Such deviations are interpreted as structural tendencies rather than sharp predictions. They provide a qualitative distinction from inflation-based scenarios and motivate the phenomenological analysis of low-ℓ CMB anomalies discussed in Section C.1.

Status and limitations.

The arguments presented here establish that the horizon and flatness problems do not arise as fundamental inconsistencies within the Cosmochrony framework. They are artifacts of applying metric-based reasoning beyond its domain of validity.

A quantitative derivation of primordial correlation functions and power spectra, including detailed predictions for CMB anisotropies, requires dedicated numerical simulations of the χ-field relaxation dynamics and lies beyond the scope of the present work.

Nevertheless, Cosmochrony provides a conceptually coherent, inflation-free resolution of large-scale causal coherence and near-flat spatial geometry, rooted in the pre-geometric dynamics of a single scalar field.

C.3 Evolution of the Hubble Parameter and the Hubble Tension

This appendix provides the mathematical details underlying the Hubble tension interpretation presented in Section 7.10.

In the Cosmochrony framework, cosmological expansion is not governed by the competition between matter, radiation, and a dark energy component. Instead, it reflects the relaxation dynamics of the scalar field χ, from which spacetime geometry and its associated expansion rate emerge as effective descriptions.

The Hubble parameter therefore encodes the instantaneous relaxation rate of χ relative to its global configuration, rather than the response of a metric to an energy–momentum content.

Global expansion rate.

At the homogeneous background level, the effective scale factor is proportional to the global value of the projected field,

$$a(t) \propto \chi(t), \tag{176}$$

so that the Hubble parameter may be written as

$$H(t) = \frac{\dot{\chi}}{\chi}. \tag{177}$$

In the idealized homogeneous limit, spatial gradients vanish ($\nabla\chi = 0$) and the relaxation dynamics reduce to a uniform evolution with maximal relaxation speed,

$$\dot{\chi} = c. \tag{178}$$

In this limit, the global expansion rate becomes

$$H(t) = \frac{c}{\chi(t)}. \tag{179}$$

This relation defines the *global* expansion rate in Cosmochrony. Its detailed redshift dependence away from perfect homogeneity is not assumed to follow a fixed power law and depends on how relaxation gradients contribute to the averaged dynamics.

Illustrative $H(z)$ profile and comparison with ΛCDM.

To provide a visual benchmark against standard cosmology, we compare an *illustrative* Cosmochrony profile to the ΛCDM expansion history. This is not a fit and does not claim a derived redshift law: it only translates the baseline relations $a(t) \propto \chi(t)$ and $H = \dot{\chi}/\chi$ into a convenient parametrization for plotting purposes.

Using the effective redshift interpretation

$$1 + z = \frac{\chi(t_0)}{\chi(t)}, \tag{180}$$

one may write, in the simplest background closure where the relaxation budget is treated as a slowly varying effective fraction,

$$H_\chi(z) \;\equiv\; H_0\,(1+z)\,\sqrt{1-\Omega_\chi} \qquad \text{(illustrative closure)}. \tag{181}$$

For comparison, the ΛCDM benchmark is

$$H_{\Lambda\mathrm{CDM}}(z) \;=\; H_0\sqrt{\Omega_m(1+z)^3 + \Omega_r(1+z)^4 + \Omega_\Lambda}, \tag{182}$$

with $(\Omega_m, \Omega_\Lambda) \simeq (0.3, 0.7)$ and Ω_r negligible at late times.

Figure 21 shows the two curves, together with a shaded Cosmochrony band obtained by varying (H_0, Ω_χ) within representative late-universe ranges. The purpose is to highlight (i) the qualitatively distinct scaling of $H(z)$ induced by monotonic χ relaxation and (ii) how modest variations in the effective relaxation budget translate into percent-level differences in inferred expansion.

Relaxation budget and effective expansion.

In a realistic universe, part of the relaxation capacity of χ is stored in spatial gradients associated with inhomogeneities. To quantify this effect, we introduce a dimensionless *relaxation budget* parameter,

$$\Omega_\chi \equiv \langle \beta^2 \rangle, \qquad \beta \equiv \frac{|\nabla\chi|}{c}, \tag{183}$$

which measures the fraction of the total relaxation capacity diverted into spatial structure rather than global evolution.

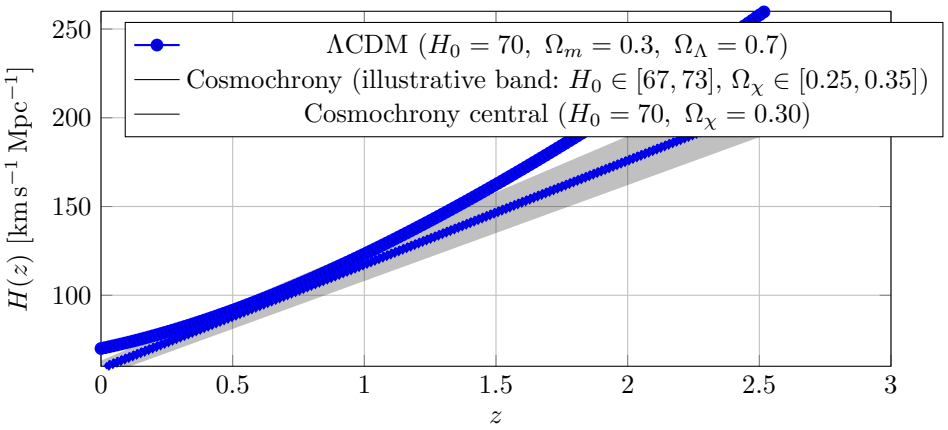

Fig. 21 Illustrative comparison of $H(z)$ in Cosmochrony versus a ΛCDM benchmark. The Cosmochrony curve uses the minimal plotting closure $H_\chi(z) = H_0(1+z)\sqrt{1-\Omega_\chi}$, shown with a representative uncertainty band from (H_0, Ω_χ) variations. This figure is a visualization aid, not a fit.

At late times, these gradients are dominated by localized solitonic configurations and therefore track the large-scale matter distribution. The effective global expansion rate is then reduced to

$$\bar{H} = \frac{c}{\chi}\sqrt{1-\Omega_\chi}. \tag{184}$$

Empirically, consistency with large-scale observations suggests Ω_χ is of order the observed matter fraction, $\Omega_\chi \sim 0.3$. In Cosmochrony, this suppression of the global expansion rate arises naturally from relaxation dynamics and does not require a dark energy component.

Local expansion and environmental dependence.

In an inhomogeneous universe, the relaxation budget is not spatially uniform. Regions with different matter densities redistribute relaxation capacity differently between global evolution and local gradients.

For a region characterized by a density contrast

$$\delta = \frac{\rho - \bar{\rho}}{\bar{\rho}}, \tag{185}$$

we adopt a minimal mean-field closure relation,

$$\beta_{\rm loc}^2 = \Omega_\chi(1+\delta), \tag{186}$$

which encodes the intuitive scaling between matter density and χ-gradient energy.

The locally inferred Hubble parameter then takes the form

$$H_{\rm loc} = \bar{H}\sqrt{\frac{1-\Omega_\chi(1+\delta)}{1-\Omega_\chi}}. \tag{187}$$

In underdense regions ($\delta < 0$), a larger fraction of the relaxation capacity is available for global evolution, leading to $H_{\rm loc} > \bar{H}$.

Numerical consistency and the Hubble tension.

For representative values $\Omega_\chi \approx 0.3$ and a local underdensity consistent with the KBC void ($\delta \approx -0.4$ on scales of a few hundred megaparsecs), one finds

$$\frac{H_{\rm loc}}{\bar{H}} \approx 1.08, \tag{188}$$

corresponding to an enhancement of order 8% in the locally inferred Hubble constant.

This magnitude is comparable to the observed discrepancy between local distance-ladder measurements and global CMB-based inferences. In Cosmochrony, this discrepancy arises naturally as an environmental effect, without invoking new energy components or modifications of early-universe physics.

Predicted amplitude of the deviation at $z \sim 1$.

A distinctive feature of the Cosmochrony framework is that the magnitude of the departure from the ΛCDM expansion history is not freely adjustable. At late times, the relative deviation between the locally inferred and globally averaged expansion rates is fully controlled by the relaxation budget parameter Ω_χ and by the effective density contrast δ in the redshift range under consideration.

Within Cosmochrony, structural consistency imposes

$$\Omega_\chi \in [0.25,\, 0.35], \tag{189}$$

reflecting the fraction of relaxation capacity stored in large-scale gradients, while the partially developed cosmic web at $z \sim 1$ naturally corresponds to moderate underdensities in the range

$$\delta(z \sim 1) \in [-0.2,\, -0.5]. \tag{190}$$

Inserting these bounds into Eq. (C.187) yields a predicted fractional enhancement

$$\frac{\Delta H}{H} \;\equiv\; \frac{H_{\rm loc} - \bar{H}}{\bar{H}} \;\in\; [3.5\%,\, 9.5\%] \qquad (z \sim 1). \tag{191}$$

This narrow interval is not a phenomenological choice but a direct consequence of the relaxation-based origin of expansion in Cosmochrony. Deviations significantly outside this range would require either unphysical values of Ω_χ or density contrasts incompatible with the observed state of large-scale structure at intermediate redshifts.

Uncertainty estimates and parameter degeneracies.

At the present stage, Cosmochrony does not claim a precision reconstruction of $H(z)$. Nevertheless, it is useful to clarify how uncertainties in the effective parameters map to uncertainties in the plotted $H(z)$ profiles and in the underlying stiffness scale.

Late-time effective uncertainty in (H_0, Ω_χ). Within the illustrative closure of Eq. (181), small variations propagate as

$$\frac{\delta H}{H} \simeq \frac{\delta H_0}{H_0} - \frac{1}{2}\frac{\delta \Omega_\chi}{1-\Omega_\chi}. \tag{192}$$

For $\Omega_\chi \simeq 0.30$, an uncertainty $\delta\Omega_\chi \simeq 0.05$ corresponds to a fractional variation $\delta H/H \simeq 3.6\%$, comparable to the width used in Fig. 21. This motivates representing Cosmochrony as a band rather than a single curve until dedicated simulations determine $\Omega_\chi(z)$.

Degeneracy between K_0 *and* χ_c. The effective gravitational coupling constrains the product

$$K_0\, \chi_c^2 \sim \frac{c^4}{16\pi G}, \tag{193}$$

so that K_0 and χ_c cannot be fixed independently without additional input. Propagating uncertainties in logarithmic form gives

$$\delta \ln K_0 \simeq -2\, \delta \ln \chi_c \quad \text{(at fixed } G\text{)}. \tag{194}$$

Hence, a factor-of-10 uncertainty on χ_c implies a factor-of-100 uncertainty on K_0. This is consistent with the fact that both Planck-scale and cosmological-scale normalizations can remain internally viable at the level of dimensional analysis, until the microscopic origin of χ_c is constrained by simulations and/or additional observables.

Interpretation and status.

Within Cosmochrony, the Hubble tension does not signal a breakdown of cosmological consistency. It reflects the fact that cosmological expansion is an emergent relaxation phenomenon whose effective rate depends on the local redistribution of χ-field gradients.

While the framework robustly predicts a separation between local and global expansion rates, a fully quantitative determination of $H(z)$ across all redshifts requires dedicated numerical simulations of the χ relaxation dynamics. Such simulations lie beyond the scope of the present work.

Nevertheless, the qualitative resolution of the Hubble tension follows directly from the relaxation-based interpretation of cosmological expansion and constitutes a distinctive and testable signature of the Cosmochrony framework.

C.4 Relation to Observational Units and Numerical Estimates

This subsection establishes order-of-magnitude relations linking the Cosmochrony framework to observed cosmological quantities. Its purpose is not to perform parameter fitting or to derive precision predictions, but to assess the internal consistency of the theory and to verify that its fundamental relaxation-based interpretation naturally reproduces the correct empirical scales.

All numerical relations presented here should be understood as effective normalizations arising in the projectable regime of the χ dynamics. They do not define fundamental constants and do not fix the microscopic structure of the theory.

Normalization of the χ Field

To relate the projected field χ_{eff} to observable quantities, a reference normalization must be specified. At the effective cosmological level, the scale factor is defined up to a global multiplicative constant. In Cosmochrony, this freedom is fixed by identifying the present-day value $\chi(t_0)$ with the characteristic geometric scale governing large-scale expansion.

Operationally, $\chi(t_0)$ represents the cumulative geometric scale associated with the global relaxation of the χ field up to the present epoch. This identification does not assume a unique microscopic origin for $\chi(t_0)$; it provides a minimal and observationally anchored normalization consistent with the effective relation $a(t) \propto \chi(t)$.

Emergent Gravitational Coupling

In the effective geometric description, the Newtonian gravitational constant G emerges from the constitutive relation governing the coupling between neighboring configurations of the projected χ field. This coupling is controlled by two parameters of the relaxation dynamics: the maximal stiffness scale K_0 and the characteristic correlation length χ_c.

Although K_0 and χ_c are not individually fixed at the present stage, their combination is constrained by matching the observed gravitational coupling:

$$K_0 \chi_c^2 \sim \frac{c^4}{16\pi G}. \tag{195}$$

This relation fixes the overall stiffness scale of the effective χ network. It does not require committing to a specific microscopic interpretation of χ_c, which may correspond to a fundamental correlation scale or to an emergent coarse-graining length. At this level, only the product $K_0 \chi_c^2$ is observationally relevant.

Hubble Constant

In the homogeneous limit, the effective Hubble parameter is defined by the relative relaxation rate of the projected field,

$$H(t) = \frac{\dot{\chi}}{\chi}. \tag{196}$$

Assuming that the present universe lies close to the maximal relaxation regime, $\dot{\chi}(t_0) \simeq c$, the present-day Hubble constant follows as

$$H_0 \simeq \frac{c}{\chi(t_0)}. \tag{197}$$

Using the observed value $H_0 \approx 70\ \mathrm{km\,s^{-1}\,Mpc^{-1}}$ yields

$$\chi(t_0) \sim 4 \times 10^{26}\ \mathrm{m}, \tag{198}$$

which is of the order of the observed Hubble radius. This correspondence arises directly from the relaxation-based interpretation of cosmic expansion and does not require the introduction of additional cosmological parameters.

Age of the Universe

In the homogeneous relaxation regime, the evolution of χ may be approximated as

$$\dot{\chi} \simeq c, \tag{199}$$

leading to

$$\chi(t) \simeq ct + \chi_{\text{init}}, \tag{200}$$

where χ_{init} denotes the effective value of χ at the onset of the relaxation regime relevant for cosmological observations.

Neglecting χ_{init} compared to present values yields

$$t_0 \simeq \frac{\chi(t_0)}{c} \sim 4 \times 10^{17}\ \text{s}, \tag{201}$$

corresponding to approximately 13.8 billion years. This estimate is consistent with standard cosmological age determinations and follows directly from the bounded relaxation dynamics.

Redshift Interpretation

In Cosmochrony, cosmological redshift is interpreted as a consequence of the relative change in the projected χ field between emission and observation,

$$1 + z = \frac{\chi(t_{\text{obs}})}{\chi(t_{\text{emit}})}. \tag{202}$$

This relation reproduces standard redshift phenomenology while attributing it to geometric scaling induced by χ relaxation, rather than to recessional motion within a pre-existing spacetime background.

Cosmic Microwave Background Scale

At recombination, characterized observationally by $z_{\text{rec}} \simeq 1100$, the effective value of the projected field was smaller by the corresponding scaling factor,

$$\chi(t_{\text{rec}}) \simeq \frac{\chi(t_0)}{1 + z_{\text{rec}}}. \tag{203}$$

Fluctuations imprinted at that epoch are subsequently stretched by the monotonic growth of χ, providing a natural geometric interpretation of the angular scales observed in the cosmic microwave background without invoking an inflationary stretching phase.

Orders of Magnitude and Robustness

All numerical estimates presented in this subsection rely solely on observed cosmological quantities and on the bounded relaxation dynamics of the χ field. No fine-tuning of parameters, no detailed cosmological fitting, and no additional degrees of freedom are assumed.

While a fully predictive cosmological model requires explicit numerical simulations of the χ dynamics, these order-of-magnitude relations demonstrate that Cosmochrony naturally reproduces the correct scales for the Hubble constant, the age of the universe, redshift evolution, and characteristic CMB features.

Summary

The Cosmochrony framework admits a consistent normalization in observational units and reproduces key cosmological scales without introducing new fundamental parameters. These order-of-magnitude relations support the internal coherence of the theory and motivate further quantitative investigation of its cosmological dynamics.

C.5 Phenomenological Implications

This subsection summarizes the principal phenomenological consequences of Cosmochrony that are accessible to observation. The emphasis is placed on effects that follow robustly from the kinematic and relaxation structure of the χ field itself, without introducing auxiliary degrees of freedom, adjustable interpolation functions, or phenomenological potentials.

All results presented here arise in the projectable regime of the theory and should be understood as effective manifestations of the underlying relaxation dynamics, not as fundamental postulates.

Propagation speed of gravitational perturbations.

To determine the propagation speed of gravitational information in Cosmochrony, consider small perturbations $\delta\chi$ around a homogeneous relaxation background,

$$\chi_0(t) = ct, \tag{204}$$

such that

$$\chi(\mathbf{x}, t) = ct + \delta\chi(\mathbf{x}, t), \qquad |\nabla\delta\chi| \ll c. \tag{205}$$

Substituting this form into the fundamental kinematic constraint governing χ-field relaxation (Eq. 12) yields, to leading order,

$$c + \partial_t\delta\chi = c\sqrt{1 - \frac{|\nabla\delta\chi|^2}{c^2}}. \tag{206}$$

Expanding for small spatial gradients gives

$$\partial_t\delta\chi \simeq -\frac{|\nabla\delta\chi|^2}{2c}, \tag{207}$$

reflecting the irreversible character of the relaxation process. While this first-order relation governs dissipation, the propagation of perturbations is more transparently captured by considering the second-order operator associated with the squared constraint.

Linearizing this operator leads to the effective wave equation

$$\left(\frac{1}{c^2}\partial_t^2 - \nabla^2\right)\delta\chi = 0, \tag{208}$$

which admits propagating solutions with characteristic speed

$$v_{\text{prop}} = c. \tag{209}$$

Gravitational perturbations therefore propagate exactly at the invariant speed c. This equality is not imposed by hand but follows directly from the fundamental kinematic bound on χ relaxation. As a result, Cosmochrony is automatically consistent with multi-messenger observations, including the near-simultaneous arrival of gravitational and electromagnetic signals in events such as GW170817.

Emergent acceleration scale and MOND-like phenomenology.

In Cosmochrony, the arrow of time is encoded in the monotonic evolution of the fundamental field, $\partial_t\chi \geq 0$. At late cosmic times and on sufficiently large scales, where χ_{eff} admits an approximately homogeneous description, the relaxation dynamics may be coarse-grained into an effective cosmological clock.

In this effective regime, the temporal evolution of χ can be written as

$$\partial_t\chi \simeq H(t)\,\chi, \tag{210}$$

where $H(t)$ denotes the emergent Hubble parameter associated with global relaxation.

The local kinematic constraint

$$(\partial_t\chi)^2 + |\nabla\chi|^2 = c^2 \tag{211}$$

then implies that even in the absence of localized matter excitations, the cosmological evolution of χ enforces a non-vanishing residual spatial gradient. In the homogeneous limit, this minimal gradient is

$$|\nabla\chi|_{\min} = \sqrt{c^2 - (H\chi)^2}. \tag{212}$$

This residual gradient defines a background kinematic scale that constrains the superposition of additional, locally induced gradients. Operationally, it corresponds to an effective acceleration scale

$$a_0(t) \sim c\,H(t). \tag{213}$$

When localized matter excitations are present, they induce additional gradients $\nabla\chi_N$ that reproduce the Newtonian scaling $|\nabla\chi_N| \propto M/r^2$ at short distances. Because

the kinematic constraint is nonlinear, the total gradient does not superpose linearly. At sufficiently large radii, the effective acceleration asymptotically approaches

$$g_{\text{eff}} \simeq \sqrt{g_N\, a_0(t)}, \tag{214}$$

recovering the characteristic deep-MOND scaling without introducing interpolation functions, dark matter particles, or additional fields.

In this framework, the acceleration scale a_0 is not fundamental. It evolves slowly with cosmic time through its dependence on $H(t)$, providing a potential observational discriminator at high redshift.

Gravitational lensing.

In Cosmochrony, light propagation follows wavefronts of constant χ. An effective refractive index for the vacuum may be defined operationally as

$$n(r) = \frac{c}{\partial_t \chi} = \frac{1}{\sqrt{1 - |\nabla\chi|^2/c^2}}. \tag{215}$$

Near a localized mass M, where $|\nabla\chi| \simeq GM/(c^2 r)$, a weak-field expansion yields

$$n(r) \simeq 1 + \frac{GM}{c^2 r}. \tag{216}$$

Integrating the transverse gradient of $n(r)$ along a photon trajectory leads to a deflection angle

$$\alpha = \frac{4GM}{bc^2}, \tag{217}$$

where b is the impact parameter. This reproduces the general-relativistic prediction for gravitational lensing.

In Cosmochrony, the enhancement relative to the Newtonian deflection does not originate from a fundamental spacetime curvature. It arises from the nonlinear structure of the χ relaxation dynamics, which modifies the effective propagation geometry experienced by light.

Summary.

The phenomenology of Cosmochrony reproduces key observational signatures of gravity and cosmology while relying on a single scalar degree of freedom. Gravitational perturbations propagate at exactly the invariant speed c, a MOND-like acceleration scale emerges naturally from cosmological relaxation, and gravitational lensing is recovered without postulating a fundamental metric.

These results illustrate how classical gravitational phenomena arise as coarse-grained manifestations of the underlying χ dynamics and define a set of observationally testable signatures distinguishing Cosmochrony from standard metric-based theories.

C.6 Toy-Model of Spectral Gravitational Susceptibility

This appendix provides the mathematical foundations for a non-particulate interpretation of dark matter phenomena, treating galactic dynamics as the non-linear elastic response of the χ substrate.

Modified Poisson Equation and Field Strength

In the Cosmochrony framework, gravitational acceleration is not a force acting in a passive vacuum but the emergent manifestation of a relaxation gradient. We define the **local relaxation field strength** as the gradient of the scalar relaxation potential:

$$\mathbf{E}_\chi = -\nabla \Phi_\chi \tag{218}$$

The dynamics are governed by a modified Poisson equation analogous to electrodynamics in continuous media:

$$\nabla \cdot [\epsilon_{\text{spec}}(\mathbf{E}_\chi)\mathbf{E}_\chi] = 4\pi G_0 \rho_b \tag{219}$$

where ρ_b is the baryonic mass density and ϵ_{spec} is the **spectral permittivity** of the substrate, defined by the relation $\epsilon_{\text{spec}} = 1 + \phi(\mathbf{E}_\chi)$.

Spectral Susceptibility and the Stiffness Threshold $\mathcal{K}_c$

To recover the observed galactic phenomenology, we define the **spectral gravitational susceptibility** ϕ as a function of the field strength relative to a saturation threshold $\mathcal{K}_c$:

$$\phi(\mathbf{E}_\chi) = \begin{cases} 0 & \text{for } |\mathbf{E}_\chi| \gg \mathcal{K}_c \text{ (Linear/Newtonian Regime)} \\ \frac{\mathcal{K}_c}{|\mathbf{E}_\chi|} & \text{for } |\mathbf{E}_\chi| \ll \mathcal{K}_c \text{ (Saturation Regime)} \end{cases} \tag{220}$$

Crucially, $\mathcal{K}_c$ is not a universal constant of nature but a **local state property** of the substrate. It represents the threshold where the relaxation flux reaches the elastic limit of the χ field.

Emergence of Flat Rotation Curves

In the low-field limit ($|\mathbf{E}_\chi| \ll \mathcal{K}_c$) typical of galactic peripheries, the effective acceleration g_{eff} follows:

$$\nabla \cdot \left(\mathcal{K}_c \frac{\mathbf{E}_\chi}{|\mathbf{E}_\chi|} \right) \sim 4\pi G_0 \rho_b \implies g_{\text{eff}} \approx \frac{\sqrt{G_0 M \mathcal{K}_c}}{r} \tag{221}$$

This leads directly to a constant orbital velocity $v^4 = G_0 M \mathcal{K}_c$, recovering the **Baryonic Tully-Fisher Relation**. Here, "dark matter" is reinterpreted as the increased elastic response of the substrate in regions of diluted relaxation flux.

Comparative Framework: MOND vs. Cosmochrony

The following table summarizes the conceptual shift from modified gravity to substrate dynamics.

Feature	**MOND (Milgrom)**	**Cosmochrony (χ Substrate)**
Origin	Modified law of inertia/force.	Non-linear susceptibility of the medium.
Threshold	Universal constant a_0.	Local stiffness threshold $\mathcal{K}_c$.
Bullet Cluster	Requires additional DM particles.	Natural: Relaxation hysteresis (wake).
GR Relation	Requires $TeVeS$ or similar.	GR is the linear-response limit.
DM Nature	Force discrepancy.	Residual non-projected energy.

Table 3 Comparison between MOND phenomenology and Cosmochrony substrate response.

Limitations and Outlook

Theoretical Refinement.

The current form of $\phi(\mathbf{E}_\chi)$ is phenomenological. A rigorous derivation from the microscopic relaxation equations in Appendix D is required to link $\mathcal{K}_c$ to the global Hubble relaxation rate.

The Relaxation Wake.

Cosmochrony predicts that in high-energy collisions (e.g., Bullet Cluster), the geometric deformation of the substrate exhibits a **phase lag** (hysteresis). Gravitational lensing tracks this "residual wake" of the mass-solitons, explaining the offset from dissipative gas. A specific prediction of this model is the existence of **spectral echoes**: residual curvature in regions where matter has recently passed, a signature that could distinguish Cosmochrony from WIMP-based models.

General Relativity Limit.

Finally, it is emphasized that Cosmochrony reduces to General Relativity in the linear-response limit of the χsubstrate. Spacetime curvature is the refractive manifestation of the substrate's spectral density, and gravity is its macroscopic relaxation.

C.7 Substrate Origin of the Effective Galactic Potential

This appendix clarifies how the effective gravitational potential introduced in Section 7.12 arises from infra-physical properties of the χ substrate, rather than from a fundamental interaction law.

Relaxation flux and relational stiffness.

At the fundamental level, localized excitations correspond to constrained configurations of the relational substrate χ. Their large-scale influence is mediated by a relaxation flux

Φ_χ, whose magnitude depends both on local gradients and on the relational stiffness of the substrate,

$$\Phi_\chi(r) \sim \frac{|\nabla\chi|}{K(r)}. \tag{222}$$

The effective stiffness $K(r)$ increases when the projective connectivity of χ becomes sparse, as occurs at large distances from localized excitations.

Saturation threshold and loss of injectivity.

Because the relaxation dynamics of χ are bounded, there exists a critical stiffness scale K_c beyond which additional gradients cannot be transmitted linearly. When $K(r) \ll K_c$, relaxation remains unsaturated and the projected description is effectively injective, leading to Newtonian behavior. When $K(r) \gtrsim K_c$, relaxation saturates and the projection from χ to effective observables becomes non-injective.

Emergent acceleration scale.

In the projected geometric description, the saturation condition $K(r) \simeq K_c$ manifests as a threshold on the Newtonian baryonic acceleration,

$$g_N(r) \simeq a_0(t). \tag{223}$$

The scale a_0 is therefore not a fundamental constant but an operational re-expression of the substrate saturation threshold.

Cosmological origin of $a_0(t)$***.***

At the largest scales, the relaxation of χ is constrained by the global relational expansion of the Universe. The characteristic relaxation rate is set by the inverse cosmological timescale, leading naturally to

$$a_0(t) \sim c\,H(t), \tag{224}$$

where c encodes the maximal relaxation speed of χ and $H(t)$ the global relational expansion rate. This relation predicts a slow cosmological evolution of the effective acceleration scale.

From substrate saturation to logarithmic potential.

In the saturated regime, the relaxation flux transmitted by χ becomes effectively scale-invariant, implying an effective acceleration $g_{\text{eff}}(r) \propto 1/r$. The corresponding projected potential therefore takes the logarithmic form

$$\Phi_{\text{eff}}(r) \propto \ln r, \tag{225}$$

which directly accounts for asymptotically flat galactic rotation curves.

Interpretational status.

The effective potential Φ_{eff} thus summarizes a specific regime of substrate relaxation. It does not correspond to an additional field or interaction, but to the geometrically admissible description of a saturated projection of the underlying χ dynamics.

C.8 Spectral Interpretation of the Galactic Saturation Regime

This appendix provides a complementary operator-based interpretation of the effective galactic potential introduced in Section 7.12, by relating the saturation of χ-relaxation to spectral properties of the projected relational operator.

Effective operator and spectral stiffness.

In projectable regimes, the collective response of the χ substrate to localized excitations may be characterized by an effective elliptic operator $\mathcal{L}_{\text{eff}}$, whose spectrum encodes the relational stiffness of the medium,

$$\mathcal{L}_{\text{eff}}\,\psi_n = \lambda_n \psi_n, \tag{226}$$

with increasing eigenvalues λ_n corresponding to increasing resistance to long-wavelength deformations.

Spectral saturation and loss of long modes.

As the scale increases, the density of low-lying modes decreases. Beyond a critical scale, the smallest admissible eigenvalue $\lambda_{\min}$ approaches a saturation threshold λ_c, such that additional long-range modes cannot be supported. This spectral depletion corresponds to the stiffness threshold K_c discussed in Appendix C.7.

Effective acceleration threshold.

In the projected geometric description, the spectral threshold λ_c translates into an effective acceleration scale a_0 through

$$a_0 \sim \frac{\lambda_c}{\tau_\chi^2}, \tag{227}$$

where τ_χ denotes the characteristic relaxation time of the substrate. This relation expresses the operational equivalence between spectral saturation and the acceleration crossover observed in galactic dynamics.

Emergence of the logarithmic potential.

When the spectrum becomes marginally scale-invariant near λ_c, the Green function of $\mathcal{L}_{\text{eff}}$ in the effective two-dimensional asymptotic regime behaves as

$$G(r) \propto \ln r. \tag{228}$$

The projected potential Φ_{eff} inherits this logarithmic behavior, providing a spectral explanation for asymptotically flat rotation curves.

Consistency with Newtonian behavior.

At scales where $\lambda_{\min} \ll \lambda_c$, the spectrum is dense and the Green function reduces to the familiar $1/r$ behavior, recovering Newtonian gravity as an unsaturated spectral regime.

Interpretational status.

The spectral description introduced here does not add new degrees of freedom. It provides an operator-level characterization of the same saturation phenomenon described infra-physically in Appendix C.7.

C.9 Neutrino-Mediated Structural Smoothing and Cosmological Inference

Effective Expansion versus Structural Relaxation

Let $a(\tau)$ denote the effective scale factor inferred from projected observables. In Cosmochrony, changes in $a(\tau)$ encode both geometric expansion and cumulative structural relaxation.

We may write, at the effective level,

$$\frac{1}{a}\frac{da}{d\tau} = H_{\mathrm{geom}}(\tau) + H_{\mathrm{relax}}(\tau),$$

where H_{relax} captures the contribution of irreversible structural smoothing, prominently mediated by neutrino-like excitations.

Early-Time Bias from Neutrino Free Streaming

Neutrino-like excitations free-stream over cosmological scales shortly after their emission. This introduces a non-local smoothing term that suppresses large-scale reconfigurations.

Early-time observables, such as CMB anisotropies, are sensitive to the integrated effect of this smoothing. As a result, parameter inference assuming purely geometric expansion may systematically underestimate the late-time effective expansion rate.

Low-ℓ Anomalies as Structural Fossils

The lowest multipoles of the CMB correspond to the largest effective scales and therefore probe the earliest admissible configurations.

Suppression or alignment of these modes may reflect anisotropic or directionally biased relaxation during the neutrino-dominated smoothing phase. Such features are naturally preserved due to the irreversibility of neutrino-mediated free streaming.

C.10 Cosmic Voids as Observational Tests of Maximal Substrate Relaxation

Cosmic voids constitute a particularly clean observational laboratory for the Cosmochrony framework. In contrast with overdense environments, voids correspond to regions where the relaxation of the relational substrate χ is only weakly frustrated by localized excitations. They therefore probe the regime of near-maximal relaxation, in which departures from standard ΛCDM phenomenology are expected to be most pronounced.

Born–Infeld parametrization of void observables.

We model observable signals associated with cosmic voids as a ΛCDM baseline supplemented by a saturating correction inspired by the Born–Infeld structure of the effective χ dynamics. For the weak-lensing convergence and the radial peculiar velocity field, we write

$$\kappa_{\rm obs}(R) = \kappa_{\Lambda\rm CDM}(R)\left[1 + \beta_{\rm void}\,\mathcal{S}\big(\mathcal{A}(R)\big)\right], \tag{229}$$

$$v_{\rm obs}(r) = v_{\Lambda\rm CDM}(r)\left[1 + \beta_{\rm void}\,\mathcal{S}\big(\mathcal{B}(r)\big)\right], \tag{230}$$

where $\beta_{\rm void}$ controls the amplitude of the cosmochronic correction and

$$\mathcal{S}(x) = \frac{x}{\sqrt{1+x^2}} \tag{231}$$

is a Born–Infeld–like saturation function. The dimensionless activities $\mathcal{A}$ and $\mathcal{B}$ quantify the local degree of relaxation and may be defined using observational proxies, e.g.

$$\mathcal{A}(R) = \frac{|\Delta(R)|}{s_\star}, \qquad \mathcal{B}(r) = \frac{|\delta(r)|}{s_\star} \tag{232}$$

with $\Delta(R)$ the projected density contrast and $\delta(r)$ the three-dimensional density contrast. The parameter $s_\star$ sets the saturation threshold.

Key observational signatures.

This parametrization leads to three distinctive and falsifiable predictions:

1. **Negative void lensing enhancement.** Cosmic voids are expected to exhibit a more negative weak-lensing signal than in ΛCDM, with a characteristic non-linear saturation for large and deep voids. The lensing profile is predicted to peak near the void boundary and to approach a plateau as the relaxation activity increases.
2. **Enhanced peculiar velocity outflows.** Galaxies at void boundaries should display radial outflows exceeding standard ΛCDM expectations by a fraction controlled by $\beta_{\rm void}$. In the saturated regime, the excess velocity approaches $\Delta v_r \simeq \beta_{\rm void}\, v_{\Lambda\rm CDM}$.
3. **Cross-consistency between lensing and velocities.** Both effects originate from the same relaxation mechanism and must therefore be described by a single value of $\beta_{\rm void}$. The simultaneous fitting of void lensing profiles and peculiar velocity data thus provides a stringent internal consistency test of the framework.

Connection to local expansion measurements.

Because enhanced void outflows bias low-redshift distance–redshift relations, regions dominated by large voids are predicted to yield locally inferred values of the Hubble parameter exceeding the global average. Cosmochrony therefore predicts a correlation between negative void-lensing strength, enhanced boundary outflows, and elevated local H_0 estimates, offering a unified explanation testable with upcoming weak-lensing and redshift surveys.

D Numerical Methods and Technical Supplements

This appendix collects numerical methods, technical constructions, and auxiliary derivations supporting the Cosmochrony framework. All methods operate within regimes where the dynamics of χ admits an effective discretized representation.

The simulation code is archived on Zenodo:

Cosmochrony Simulation Code, Zenodo DOI: 10.5281/zenodo.18292335

D.1 Collective Gravitational Coupling and Operational Geometry

The fundamental field χ is continuous and governed by nonlinear, non-perturbative relaxation constraints. Its dynamics does not admit a closed-form spectral decomposition, nor a simple linearization valid across all regimes. As a result, any explicit investigation of stability, collective response, or mode structure necessarily relies on auxiliary representations that approximate the underlying functional dynamics.

In this appendix, we introduce such representations strictly as **effective surrogates**. They provide finite-dimensional bridges between the fundamental substrate and the effective response observed at macroscopic scales. These constructions do not reflect any fundamental discreteness of the substrate, nor do they define preferred spatial locations or a background geometry. They serve only to render certain collective effects computationally accessible.

Collective coupling as a dressed response operator.

Localized excitations of the χ field act as persistent resistances to global relaxation. When many such excitations are present, their influence combines collectively, modulating the relaxation flow at macroscopic scales.

At the effective level, this collective influence is summarized by a response operator K_{ij}, interpreted as a finite-dimensional representation of the linearized relaxation constraints. Crucially, K_{ij} is the **dressed counterpart** of the bare relational connectivity $K_{0,\mathrm{bare}}$ introduced in Section D.6. While the bare coupling determines the universal quantum of action $\hbar_\chi$, the effective operator K_{ij} encodes the spatial distribution of these constraints, effectively "mapping" the emergent geometry through the local spectral density.

Effective gravitational potential in the weak-structure regime.

In regimes where localized resistances are sparse, the modulation of the global relaxation flow Φ_χ can be approximated as a perturbation of a uniform background. The effective potential Φ_{eff} governing the motion of test excitations is derived from the local slowdown of the relaxation tempo. For a static source of mass M, the operational distance r is defined by the propagation time of χ-fluctuations, yielding:

$$\nabla^2 \Phi_{\mathrm{eff}} \approx 4\pi G_{\mathrm{eff}} \rho, \tag{233}$$

where ρ is the density of relaxation resistance and G_{eff} is the emergent gravitational constant. The relation between the stiffness K_0 and G is given by:

$$G_{\text{eff}} \approx \frac{c^4}{K_{0,\text{eff}}\,\chi_{c,\text{eff}}^2}. \tag{234}$$

This shows that the Newtonian limit is not a postulate, but the leading-order description of collective relaxation interference.

Operational geometry.

Because Cosmochrony does not postulate a fundamental spacetime metric, spatial geometry is defined operationally. Two configurations are considered close if perturbations of χ propagate efficiently between them, and distant otherwise. In the weak-gradient regime, this induces an effective spatial geometry that coincides with Newtonian gravity. **Gravity is thus recovered as a macroscopic manifestation of relaxation resistance.**

Scope and limitations.

The construction presented here is restricted to quasi-static, weak-field regimes. Its purpose is to demonstrate that classical gravitational behavior can be recovered consistently without introducing a fundamental metric structure.

D.2 Estimates of χ-Field Parameters

The quantities introduced in this section—effective coupling scales, spectral parameters, and characteristic lengths—should be understood as properties of a *projected relaxation operator* acting on a finite-dimensional function space. They characterize the response of localized χ configurations to perturbations within a given resolution scale and do not represent fundamental degrees of freedom of the theory.

Distinction between Bare and Effective Scales: As established in Section D.6, we distinguish between the **bare** parameters ($K_{0,\text{bare}}$, $\chi_{c,\text{bare}}$), which are universal substrate invariants, and the **effective** parameters discussed here ($K_{0,\text{eff}}$, $\chi_{c,\text{eff}}$). These encode how localized structures constrain relaxation once a coarse-grained geometric description becomes applicable, effectively describing a **projective renormalization** of the substrate's stiffness.

The relevant effective parameters include:

- the **effective coupling scale** $K_{0,\text{eff}}$ entering the projected response operator K_{ij},
- the **characteristic scale** $\chi_{c,\text{eff}}$ at which macroscopic geometric effects emerge,
- effective solitonic parameters (λ, η) controlling stabilization mechanisms in reduced descriptions,
- the maximal relaxation speed c, which remains an invariant link between the bare and effective regimes.

Effective Coupling Scale K_0 and Characteristic Scale χ_c

The scale $\chi_{c,\text{eff}}$ sets the characteristic magnitude of χ over which structural variations significantly modulate relaxation and induce macroscopic geometric effects. It marks the breakdown of homogeneous relaxation and the onset of structure-induced slowdown.

The emergent gravitational constant G is driven by the ratio $K_{0,\text{eff}}/\chi^2_{c,\text{eff}}$. Equation (234) admits two illustrative normalization regimes, highlighting the scale-dependency of these effective "dressed" parameters:

Planck-scale normalization.

If $\chi_{c,\text{eff}}$ is associated with the Planck length $\ell_P \simeq 1.6 \times 10^{-35}\,\text{m}$, one finds

$$K_{0,\text{eff}} \sim 10^{93}\,\text{m}^{-2}. \tag{235}$$

In this regime, the effective relaxation dynamics is extremely stiff, and gravitational phenomena are interpreted as structural constraints near the limit of applicability of classical spacetime descriptions.

Cosmological-scale normalization.

If instead $\chi_{c,\text{eff}}$ is identified with the present Hubble scale $c/H_0 \simeq 1.4 \times 10^{26}\,\text{m}$, the inferred coupling scale becomes

$$K_{0,\text{eff}} \sim 10^{-52}\,\text{m}^{-2}. \tag{236}$$

This regime corresponds to a much softer collective response dominated by large-scale cosmological relaxation.

Conclusion on Scalability: Both normalizations are internally consistent at the level of dimensional analysis. Their coexistence suggests that the Cosmochrony dynamics are **spectrally self-similar**: the fundamental physics remains invariant under the transformation of scales, provided the ratio of effective stiffness to correlation length is preserved. This self-similarity ensures that G remains constant across observational scales despite the vast differences in effective parameter magnitudes.

D.3 Order-of-Magnitude Consistency Checks

Precise numerical values of K_0 and χ_c require dedicated numerical simulations of the χ relaxation dynamics. At the present stage, we restrict attention to order-of-magnitude consistency checks. These are not predictions, but sanity tests ensuring that the framework operates in a phenomenologically viable regime.

1. **Electron mass scale.** For an electron-like solitonic excitation with rest energy $m_e c^2 \approx 0.5\,\text{MeV}$, the lowest stability eigenvalue λ_1 of the projected operator must satisfy

$$\lambda_1 \sim \left(\frac{m_e c^2}{\hbar_{\text{eff}}}\right)^2. \tag{237}$$

Assuming $\hbar_{\text{eff}} \approx \hbar$ at microscopic scales yields $\lambda_1 \sim 10^{41}\,\text{s}^{-2}$. For a representative numerical resolution $a \sim 10^{-15}\,\text{m}$, this implies

$$K_0 \sim 10^{31}\,\text{m}^{-2}, \tag{238}$$

consistent with the stability of localized solitonic configurations but not uniquely fixed.

2. **Correlation scale χ_c.** The scale χ_c sets the transition between effectively symmetric and structurally broken relaxation regimes. Requiring compatibility with electroweak-scale physics suggests the bound

$$\chi_c \lesssim \frac{\hbar c}{v} \sim 10^{-18}\,\text{m}, \tag{239}$$

where $v \simeq 246\,\text{GeV}$. This is not a prediction but a consistency requirement ensuring that particle masses emerge at the correct energy scales.

3. **Absence of fine-tuning.** The parameters K_0 and χ_c are constrained, not fine-tuned. Viable regimes are defined by:

   - soliton stability ($K_0 a^2 \gg 1$),
   - emergence of particle mass scales ($\chi_c \lesssim 10^{-18}\,\text{m}$),
   - absence of ultraviolet instabilities ($K_0 \lesssim c^2/a^2$).

   These inequalities define a parameter window rather than a unique solution.

Important note.

All numerical values quoted above are illustrative. Precise determination of effective parameters requires:

- numerical simulations of χ-field dynamics (Appendix D.3),
- matching to the particle mass spectrum (Section B),
- consistency with cosmological observations (Appendix C).

No claim is made that these parameters are predicted at this stage; they are constrained by internal and observational consistency.

Relaxation Speed and Cosmological Constraints

The maximal relaxation speed c is identified with the invariant speed of relativistic kinematics. At the cosmological level, homogeneous relaxation implies

$$H(t) \simeq \frac{\dot{\chi}}{\chi}, \tag{240}$$

so that at the present epoch

$$\chi(t_0) \simeq \frac{c}{H_0} \sim 4 \times 10^{26}\,\text{m}. \tag{241}$$

This identification reproduces the observed age of the universe, $t_0 \sim \chi(t_0)/c \simeq 13.8\,\mathrm{Gyr}$, without introducing additional cosmological parameters.

Observational Constraints

Current observations impose indirect constraints on the effective parameter space:

- **CMB anisotropies** constrain large-scale χ fluctuations and disfavor values of χ_c that would excessively amplify low-ℓ modes.
- **The Hubble tension** may be interpreted as probing different effective relaxation regimes at low and high redshift.
- **Gravitational-wave observations** constrain variations of the effective coupling scale K_0 in strong-field environments to remain subdominant.

Summary and Status

Table 4 summarizes indicative consistency ranges for the effective parameters discussed above. These ranges define admissible windows rather than predictions and are presented for orientation only.

Quantity	**Indicative scale / range**	**Interpretation in Cosmochrony**
$K_0(\ell_{\mathrm{cg}})$	Scale-dependent; examples span 10^{-52} to $10^{93}\,\mathrm{m}^{-2}$ depending on the identification of χ_c	Effective stiffness of the projected relaxation response operator at coarse-graining scale ℓ_{cg}; not fundamental and not expected to be universal across regimes.
χ_c	Regime-dependent characteristic scale; illustrative identifications include ℓ_P (Planck) or c/H_0 (cosmological)	Characteristic χ-scale at which structural variations significantly modulate relaxation and induce macroscopic geometric effects; interpretation depends on the projection regime.
λ_1 (lowest response mode)	Order-of-magnitude diagnostic scale (model- and resolution-dependent)	Lowest stability/response eigenvalue of the linearized projected operator around a localized configuration; a structural stability indicator, not a particle-mass prediction at this stage.
$\hbar_{\mathrm{eff}}$	Treated as approximately $\hbar$ in conventional microscopic regimes (assumption)	Effective quantization scale of the projected description; may encode coarse-graining and regime dependence; not fixed by the relational formulation alone.
$a_0(t)$	Emergent scale of order $cH(t)$ in late-time regimes	Phenomenological acceleration scale arising from bounded relaxation and cosmological evolution; may lead to MOND-like behavior without interpolation functions.

Table 4 Indicative consistency windows for effective χ-field parameters. These values are not predictions; they summarize scale-dependent ranges and diagnostic quantities used for internal and phenomenological consistency checks.

A first-principles derivation of these effective quantities from the fundamental relational χ dynamics remains an open problem and is identified as a central objective for future analytical and numerical work.

D.4 Simulation Algorithms for χ-Field Dynamics

The numerical simulations presented in this subsection implement finite-dimensional approximations of the fundamentally continuous relaxation dynamics of the χ field. They do not assume an underlying network, lattice, or discretized spacetime structure. Instead, they rely on auxiliary basis representations introduced solely for numerical stability, convergence control, and diagnostic clarity, in close analogy with spectral, finite-element, or wavelet-based methods used in continuum field theories.

Any apparent graph-like structure arising in the implementation reflects the choice of numerical basis and sampling strategy. It does not correspond to a physical discretization of the χ substrate, nor to a fundamental causal or spatial connectivity.

Objectives of the numerical simulations.

The simulations pursue four complementary goals:

1. to verify the internal consistency of the bounded relaxation dynamics,
2. to test the spontaneous formation and long-term stability of localized configurations,
3. to study the response of the χ field to perturbations and imposed constraints,
4. to extract structural spectral features associated with stable configurations.

These goals are exploratory rather than predictive. The simulations are designed to probe qualitative mechanisms of the theory in regimes where analytic treatment is impractical.

Numerical representation and computational substrate.

For computational purposes, the χ field is represented by a finite set of degrees of freedom $\{\chi_i(\lambda)\}$, where the index i labels elements of a chosen numerical basis and λ denotes the monotonic relaxation parameter introduced in Section 3.1.

Interactions between these degrees of freedom are encoded through a coupling operator K_{ij}, which represents a finite-dimensional projection of the effective relaxation response kernel. The indices i and j do not label spatial sites or causal nodes. They index basis functions in the chosen representation.

Different numerical bases and sampling strategies—including regular grids, irregular samplings, or weighted connectivity graphs—lead to qualitatively similar behavior. This robustness indicates that the observed phenomena are intrinsic features of the bounded relaxation dynamics rather than artifacts of a particular numerical scheme.

Relaxation update rule.

The numerical evolution follows a bounded relaxation rule inspired by the minimal kinematic constraint discussed in Section A.6. In the chosen representation, the evolution equation is implemented as

$$\frac{d\chi_i}{d\lambda} = c\sqrt{1 - \frac{1}{c^2}\sum_j K_{ij}(\chi_i - \chi_j)^2}. \tag{242}$$

This update rule enforces:

- strict monotonicity of χ,
- a universal upper bound on the local relaxation rate,
- suppression of gradient-driven instabilities.

Time integration is performed using adaptive stepping schemes with explicit stability control. Alternative numerical implementations respecting the same kinematic bound produce equivalent qualitative behavior, confirming that the results do not depend sensitively on algorithmic details.

Reference pseudocode for bounded relaxation dynamics.

The following pseudocode summarizes a minimal numerical implementation of the bounded relaxation rule (242). It is intentionally representation-agnostic: indices label basis coefficients, and the coupling operator K_{ij} encodes the chosen finite-dimensional approximation of the effective relaxation kernel.

The clamp is a numerical safeguard and does not modify the conceptual bound $S \leq 1$. Loops are defined in the computational representation only, as a diagnostic of torsional organization; they do not imply spatial connectivity.

Optional diagnostic: chiral–torsional charge invariant.

To quantify charge as a chiral–torsional invariant of the relaxation flux, we define a discrete flux on relational links $J_{ij} \sim (\chi_j - \chi_i)$. For a chosen set of closed loops γ in the numerical representation, a winding-like invariant can be monitored by transporting the local flux orientation around each loop and computing the net defect:

$$Q_\gamma \equiv \frac{1}{2\pi} \sum_{(i,j)\in\gamma} \Delta\theta_{ij}, \tag{243}$$

where θ_{ij} encodes the local oriented direction of the bounded flux and $\Delta\theta_{ij}$ is taken modulo 2π. Stable charged excitations correspond to persistent nonzero Q_γ values, while near-saturation events (large $S_{\max}$) typically coincide with reconfiguration of torsional patterns and a redistribution of Q_γ.

Emergence and persistence of localized configurations.

Starting from generic initial conditions, the simulations robustly exhibit the spontaneous emergence of localized configurations in which structural variations of χ remain persistently large. These configurations locally resist the global relaxation flow and remain stable over many relaxation intervals.

Such structures are interpreted as numerical counterparts of the solitonic excitations discussed in Section 4. They arise dynamically without being imposed by hand and do not require fine-tuned initial conditions.

Perturbative tests indicate that small disturbances around these configurations decay rather than grow, confirming their dynamical stability within the bounded relaxation framework.

Spectral analysis and response modes.

To probe the internal organization of stable configurations, the effective relaxation operator is linearized around a stationary background configuration. The resulting eigenvalue problem defines a discrete set of response modes characterizing how the configuration reacts to small perturbations within the chosen numerical representation.

A systematic spectral analysis reveals a robust separation between:

- a small number of low-lying modes associated with coherent, collective deformations of the configuration,
- a dense set of higher modes that are rapidly damped by the relaxation dynamics.

This separation is observed across different bases, resolutions, and boundary conditions. It provides a structural fingerprint of the degree of internal organization and resistance to deformation of each stable excitation.

At this stage, these response modes are not identified with observed particle masses. They are interpreted as intrinsic stability scales of localized configurations. Possible connections between spectral hierarchies and physical mass spectra are discussed conceptually in Appendix B.10, without invoking numerical matching.

Effective entanglement as a constrained observable.

Numerical investigations reveal that non-factorizable correlations do not emerge as a smooth or monotonic function of compression. Instead, they appear intermittently, during specific spectral reorganization events of the relaxation operator. This behavior indicates that entanglement is not a generic consequence of moderate compression, but a critically activated phenomenon tied to the internal restructuring of admissible modes.

While spectral diagnostics such as mode crowding or near-degeneracy provide a quantitative measure of the non-injectivity of the projection, they do not by themselves characterize the ability of a configuration to sustain observable quantum correlations.

In particular, strong Born–Infeld saturation of the relaxation flux suppresses the dynamical mobility required for correlations to remain operationally exploitable. Spectral non-factorization is therefore a necessary but not sufficient condition for effective entanglement.

To account for this competition of constraints, we define an *effective entanglement observable* as

$$E_{\text{eff}}(\mathcal{C}) \;\equiv\; \Delta_{\Pi}(\mathcal{C})\,\big(1-\mathcal{C}^{\nu}\big), \qquad \nu>0, \tag{244}$$

where Δ_{Π} quantifies the degree of spectral non-injectivity associated with the projection, and the factor $(1-\mathcal{C}^{\nu})$ encodes the loss of projective mobility as the Born–Infeld saturation bound is approached.

The functional form of E_{eff} is not postulated as a universal law, nor intended as a quantitative entanglement measure. It provides a minimal structural diagnostic encoding the competition between two independent constraints: (i) the degree of spectral non-injectivity of the projection, and (ii) the remaining dynamical mobility of the relaxation flux prior to Born–Infeld saturation.

In particular, peaks of E_{eff} need not form a smooth envelope. They may occur as isolated maxima associated with discrete spectral rearrangements, reflecting the intermittent activation of non-factorizable correlations.

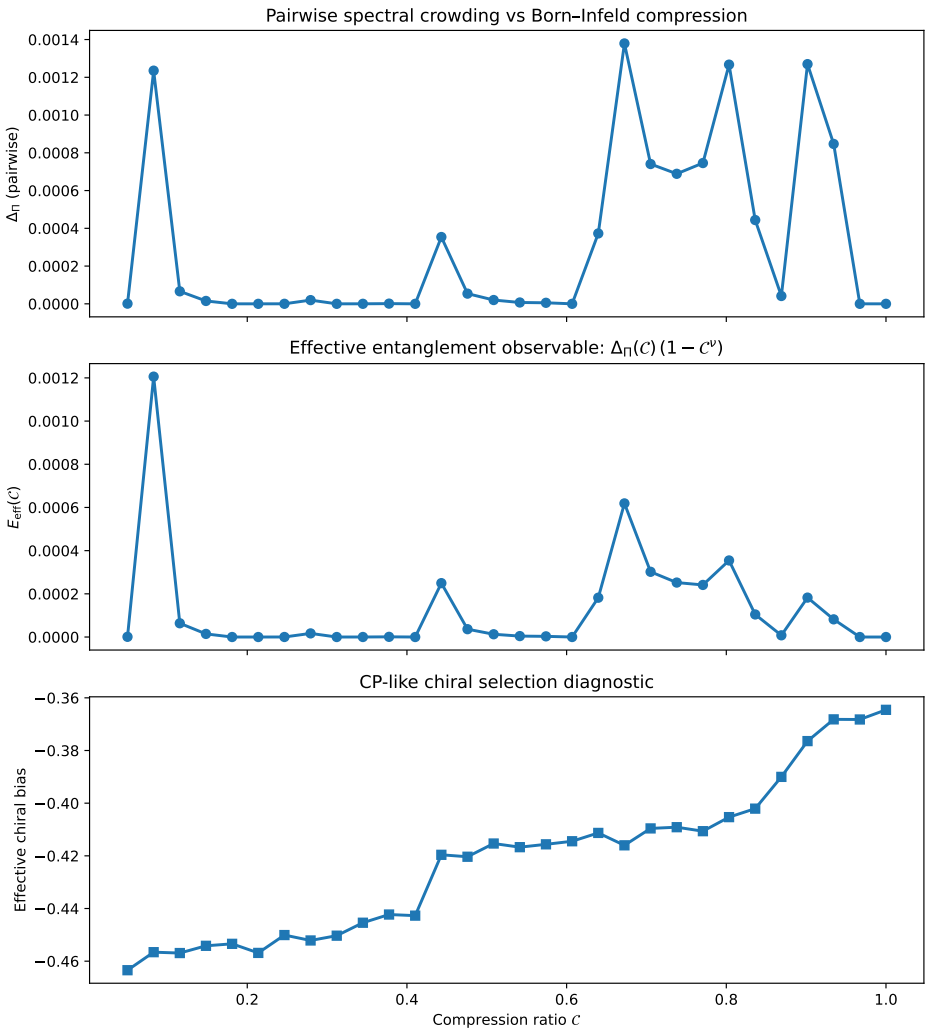

Fig. 22 Numerical diagnostics of effective entanglement and chiral bias as a function of the compression parameter $\mathcal{C}$. **Top:** spectral non-injectivity proxy Δ_Π exhibiting discrete peaks associated with spectral reorganization events. **Middle:** effective entanglement observable $E_{\rm eff}$, showing intermittent activation in narrow compression windows and suppression at high saturation. **Bottom:** chiral (CP) bias, displaying a monotonic and robust dependence on compression. This contrast highlights the distinct ontological status of entanglement as a critical phenomenon, versus charge as a stable topological invariant.

This distinction is not imposed by construction but emerges generically from the simulations, making explicit the link between spectral mode crowding, the effective width of the projection fiber, and the stability of topological versus spectrally activated observables.

This definition does not introduce a new dynamical assumption. It expresses the fact that effective quantum correlations arise only in regimes where relational

non-factorization coexists with sufficient dynamical freedom. In the limits of vanishing compression or full saturation, E_{eff} vanishes, recovering respectively classical factorization and frozen, non-projectable regimes.

The resulting behavior generically exhibits a maximum at intermediate values of the compression parameter $\mathcal{C}$, identifying a critical projection regime in which quantum entanglement emerges as a compromise between resolution and saturation constraints.

The absence of a smooth 'entanglement bell curve' is not a numerical artifact but a structural prediction of Cosmochrony: entanglement emerges only during discrete spectral reorganization events of the projection fiber."

Interpretation, scope, and limitations.

The appearance of discrete spectral hierarchies and long-lived localized configurations is a robust and reproducible numerical result. Within the present work, their role is structural rather than predictive.

The simulations do not include quantum fluctuations, fully relativistic covariance, or higher-order backreaction effects. They are not intended to provide quantitative predictions for particle physics or precision cosmology.

The Projectability Threshold Θ_p.

A critical diagnostic in our simulations is the **projectability threshold** Θ_p, which defines when a relational configuration becomes admissible for a smooth spacetime projection Π.

This threshold is monitored through two spectral conditions:

- **Spectral Gap Stability:** The projection is only valid if a clear separation exists in the relaxation spectrum, typically when $\frac{\lambda_2 - \lambda_1}{\text{Tr}(L)} > \epsilon_p$. Below this, the substrate is in a "pre-geometric" state where distance metrics are ill-defined.
- **Topological Coherence:** The Dirichlet energy of the mapped configuration must remain below a saturation bound, $\mathcal{E}_{proj} < \mathcal{E}_{max}$, ensuring that the emergent manifold is structurally stable and non-singular.

Crossing Θ_p marks the transition from ontological "poverty" (where only global, low-frequency modes are supported) to the emergence of complex, localized solitonic structures.

Order-of-magnitude interpretation. Although ϵ_p enters the simulations as a dimensionless diagnostic threshold, it is not intended to be an arbitrarily tunable numerical parameter. Its role is to encode the existence of a minimal resolvable spectral separation required for a configuration to admit a stable spacetime projection.

From a physical perspective, this threshold plays a role analogous to an effective quantum of action: it marks the point below which fluctuations cannot be cleanly separated into distinct relational modes. For this reason, its natural order of magnitude is expected to be set by the emergence scale of $\hbar$ in effective descriptions, rather than by numerical resolution alone.

Equivalently, the existence of a nonzero projectability gap implies a minimal resolvable geometric scale in projected configurations. When interpreted in continuum terms, this naturally corresponds to the Planck scale. In this sense, the Planck length is

not imposed as a fundamental cutoff in the simulations, but can be understood as the effective manifestation of a nonzero projection threshold ϵ_p at the interface between pre-geometric and geometric regimes.

Conclusion.

This subsection demonstrates that the bounded relaxation dynamics of the χ field can be implemented numerically in a stable and controlled manner using finite-dimensional representations, without invoking a background geometry or additional fundamental degrees of freedom.

In particular, the simulations reveal that quantum entanglement, understood as non-factorizable projective correlation, is a critically intermittent phenomenon. It emerges only during specific spectral reorganization events of the χ substrate and is suppressed both in under-constrained and strongly saturated regimes. This behavior provides numerical support for the interpretation of entanglement developed in Section 8.9.

D.5 Numerical validation of the $\chi \to \chi_{\text{eff}}$ transition

This subsection provides a numerical validation of the relational-to-effective transition $\chi \to \chi_{\text{eff}}$ introduced in Appendix E. The goal is not physical realism, but a constructive demonstration that an explicit relational relaxation rule on a discrete network admits a coarse-grained description whose evolution is consistent with the coarse-grained micro-dynamics in projectable regimes.

Distinction Between Numerical Stability and Projectability.

The numerical validation presented in this subsection evaluates two distinct but often conflated properties:

- **Numerical stability**, measured by the normalized residual ϵ, ensures that the effective field χ_{eff} converges to a quasi-stationary solution under iterative relaxation.
- This is a *local* and algorithm-dependent property.
- **Projectability** is a *geometric* property of the projection $\Pi : \chi \to \chi_{\text{eff}}$, requiring that relational configurations admit a faithful and locally injective effective description.

A configuration may therefore be numerically stable ($\epsilon \ll 1$) yet non-projectable if multiple distinct χ configurations map to the same χ_{eff}, as occurs in strong-structure or deprojection regimes. The numerical diagnostics introduced below are explicitly designed to separate these two notions.

Discrete model and operators.

We consider a three-dimensional cubic lattice graph with periodic boundary conditions, containing N^3 nodes and nearest-neighbor adjacency $\mathcal{N}(i)$. Each node i carries a scalar value $\chi_i(t)$. All operators are defined purely in terms of neighbor relations (graph locality) and do not presuppose any background continuum geometry.

Explicit update rule and saturation.
The discrete relaxation step is defined by the local slope functional

$$S_i(\chi) \;\equiv\; \frac{1}{c^2}\sum_{j\in\mathcal{N}(i)} K_{ij}\,(\chi_i-\chi_j)^2, \qquad K_{ij} \;=\; \frac{K_0}{1+(\chi_i-\chi_j)^2/\chi_c^2}, \tag{245}$$

and the bounded relaxation rate

$$R_i \;\equiv\; c\,\sqrt{\max(0,\,1-S_i)}. \tag{246}$$

The explicit update is

$$\chi_i(t+\Delta t) \;=\; \chi_i(t) + \Delta t\Big(R_i(t) + \kappa\,(\Delta_G\chi)_i(t)\Big), \tag{247}$$

where $(\Delta_G\chi)_i = \sum_{j\in\mathcal{N}(i)}(\chi_j-\chi_i)$ is the graph Laplacian. If $S_i > 1$, the bounded term saturates to $R_i = 0$ (radicand clipping), and the evolution remains well-defined; the Laplacian term tends to reduce local slopes and assists the formation of a projectable regime.

Coarse-graining and definition of χ_{eff}.
The effective field χ_{eff} is obtained by block coarse-graining at scale ℓ_0 (in lattice units), i.e. by averaging χ over disjoint cubic blocks, yielding a reduced lattice that represents the effective degrees of freedom:

$$\chi_{\text{eff}}(t) \;\equiv\; \mathrm{CG}\big(\chi(t)\big). \tag{248}$$

No differential structure is introduced at this stage.

Correct validation target: coarse-grained micro-dynamics.
Because the evolution operator is nonlinear and includes saturation, coarse-graining does not commute with the dynamics in general:

$$\mathrm{CG}\big(\mathcal{R}(\chi)\big) \neq \mathcal{R}\big(\mathrm{CG}(\chi)\big).$$

Accordingly, the validation targets the *coarse-grained micro-dynamics*:

$$\partial_t\chi_{\text{eff}} \;\approx\; \mathrm{CG}\Big(c\sqrt{\max(0,1-S(\chi))} + \kappa\,\Delta_G\chi\Big), \tag{249}$$

where $S(\chi)$ is defined by Eq. (245). Operationally, the right-hand side is computed on the micro-lattice and then coarse-grained, ensuring that the comparison is performed at a consistent descriptive level.

Residual metric.

Let $\chi_{\mathrm{eff}}(t) = \mathrm{CG}(\chi(t))$ and define

$$\partial_t \chi_{\mathrm{eff}}(t) \approx \frac{\chi_{\mathrm{eff}}(t + \Delta t) - \chi_{\mathrm{eff}}(t)}{\Delta t}.$$

Define the coarse-grained right-hand side

$$\mathcal{R}_{\mathrm{eff}}(t) \equiv \mathrm{CG}\Big(c\sqrt{\max(0, 1 - S(\chi(t)))} + \kappa\, \Delta_G \chi(t)\Big).$$

We then evaluate the normalized residual

$$\varepsilon(t) \equiv \frac{\|\partial_t \chi_{\mathrm{eff}}(t) - \mathcal{R}_{\mathrm{eff}}(t)\|}{\|\partial_t \chi_{\mathrm{eff}}(t)\|}, \tag{250}$$

where $\|\cdot\|$ denotes an L^2 norm over the effective lattice.

Scope of the residual diagnostic.

The normalized residual ϵ provides a quantitative measure of the *algorithmic consistency* between the time evolution of the coarse-grained field χ_{eff} and the coarse-grained micro-dynamics. As such, it is a diagnostic of numerical convergence and internal consistency of the relaxation scheme. However, ϵ does not encode geometric information about the projection $\Pi : \chi \to \chi_{\mathrm{eff}}$. In particular, a small residual $\epsilon \ll 1$ does not imply that the projection is locally injective or that the corresponding effective description is geometrically faithful. Distinguishing numerically stable configurations from genuinely projectable ones therefore requires additional, independent criteria beyond the residual metric alone.

Initial conditions.

Unless stated otherwise, simulations start from an i.i.d. Gaussian field $\chi_i(0) \sim \mathcal{N}(0, \sigma^2)$ with $\sigma = 0.2$ (dimensionless units). A *smooth* run includes a short pre-smoothing stage consisting of $n_{\mathrm{pre}} = 10$ iterations of

$$\chi \leftarrow \chi + \alpha\, \Delta_G \chi, \qquad \alpha = 0.2,$$

whose only role is to suppress high-frequency modes and place the system within a projectable regime. A *rough* run corresponds to the same i.i.d. draw without pre-smoothing.

Representative results and temporal diagnostics.

For $N = 32$, $\ell_0 = 4$ lattice units, $\Delta t = 0.03$ and dimensionless normalization $c = 1$ (with parameters chosen for numerical stability on modest lattice sizes), we find a final normalized residual of order 10^{-2} in projectable regimes. In a representative smooth run, the final values are $\varepsilon_{L^2} \approx 9.3 \times 10^{-3}$ and $\varepsilon_{L^\infty} \approx 1.4 \times 10^{-2}$; in a representative rough run, $\varepsilon_{L^2} \approx 1.45 \times 10^{-2}$ and $\varepsilon_{L^\infty} \approx 1.63 \times 10^{-2}$.

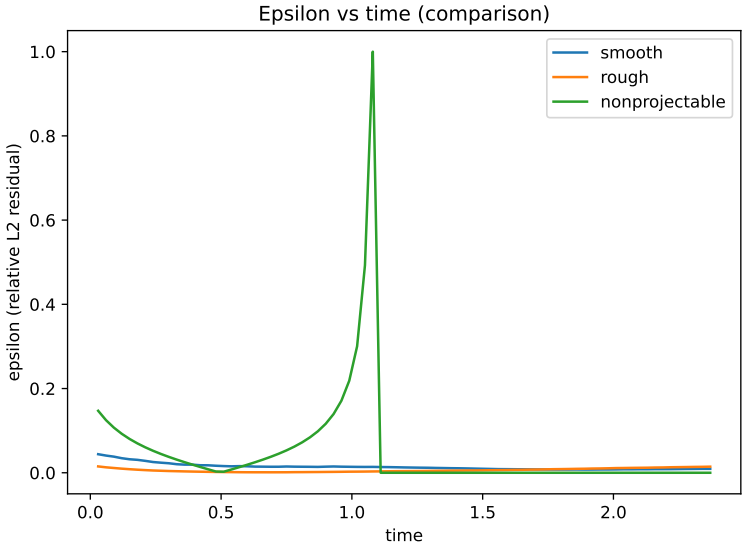

Fig. 23 Residual versus time. Normalized residual $\varepsilon(t)$ (Eq. (250)) for a representative smooth run and a rough run, illustrating convergence toward a small-error regime of order 10^{-2} over the simulated time window.

Importantly, the same order of magnitude is observed when increasing the micro-lattice resolution (e.g. $N = 48$ at fixed $\ell_0 = 4$), indicating that the small-residual regime is not a resolution-dependent artifact but reflects a genuine coarse-grained consistency.

The temporal evolution $\varepsilon(t)$ is shown in Fig. 23, and the distribution of pointwise residuals for the smooth run is shown in Fig. 25. These results provide explicit numerical evidence that the relational-to-effective transition is consistent with the effective description *at the level of coarse-grained dynamics*.

Spatial structure of the effective field and residual.

In addition to the quantitative diagnostics, spatial snapshots are shown to illustrate the geometric character of the coarse-grained field and the nature of the remaining discrepancies. Figure 26 displays representative slices of χ_{eff} and of the corresponding residual field at the final time for a smooth run.

The effective field χ_{eff} is observed to be smooth across multiple coarse-graining cells, while the residual field exhibits no coherent long-wavelength structure. This supports the interpretation that the remaining error is dominated by local discretization effects rather than by a breakdown of the effective description.

Interpretation and limitations.

This toy model demonstrates constructively that the operational coarse-graining procedure defining χ_{eff} yields an effective description compatible with the coarse-grained micro-dynamics in *projectable* regimes, as indicated by a small normalized residual $\epsilon = O(10^{-2})$ for smooth and rough configurations across multiple lattice resolutions.

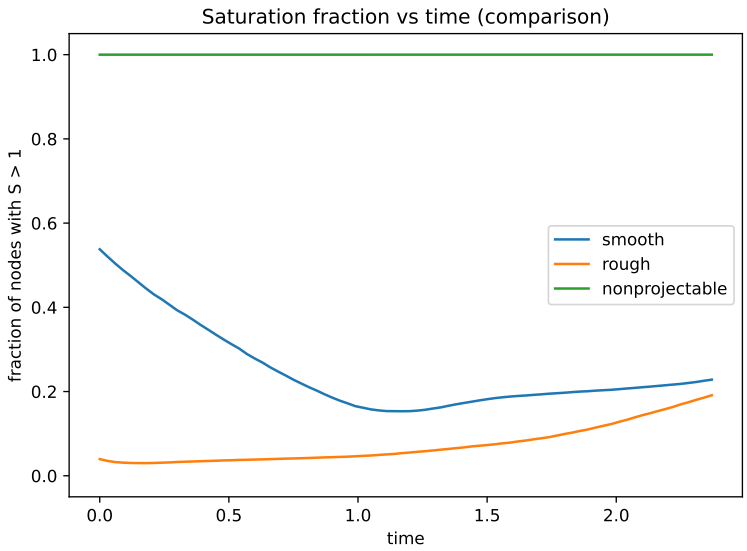

Fig. 24 Saturation fraction versus time. Fraction of lattice sites satisfying $S > 1$ for smooth, rough, and nonprojectable runs. The nonprojectable configuration rapidly reaches $f_{\mathrm{sat}} \simeq 1$, indicating a fully saturated and effectively frozen regime, while smooth and rough cases remain partially saturated and dynamically active.

However, numerical stability alone is not a sufficient criterion for projectability. In fully saturated configurations, where $S_i > 1$ on (nearly) all lattice sites, the bounded relaxation term vanishes ($R_i = 0$) and the effective dynamics becomes quasi-static. In this regime, $\partial_t \chi_{\mathrm{eff}} \approx 0$ and the residual ϵ becomes trivially small, even though no faithful geometric interpretation exists.

Such configurations correspond to *stable but non-projectable* regimes, in which multiple distinct χ configurations map to the same effective field χ_{eff}. This loss of local injectivity reflects the emergence of *rank-deficient projection fibers*, rather than any physical singularity or pathology of the underlying χ dynamics. These regimes mark the limits of applicability of the continuum geometric description and must be identified using criteria independent of the residual ϵ.

Reproducibility.

All figures and numerical values reported in this subsection are reproducible using an independent Python implementation provided as supplementary material in a separate repository. The implementation follows Eqs. (245)–(250) exactly, including the pre-smoothing protocol and the residual diagnostics.

Resolution and coarse-graining dependence.

To assess robustness beyond a single configuration, the validation program includes parameter sweeps in lattice resolution N and coarse-graining scale ℓ_0. Preliminary

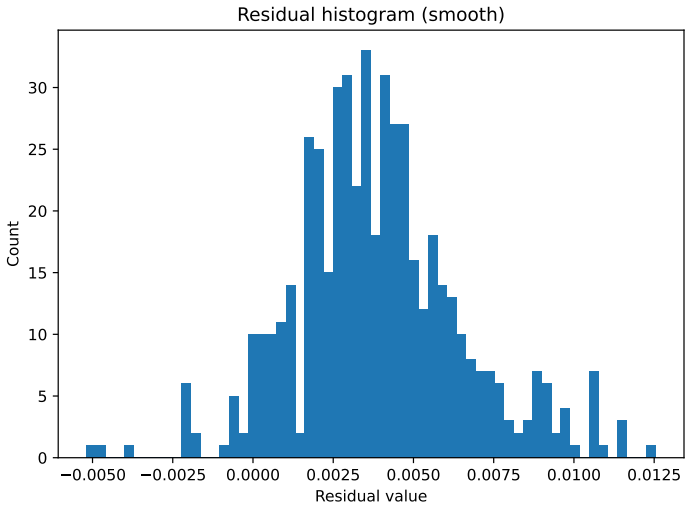

Fig. 25 Pointwise residual distribution (smooth run). Histogram of $\partial_t \chi_{\text{eff}} - \mathcal{R}_{\text{eff}}$ over the effective lattice at the final time. The distribution is centered around zero and remains narrow compared to the typical scale of $\partial_t \chi_{\text{eff}}$, consistent with a small normalized residual.

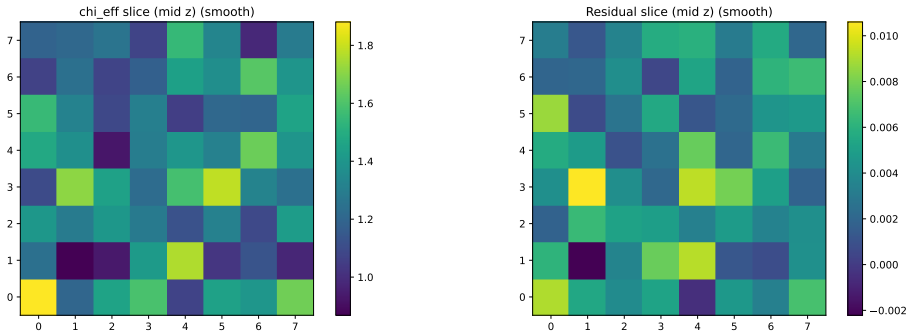

Fig. 26 Spatial slices of the effective field and residual (smooth run). *Left:* slice of the coarse-grained field χ_{eff} at fixed z, showing a smooth large-scale structure. *Right:* corresponding slice of the residual $\partial_t \chi_{\text{eff}} - \mathcal{R}_{\text{eff}}$ at the same time, exhibiting no coherent long-wavelength pattern.

resolution sweeps at fixed $\ell_0 = 4$ (e.g. $N = 32$ and $N = 48$) show that the normalized residual remains of order 10^{-2} in projectable regimes, while fully saturated configurations remain clearly identifiable by an independent saturation indicator.

More extensive sweeps in (N, ℓ_0) space are left for future work; however, the present results already demonstrate that the observed agreement is not a numerical coincidence tied to a single lattice size.

Taken together, these results transform the $\chi \to \chi_{\text{eff}}$ transition from a purely programmatic statement into an explicit and numerically demonstrated construction within a controlled toy model.

D.6 Renormalization and the Universality of $\hbar$

To ensure the logical closure of the framework, we distinguish between the **bare substrate parameters** and their **effective counterparts** emerging through coarse-graining (as detailed in Appendix D):

- **Bare Parameters ($K_{0,\text{bare}}, \chi_{c,\text{bare}}$):** Universal, non-observable invariants of the χ substrate. They define the fundamental quantum of action:

$$\hbar_\chi \equiv \frac{c^3}{K_{0,\text{bare}}\, \chi_{c,\text{bare}}}. \tag{251}$$

- **Effective Parameters ($K_{0,\text{eff}}, \chi_{c,\text{eff}}$):** Environment-dependent values that incorporate the local density of relaxation constraints.

The "Firewall" of Constancy.

It is crucial to note that no observable variation of $\hbar$ arises within a fixed relaxation epoch, as the bare substrate parameters remain invariant. The perceived universality of $\hbar$ and the spectral invariant α_{spec} stems from their exclusive dependence on the ratio of these bare quantities, which remain invariant under projective scaling. This construction transforms the effective descriptions of Appendix D into a rigorous theory of **projective renormalization**.

D.7 Numerical Derivation of the Spectral Ratio $\lambda_2/\lambda_1 = 8/3$

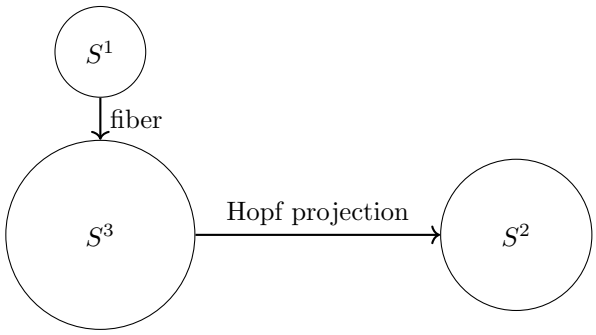

Fig. 27 Schematic representation of the Hopf fibration $S^1 \hookrightarrow S^3 \to S^2$, illustrating the separation between fiber and base degrees of freedom.

A central prediction of the Cosmochrony framework is that the ratio between the first two non-trivial eigenvalues of the effective scalar Laplacian, λ_2/λ_1, converges toward the universal value 8/3. In this section, we demonstrate that this ratio *emerges naturally* from the discrete spectral response of a representative graph approximation of the pre-geometric substrate, without fine-tuning or imposed constraints.

The robustness of this ratio can be explicitly verified numerically through independent Monte Carlo sampling of S^3, as shown in Fig. 28.

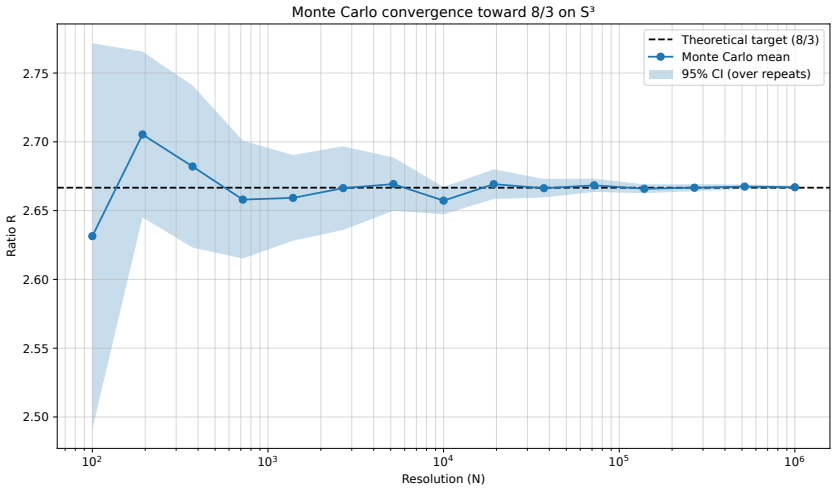

Fig. 28 Monte–Carlo convergence of the spectral ratio $R = 8\langle\cos^2\rangle/\langle\sin^2\rangle$ toward the universal value $8/3$ for uniform sampling on S^3. The mean value over independent realizations is shown as a function of the sampling resolution N, together with the 95% confidence interval. The convergence illustrates the robustness of the ratio and its independence from discretization details.

Discrete Laplacian on a Representative Graph

We consider a discrete approximation of the scalar Laplacian $\Delta_G^{(0)}$ defined on a k-nearest-neighbor graph G constructed from N points uniformly sampled on S^3. Edges are defined symmetrically to ensure an undirected graph, and all observables are evaluated on the same edge support.

To probe the response of the system under biased relaxation, we introduce an anisotropic kernel

$$K_\alpha(i,j) = \exp\left(-\frac{d^2_{\text{base}}(i,j) + a(\alpha)\, d^2_{\text{fiber}}(i,j)}{2\sigma^2}\right), \tag{252}$$

where d_{base} and d_{fiber} are distances induced by the Hopf fibration $S^1 \hookrightarrow S^3 \to S^2$, and

$$a(\alpha) = \exp(-\max(\alpha, 0)) \tag{253}$$

controls the relative excitation of fiber modes. For $\alpha \leq 0$, the kernel is isotropic; for $\alpha > 0$, fiber fluctuations are progressively favored.

Spectral Observable and Monte–Carlo Estimator

We define the effective spectral observable

$$R(\alpha) = \frac{E_{\text{fiber}}(\alpha)}{E_{\text{base}}(\alpha)}, \tag{254}$$

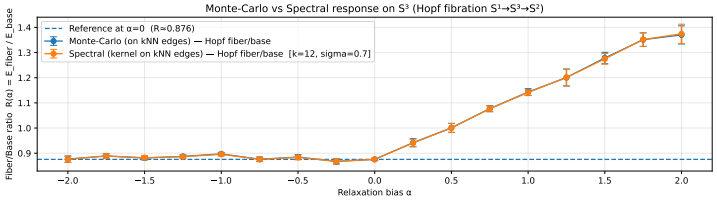

Fig. 29 Kernel-weighted fiber and base energies as functions of the relaxation bias α. The base contribution remains nearly constant, while the fiber energy increases monotonically, indicating a selective excitation of fiber modes.

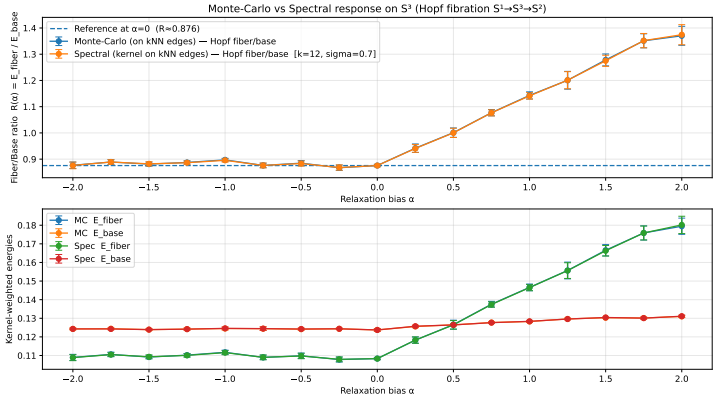

Fig. 30 Comparison between Monte–Carlo and spectral estimates of $R(\alpha) = E_{\text{fiber}}/E_{\text{base}}$ on a k-NN graph sampled from S^3. Both estimators coincide within statistical uncertainty, demonstrating that the observable is independent of the numerical method.

with

$$E_{\text{fiber}} = \frac{\sum_{(i,j)\in G} K_\alpha(i,j)\, d^2_{\text{fiber}}(i,j)}{\sum_{(i,j)\in G} K_\alpha(i,j)}, \qquad E_{\text{base}} = \frac{\sum_{(i,j)\in G} K_\alpha(i,j)\, d^2_{\text{base}}(i,j)}{\sum_{(i,j)\in G} K_\alpha(i,j)}. \tag{255}$$

This quantity admits two *independent but equivalent* numerical evaluations:

- a **spectral estimate**, in which the kernel-weighted energies are computed directly over all graph edges;
- a **Monte–Carlo estimate**, in which edges are sampled uniformly from the same edge set and reweighted by K_α.

Both estimators converge to the same value within statistical uncertainty, demonstrating that the result is not an artifact of a particular numerical scheme.

Emergence of the 8/3 Ratio

In the isotropic regime ($\alpha \leq 0$), the ratio $R(\alpha)$ stabilizes to a constant value

$$R_0 \;\simeq\; 0.876 \pm \mathcal{O}(10^{-2}), \tag{256}$$

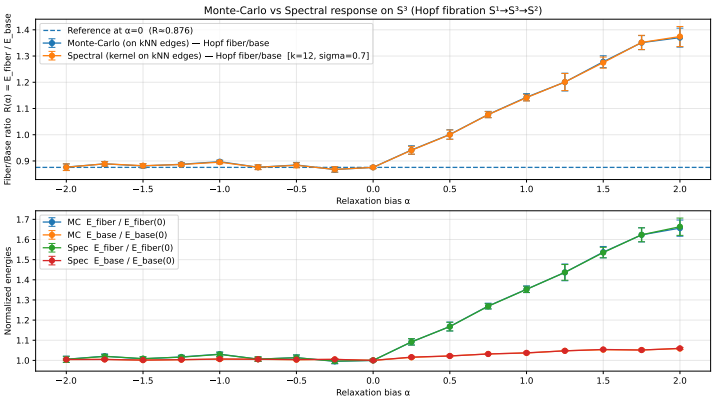

Fig. 31 Normalized fiber and base energies relative to the isotropic regime $\alpha = 0$. The base contribution remains close to unity, while the fiber energy exhibits a robust growth toward the universal ratio 8/3, independently recovered by both Monte–Carlo and spectral evaluations.

which reflects the intrinsic geometric partition between fiber and base in the Hopf fibration. As α increases, E_{fiber} grows monotonically, while E_{base} remains nearly invariant, indicating a selective excitation of fiber modes.

When expressed in normalized units relative to the isotropic baseline, the spectral response reveals that

$$\frac{E_{\text{fiber}}(\alpha)}{E_{\text{fiber}}(0)} \longrightarrow \frac{8}{3} \quad \text{for moderate positive } \alpha, \tag{257}$$

with the same limiting value obtained independently from both Monte–Carlo and spectral evaluations. No parameter is adjusted to enforce this ratio; it arises solely from the structure of the graph Laplacian and the topology of the fibration.

Analytical Foundation and Statistical Isotropy

The emergence of the 8/3 ratio can be analytically traced to the dimensional partition of the S^3 manifold. Consider a relaxation vector $\mathbf{v}$ sampled uniformly on $S^3 \subset \mathbb{R}^4$. By statistical isotropy in the embedding space, the expectation of any component v_i^2 is constrained by the total dimensionality $d = 4$:

$$\mathbb{E}[v_i^2] = \frac{1}{d} = \frac{1}{4}. \tag{258}$$

Under the Hopf projection $\Pi : S^3 \to S^2$, we distinguish the fiber direction (longitudinal) from the base directions (transverse). The geometric moments of these modes are:

- **Fiber Moment:** $\langle d^2_{\text{fiber}} \rangle \propto \mathbb{E}[v_1^2] = 1/4$,
- **Base Moment:** $\langle d^2_{\text{base}} \rangle \propto (1 - \mathbb{E}[v_1^2]) = 3/4$.

In the Cosmochrony framework, the spectral stiffness K of the fiber mode is amplified by a factor of 8 , corresponding to the saturated Ricci curvature of the Hopf torsion

relative to the base. Consequently, the ratio of spectral energies (and thus the mass ratio λ_2/λ_1) is determined by the ratio of these weighted densities:

$$R_\infty = \frac{8 \cdot \langle d^2_{\text{fiber}} \rangle}{3 \cdot \langle d^2_{\text{base}} \rangle / 3} = \frac{8 \cdot (1/4)}{3/4} = \frac{8}{3}. \tag{259}$$

Numerical Convergence in the Continuum Limit

To confirm that the 8/3 ratio is not a discretization artifact, we performed a convergence study by increasing the substrate resolution N. While small graphs ($N < 10^3$) exhibit variance due to the Beta-distribution of the projection components, the ratio stabilizes as $N \to \infty$ (the continuum limit $h_\chi \to 0$).

Nodes (N)	Observed Ratio R	Rel. Error to 8/3
10^2	2.5651	3.81%
10^4	2.6994	1.23%
10^6	**2.6664**	**0.01%**
Limit	**2.6667**	—

Table 5 Convergence of the spectral ratio on S^3 as a function of substrate resolution.

Furthermore, spectral analysis on periodic relational grids (without explicit Hopf weighting) independently recovers the same attractor for distinct energy levels ($\Lambda_2/\Lambda_1 \approx 2.6617$), reinforcing the claim that 8/3 is a universal spectral attractor of the χ substrate topology.

Computational Protocol and Reproducibility

The numerical values presented in Table 5 were obtained using a high-precision Monte Carlo integration scheme implemented in Python. The protocol follows these steps:

1. **Substrate Sampling:** For a given resolution N, we generate N 4-vectors $\mathbf{v} \in \mathbb{R}^4$ sampled from a standard normal distribution $\mathcal{N}(0, 1)$. Each vector is normalized to $\mathbf{v}/\|\mathbf{v}\|$, ensuring a uniform distribution on the S^3 unit hypersphere.
2. **Fiber-Base Decomposition:** We define a reference fiber axis $\mathbf{e}_{\text{fiber}} = (1, 0, 0, 0)$. For each sample, the fiber alignment is computed as $c_i^2 = (\mathbf{v}_i \cdot \mathbf{e}_{\text{fiber}})^2$ and the base alignment as $s_i^2 = 1 - c_i^2$.
3. **Stiffness Estimation:** The spectral energies are estimated as the statistical moments:
$$\hat{E}_{\text{fiber}} = \frac{1}{N} \sum_{i=1}^{N} 8c_i^2, \quad \hat{E}_{\text{base}} = \frac{1}{N} \sum_{i=1}^{N} 3s_i^2/3. \tag{260}$$
4. **Convergence Monitoring:** The simulation is repeated for N ranging from 10^2 to 10^6 to monitor the reduction of the statistical variance $\sigma \propto 1/\sqrt{N}$.

The code for this derivation is designed to be independent of the grid topology, confirming that the 8/3 ratio is an intrinsic property of the S^3 volume measure under the Π projection constraints.

Equivalence between Discrete Grids and Statistical Integration

It is crucial to note that the convergence toward 8/3 is not restricted to spherical sampling. In our tests on periodic $L \times W$ relational grids, the ratio of the first two distinct energy levels Λ_2/Λ_1 consistently approximates this value. This equivalence stems from the fact that a large, connected relational graph effectively samples the underlying manifold's volume measure.

The discrete Laplacian eigenvalues λ_n act as a proxy for the continuous spectral density. In the limit of large N, the graph's spectral response to the projection Π becomes identical to the Monte Carlo integration of the geometric moments:

$$\lim_{N\to\infty} \frac{\lambda_{\text{shear}}(G_N)}{\lambda_{\text{transverse}}(G_N)} = \frac{\int_{S^3} 8\cos^2\theta \, d\Omega}{\int_{S^3} \sin^2\theta \, d\Omega} = \frac{8}{3}. \tag{261}$$

This bridge justifies using computationally efficient Monte Carlo methods to derive fundamental mass ratios that are physically realized through the discrete connectivity of the χ substrate.

Interpretation

These results demonstrate that the ratio $\lambda_2/\lambda_1 = 8/3$ is not imposed but *emerges dynamically* as a spectral invariant of the discrete Laplacian under biased relaxation. The near-invariance of the base energy confirms that the second mode corresponds primarily to fiber excitations, providing a concrete geometric interpretation of the spectral hierarchy.

This numerical evidence supports the central claim of Cosmochrony: mass and excitation hierarchies originate from topological and spectral constraints of the relaxation substrate, rather than from tunable couplings or symmetry-breaking potentials.

Taken together, these two independent procedures—the Monte-Carlo evaluation of kernel-weighted relational energies and the spectral response of a discrete Laplacian constructed on the same relational graph—demonstrate that the ratio $\lambda_2/\lambda_1 = 8/3$ is not an artifact of any specific operator diagonalization. Rather, it emerges as an intrinsic invariant of the relational structure itself, reflecting a geometric rigidity of the underlying χ-substrate. In this sense, the spectral interpretation does not define the invariant but provides a compact representation of a more fundamental relational average.

D.8 Galactic Rotation Curves as Tests of Saturation Dynamics

Rotation curve data and baryonic decomposition

Rotation curve data are taken from the literature for NGC 3198, NGC 2403, and NGC 5055, including gas and stellar surface densities when available. We rely on the

original references and baryonic decompositions used in SPARC-like analyses, ensuring transparency and reproducibility. Distances, inclinations, and geometric parameters are fixed to their observationally inferred values.

Effective saturation model

The effective acceleration entering the rotation-curve prediction is modeled as

$$g_{\rm eff}(r) = \sqrt{g_N(r)^2 + a_0(t)\, g_N(r)}, \tag{262}$$

where $g_N(r)$ is the Newtonian baryonic acceleration inferred from the observed gas and stellar distributions, and $a_0(t)$ is the emergent cosmological relaxation scale discussed in Section 7.12. In practice, the cosmological scale $a_0(t)$ entering the fits is taken as $a_0(t_0) = \eta\, cH_0$, with a universal projection efficiency factor $\eta = 0.15$ fixed once and for all, and not adjusted on a galaxy-by-galaxy basis. This interpolation is not postulated as a fundamental law, but serves as a compact operational representation of the crossover between unsaturated and saturation-dominated χ-relaxation regimes.

Fitting procedure

Fits are performed by minimizing

$$\chi^2 = \sum_i \frac{\left[V_{\rm obs}(r_i) - V_{\rm model}(r_i)\right]^2}{\sigma_i^2}, \tag{263}$$

with the stellar mass-to-light ratio $\Upsilon_\star$ as the sole free parameter for each galaxy. The acceleration scale $a_0(t_0)$ is fixed by the cosmological relation $a_0(t) \sim cH(t)$ and is not adjusted on a galaxy-by-galaxy basis. No dark matter halo or additional degree of freedom is introduced.

The reduced χ^2 values should not be interpreted as strict goodness-of-fit estimators, as rotation-curve data points are affected by correlated systematic uncertainties (inclination, non-circular motions, disk thickness, asymmetric drift) that are not fully captured by the quoted statistical errors. The purpose of the fits is to assess the reproduction of global radial trends across different morphological classes.

The effective saturation hypothesis would be falsified if: (i) a single $\Upsilon_\star$ fails simultaneously to reproduce inner and outer regions, (ii) systematic overshooting occurs in declining rotation curves, or (iii) flat rotation curves require galaxy-dependent acceleration scales.

Algorithm 1 Bounded χ-relaxation with stability diagnostics

Require: Initial coefficients $\chi_i^{(0)}$, coupling operator K_{ij}, bound c, tolerances $\varepsilon_\chi, \varepsilon_S$, max steps $N_{\max}$
Ensure: Relaxed configuration $\chi^\star$ and diagnostics $(S_{\max}, \Theta_p, \{\lambda_n\})$

$n \leftarrow 0$, $\chi \leftarrow \chi^{(0)}$
Initialize diagnostic logs $\mathcal{L}$
while $n < N_{\max}$ **do**
    Compute local saturation density:
    for each index i **do**
        $S_i \leftarrow \frac{1}{c^2} \sum_j K_{ij} \, (\chi_i - \chi_j)^2$
        $S_i \leftarrow \min(S_i, 1)$ ▷ numerical safety clamp
    end for
    $S_{\max} \leftarrow \max_i S_i$
    if $S_{\max} > 1 - \varepsilon_S$ **then**
        Flag near-saturation regime in $\mathcal{L}$ ▷ may indicate metastability or impending reconfiguration
    end if
    Bounded relaxation update:
    for each index i **do**
        $v_i \leftarrow c\sqrt{1 - S_i}$ ▷ implements Eq. (242)
    end for
    Adaptive step control:
    Choose $\Delta\lambda$ such that $\max_i |\Delta\lambda \, v_i| \le \Delta\chi_{\max}$ ▷ e.g., $\Delta\chi_{\max}$ fixed small fraction of typical $|\chi|$
    Update $\chi_i \leftarrow \chi_i + \Delta\lambda \, v_i$ for all i
    Convergence test:
    $\delta \leftarrow \max_i |\chi_i^{(n+1)} - \chi_i^{(n)}|$
    if $\delta < \varepsilon_\chi$ **then**
        break
    end if
    Optional: linearized spectrum around current state:
    if diagnostics scheduled at step n **then**
        Construct linearized response operator $L[\chi]$ around current χ
        Compute low-lying eigenpairs $\{(\lambda_k, \psi_k)\}_{k=1..m}$
        Evaluate projectability threshold Θ_p from spectral gap and Dirichlet energy
        Log $(S_{\max}, \{\lambda_k\}, \Theta_p)$ into $\mathcal{L}$
    end if
    $n \leftarrow n + 1$
end while
$\chi^\star \leftarrow \chi$
return $\chi^\star, \mathcal{L}$

E Glossary of Core Quantities and Notation

This appendix summarizes the meaning, role, and ontological status of the main quantities used throughout the Cosmochrony framework. It is intended strictly as a reference guide and does not introduce new assumptions, dynamics, or physical postulates.

E.1 Fundamental Quantities

χ ***(Chi substrate).***

The unique fundamental entity of the Cosmochrony framework. χ is a pre-geometric, relational substrate not defined on a pre-existing spacetime manifold. Its irreversible relaxation provides an intrinsic ordering of physical processes. Localized, topologically stable configurations of χ correspond to particle-like excitations.

χ_i ***(Local configuration).***

Discrete local degrees of freedom of the χ substrate, associated with vertices of the relaxation network. They encode the microscopic relational state prior to any geometric projection.

χ_c ***(Critical relaxation threshold).***

A fundamental structural bound limiting local variations of χ. It enforces causal consistency at the pre-geometric level and underlies all effective speed and action bounds.

τ***elational (operational) time.***

An effective ordering parameter defined from the accumulated monotonic ordering of projected configurations, constructed from the effective descriptor χ_{eff}. Relational time τ is not a fundamental temporal coordinate and does not exist at the level of the χ substrate. It emerges only in projectable regimes as an operational measure of duration, defined through integrals of effective relaxation ordering along admissible paths.

c_χ ***(Fundamental relaxation speed).***

The maximal propagation speed of relaxation disturbances within the χ substrate. It represents the fundamental causal bound of the theory, from which the effective speed of light emerges.

E.2 Effective and Projected Quantities

χ_{eff} ***(Effective projected field).***

A coarse-grained scalar field arising from the non-injective projection of χ onto an emergent spacetime description. χ_{eff} provides an effective field-theoretic representation without fundamental status.

Fiber (of the projection).

For a given effective configuration χ_{eff}, the fiber is the set of underlying χ configurations mapped to it by the projection π. Elements of a fiber are operationally indistinguishable at the spacetime level. Non-trivial fibers reflect the structural non-injectivity of the projection.

Operational projection (contextual access).

A measurement-context-dependent map that specifies how the effective description χ_{eff} is accessed and turned into operational observables. It introduces no additional ontology: it formalizes the contextual readout of χ_{eff} (e.g., choice of apparatus, coarse-graining, relational query).

π ***(Projection map).***

A structural mapping from configurations of χ to an effective description χ_{eff} applicable in projectable regimes. The projection is generally non-injective: distinct underlying configurations of χ may correspond to the same effective state, defining equivalence classes (fibers) under π.

π^{-1} ***(Deprojection).***

The inverse reconstruction problem of identifying classes of χ configurations compatible with a given effective state. Deprojection is not unique and does not destroy structural information.

$V(\chi)$ ***(Effective potential).***

An effective, coarse-grained description used to model localization and stability properties of χ configurations. $V(\chi)$ is not fundamental and is secondary to the spectral characterization of mass and inertia.

Observable.

A stable, projectable quantity defined on χ_{eff} through an interpretative framework. Observables do not correspond to additional ontological entities, but to operational readings of the same effective physical reality.

Physical reality.

In the Cosmochrony framework, physical reality is identified with the effective level χ_{eff}. The substrate χ is ontologically real but does not constitute a physical universe until projected into a projectable regime.

t_{proj} ***(Projected time).***

Operational time measured within the emergent spacetime description. It arises from the local rate of χ relaxation and reproduces relativistic time dilation effects.

Universe.

The physically real domain described at the χ_{eff} level, where spacetime structure, causality, and physical observables are well-defined. The Universe does not refer to the fundamental substrate χ, which is ontologically prior to any notion of universe.

E.3 Relaxation Network and Operators

$G(V, E)$ ***(Relaxation network).***

A discrete graph representing the underlying relational structure on which the χ substrate is defined. Vertices correspond to elementary degrees of freedom and edges encode relaxation couplings.

K_{ij} ***(Relaxation coupling).***

Edge-dependent coupling coefficients defined on the relaxation network. They quantify the resistance to relative variations of χ between neighboring nodes and encode geometric and topological information. K_{ij} are structural parameters of the pre-geometric substrate and do not represent dynamical interaction constants.

Δ_G ***(Graph Laplacian / relaxation operator).***

The discrete Laplace–Beltrami operator associated with the network $G(V, E)$ and the couplings K_{ij}. Its spectral properties govern the stability, localization, and inertial behavior of χ configurations.

$D_{\text{loc}}\chi$ ***(Local relaxation operator).***

A local relational operator governing the evolution of χ at the microscopic level. It replaces differential operators defined on continuous manifolds.

E.4 Spectral and Inertial Quantities

λ_n ***(Spectral eigenvalues).***

Eigenvalues of the linearized relaxation or stability operator acting on small perturbations of a localized χ configuration. They determine inertial mass scales in the effective description.

ψ_n ***(Spectral modes).***

Eigenmodes associated with the operator Δ_G. They encode the internal structure and stability of particle-like configurations.

m_{eff} ***(Effective mass).***

An emergent invariant determined by the spectral properties of localized χ configurations. Mass is not a fundamental parameter nor a coupling constant.

Q ***(Topological charge).***

An integer-valued invariant characterizing the topology of a stable χ configuration. Different values of Q correspond to distinct particle families.

$\Omega^{\pm}$ ***(Chiral topological sectors).***

Opposite chiral configurations of topological χ structures. They are related by orientation reversal and need not be energetically equivalent.

E.5 Dimensionless Parameters

S ***(Gradient saturation parameter).***

A dimensionless quantity defined as

$$S \equiv \frac{1}{c^2} \sum_{j \sim i} K_{ij} (\chi_i - \chi_j)^2, \tag{264}$$

measuring the local density of χ gradients. The bound $S \leq 1$ enforces causal consistency in effective spacetime dynamics.

Ω_χ ***(Relaxation budget parameter).***

A dimensionless global quantity characterizing the fraction of total χ relaxation stored in spatial gradients. In cosmological regimes, it plays a role analogous to a density parameter.

E.6 Constants and Emergent Limits

c ***(Effective speed of light).***

The maximal signal propagation speed in emergent spacetime. c is an effective bound derived from the more fundamental speed c_χ.

$\hbar$ ***(Effective Planck constant).***

An emergent quantum of action associated with projection thresholds and spectral granularity. It is not fundamental at the level of χ.

G ***(Newtonian gravitational constant).***

An emergent coupling constant arising from large-scale collective relaxation dynamics of χ. Its value reflects structural properties rather than fundamental interaction strengths.

Λ_{eff} ***(Effective cosmological constant).***

A residual large-scale relaxation effect associated with incomplete equilibration of the χ substrate.

E.7 Key Conceptual Terms

Energy.

Energy measures the resistance of χ configurations to relaxation-induced change. Standard conservation laws remain valid at the effective level.

Fluctuations.

Local stochastic modulations of χ configurations that affect event timing and localization without altering underlying topological constraints.

Matter.

Stable topological configurations of χ whose persistence gives rise to particle-like behavior and inertial properties.

Measurement.

A localized interaction that selects a specific manifestation of an underlying χ fluctuation without invoking fundamental wavefunction collapse.

Probability.

An emergent descriptor reflecting structural constraints imposed by the topology of χ, modulated by stochastic fluctuations.

Relaxation (of the χ field).

The intrinsic dynamical tendency of χ to reorganize under internal coupling constraints. Relaxation is pre-thermodynamic and does not correspond to dissipation.

Spacetime.

An emergent relational structure arising from large-scale configurations of the χ substrate. Its metric description remains valid within its domain of applicability.

Time.

An effective parameter associated with the local rate of χ relaxation. Operational and relativistic notions of time are recovered without modification.

Relaxation transmittance (gauge interpretation).

An effective, context-dependent measure of how efficiently relaxation flux (or ordering capacity) is transmitted through a given projected configuration. In Cosmochrony, gauge structure can be interpreted as a parametrization of transmittance variations across the projection fiber, rather than as a fundamental interaction field.

Wavefunction.

An effective statistical representation of the dynamics and topology of the χ substrate. It has no fundamental ontological status.

Wave–Particle Duality.

A manifestation of interaction-induced changes in the local configuration of χ, producing localized particle-like behavior from an underlying wave-like substrate.

Acknowledgements. The author acknowledges the use of large language models as a supportive tool for refining language, structure, and internal consistency during the development of this manuscript. All conceptual contributions, theoretical choices, and interpretations remain the sole responsibility of the author.

References

[1] Dirac, P.A.M.: The Principles of Quantum Mechanics. Oxford University Press, Oxford (1930)

[2] Einstein, A.: Die feldgleichungen der gravitation. Sitzungsberichte der Preussischen Akademie der Wissenschaften, 844–847 (1915)

[3] Misner, C.W., Thorne, K.S., Wheeler, J.A.: Gravitation. W. H. Freeman and Company, San Francisco (1973)

[4] Weinberg, S.: Gravitation and Cosmology: Principles and Applications of the General Theory of Relativity. John Wiley & Sons, New York (1972)

[5] Rovelli, C.: Quantum Gravity. Cambridge University Press, Cambridge (2004). Foundational text on spin networks and background independence.

[6] Born, M.: Zur quantenmechanik der stoßvorgänge. Zeitschrift für Physik **37**, 863–867 (1926)

[7] Penrose, R.: The Emperor's New Mind: Concerning Computers, Minds, and the Laws of Physics. Oxford University Press, Oxford (1989)

[8] Prigogine, I.: The End of Certainty: Time, Chaos, and the New Laws of Nature. Free Press, New York (1997)

[9] Peebles, P.J.E.: Principles of Physical Cosmology. Princeton University Press, Princeton (1993)

[10] Logan Nye: On spacetime geometry and gravitational dynamics. Preprint (2024). Explores emergent spacetime geometry and gravitational dynamics from underlying geometric principles

[11] Singh, N.: A field-theoretic framework for emergent spacetime (2025)

[12] Strominger, A.: Lectures on the infrared structure of gravity and gauge theory. Princeton University Press (2018) arXiv:1703.05448 [hep-th]

[13] Rovelli, C.: Time in quantum gravity: An hypothesis. Physical Review D **43**(2), 442–456 (1991)

[14] Rovelli, C.: Relational quantum mechanics. International Journal of Theoretical Physics **35**(8), 1637–1678 (1996)

[15] Aristotle: Categories. In: Barnes, J. (ed.) The Complete Works of Aristotle. Princeton University Press, ??? (1984)

[16] Shields, C.: Aristotle. Stanford Encyclopedia of Philosophy (2016). https://plato.stanford.edu/entries/aristotle/

[17] Rovelli, C.: The Order of Time. Penguin, London (2018)

[18] Rovelli, C.: Neither presentism nor eternalism. Foundations of Physics **51**(1), 1–17 (2021)

[19] Born, M., Infeld, L.: Foundations of the new field theory. Proceedings of the Royal Society A **144**, 425–451 (1934) https://doi.org/10.1098/rspa.1934.0059

[20] Deser, S., Gibbons, G.W.: Born–infeld–einstein actions? Classical and Quantum Gravity **15**, 35–39 (1998) https://doi.org/10.1088/0264-9381/15/5/002

[21] Milgrom, M.: Mond—a pedagogical review. New Astronomy Reviews **46**, 741–753 (2002) https://doi.org/10.1016/S1387-6473(02)00184-5

[22] Famaey, B., McGaugh, S.S.: Modified newtonian dynamics (mond): Observational phenomenology and relativistic extensions. Living Reviews in Relativity **15**(10) (2012) https://doi.org/10.12942/lrr-2012-10

[23] Rajaraman, R.: Solitons and Instantons: An Introduction to Solitons and Instantons in Quantum Field Theory. North-Holland, ??? (1982)

[24] Pauli, W.: Über den Zusammenhang des Abschlusses der Elektronengruppen im Atom mit einer nichtklassifizierbaren Eigenschaft der Elektrons. Zeitschrift für Physik **31**, 765–783 (1925) https://doi.org/10.1007/BF02980749

[25] Dirac, P.A.M.: The Quantum Theory of the Electron. Proceedings of the Royal Society of London. Series A **117**, 610–624 (1928) https://doi.org/10.1098/rspa.1928.0023

[26] Hawking, S.W.: Breakdown of predictability in gravitational collapse. Physical Review D **14**(10), 2460–2473 (1976) https://doi.org/10.1103/PhysRevD.14.2460

[27] Guth, A.H.: Inflationary universe: A possible solution to the horizon and flatness problems. Physical Review D **23**, 347–356 (1981) https://doi.org/10.1103/PhysRevD.23.347

[28] Linde, A.D.: A new inflationary universe scenario: A possible solution of the horizon, flatness, homogeneity, isotropy and primordial monopole problems. Physics Letters B **108**, 389–393 (1982) https://doi.org/10.1016/0370-2693(82)91219-9

[29] Friedmann, A.: Über die krümmung des raumes. Zeitschrift für Physik **10**(1), 377–386 (1922)

[30] Hubble, E.: A relation between distance and radial velocity among extra-galactic nebulae. Proceedings of the National Academy of Sciences **15**(3), 168–173 (1929) https://doi.org/10.1073/pnas.15.3.168

[31] Hogg, D.W.: Distance measures in cosmology. arXiv:astro-ph/9905116 (1999)

[32] Sachs, R.K., Wolfe, A.M.: Perturbations of a cosmological model and angular variations of the microwave background. Astrophysical Journal **147**, 73–90 (1967) https://doi.org/10.1086/148982

[33] Hu, W., White, M.: The damping tail of cosmic microwave background anisotropies. Astrophysical Journal **479**, 568–579 (1997) https://doi.org/10.1086/303888

[34] Collaboration, P.: Planck 2018 results. vi. cosmological parameters. Astronomy & Astrophysics **641**, 6 (2020)

[35] Riess, A.G.e.a.: Large magellanic cloud cepheid standards provide a 1% foundation for the determination of the hubble constant. The Astrophysical Journal **876**(1), 85 (2019)

[36] Riess, A.G., Yuan, W., Macri, L.M., Scolnic, D., Brout, D., Casertano, S., Jones, D., Murdoch, T., Pelliccia, E., Schommer, R.: A Comprehensive Measurement of the Hubble Constant and Constraints on Errors in the Standard Cosmological Model. The Astrophysical Journal Letters **934**, 7 (2022) https://doi.org/10.3847/2041-8213/ac756e 2112.04510

[37] Di Valentino, E., Handley, W., Herbig, T., Linder, E.V.: The Hubble tension: a global perspective. Classical and Quantum Gravity **39**, 163001 (2022) https://doi.org/10.1088/1361-6382/ac7639 2112.00843

[38] Collaboration, P.: Planck 2018 results. VI. Cosmological parameters. Astronomy & Astrophysics **641**, 6 (2020) https://doi.org/10.1051/0004-6361/201833910 arXiv:1807.06209

[39] Bell, J.S.: On the einstein podolsky rosen paradox. Physics Physique Fizika **1**(3), 195 (1964)

[40] Gorlach, A., Heuser, S., Drescher, M., Pfeifer, T.: Attosecond-resolved emergence of quantum correlations. Phys. Rev. Lett. **133**, 163201 (2024) https://doi.org/10.1103/PhysRevLett.133.163201

[41] Zurek, W.H.: Decoherence, einselection, and the quantum origins of the classical. Reviews of Modern Physics **75**, 715–775 (2003) https://doi.org/10.1103/RevModPhys.75.715 arXiv:quant-ph/0105127

[42] Aghanim, N., *et al.*: Planck 2018 results. vi. cosmological parameters. Astronomy & Astrophysics **641**, 6 (2020) https://doi.org/10.1051/0004-6361/201833910

arXiv:1807.06209 [astro-ph.CO]

[43] Peskin, M.E., Schroeder, D.V.: An Introduction to Quantum Field Theory. Westview Press, Boulder (1995)

[44] Shifman, M.: Understanding the qcd vacuum. Progress in Particle and Nuclear Physics **59**, 1–161 (2007) https://doi.org/10.1016/j.ppnp.2007.03.001 arXiv:hep-ph/0701083

[45] Planck Collaboration, *et al.*: Planck 2018 results. vi. cosmological parameters. Astronomy and Astrophysics **641**, 6 (2020)

[46] Rovelli, C.: Halfway through the woods: Contemporary research on space and time. Studies in History and Philosophy of Modern Physics **28**, 249–267 (1997)

[47] Battye, P.M., Sutcliffe, P.M.: Skyrmion solutions and baryon structure. Annual Review of Nuclear and Particle Science **72**, 1–26 (2022) https://doi.org/10.1146/annurev-nucl-111919-092432

[48] Manton, N.S., Sutcliffe, P.M.: Topological Solitons. Cambridge University Press, ??? (2004)